COMPACT PULSED POWER SYSTEMS USING LIQUID DIELECTRICS

By

G. VEDA PRAKASH

ENGG06201104001

Institute for Plasma Research, Gandhinagar

A thesis submitted to the

Board of Studies in Engineering Sciences

In partial fulfillment of requirements

for the Degree of

DOCTOR OF PHILOSOPHY

of

HOMI BHABHA NATIONAL INSTITUTE

August 2015

Homi Bhabha National Institute[1]

Recommendations of the Viva Voce Committee

As members of the Viva Voce Committee, we certify that we have read the dissertation prepared by **G. Veda Prakash** entitled "**Compact Pulsed Power Systems using Liquid Dielectrics**" and recommend that it may be accepted as fulfilling the thesis requirement for the award of Degree of Doctor of Philosophy.

Archana — 28-06-2016

Chairman – Dr. Archana Sharma — **Date:**

Anurag Shyam — 28-06-2016

Guide / Convener – Prof. Anurag Shyam — **Date:**

28-06-2016

K. V. Nagesh

Examiner – Dr. K. V. Nagesh — **Date:**

Subroto Mukherjee — 28-06-2016

Member 1- Prof. Subroto Mukherjee — **Date:**

S. V. Kulkarni — 28-06-2016

Member 2- Dr. S. V. Kulkarni — **Date:**

Final approval and acceptance of this thesis is contingent upon the candidate's submission of the final copies of the thesis to HBNI.

I/We hereby certify that I/we have read this thesis prepared under my/our direction and recommend that it may be accepted as fulfilling the thesis requirement.

Date: 28th June 2016

Place: Gandhinagar

Anurag Shyam

Prof. Anurag Shyam

Guide

[1] This page is to be included only for final submission after successful completion of viva voce.

STATEMENT BY AUTHOR

This dissertation has been submitted in partial fulfillment of requirements for an advanced degree at Homi Bhabha National Institute (HBNI) and is deposited in the Library to be made available to borrowers under rules of the HBNI.

Brief quotations from this dissertation are allowable without special permission, provided that accurate acknowledgement of source is made. Requests for permission for extended quotation from or reproduction of this manuscript in whole or in part may be granted by the Competent Authority of HBNI when in his or her judgment the proposed use of the material is in the interests of scholarship. In all other instances, however, permission must be obtained from the author.

G. Veda Prakash

DECLARATION

I, hereby declare that the investigation presented in the thesis has been carried out by me. The work is original and has not been submitted earlier as a whole or in part for a degree/diploma at this or any other Institution/University.

G. Veda Prakash

List of Publications arising from the thesis

1. Tesla based pulse generator for electrical breakdown study of liquid dielectrics, **G.Veda Prakash**, R.Kumar, J.Patel, K.Saurabh, and A.Shyam Rev. Sci. Instrum. 84, 126108 (2013), dx.doi.org/10.1063/1.4850529.
2. Comparative study of Electrical breakdown properties of Deionized Water and Heavy water under pulsed power conditions, **G.Veda Prakash**, R.Kumar, J.Patel, K.Saurabh, and Anitha V.P, M.B. Chowdari and A.Shyam,. Rev. Sci. Instrum. 87, 015115 (2016), dx.doi.org/10.1063/1.4940420
3. Study of anode initiated breakdown properties of water, **G.Veda Prakash**, R. Kumar, S. Kumar, A.Shyam, IEEE transactions on plasma science (Under Review-TPS9117 R1)

International Proceedings published online

1. Electrical breakdown study of water under nanosecond pulsed conditions using optical diagnostic, **G.Veda Prakash**, Kumar, R. Kumar, S. A.Shyam, in *Pulsed Power Conference (PPC), 2015 IEEE* , pp.1-3, May 31 2015-June 4 2015, doi: 10.1109/PPC.2015.7296947

Contribution in conference Presentation/Proceedings

International conference

1. Electrical breakdown study of liquid dielectrics under pulsed conditions, **G.Veda Prakash**, R.Kumar,J.Patel, A. Shyam, Page-105, EAPPC/BEAMS-September,2012, 4th Euro- Asian Pulsed Power conference and 19th international conference on High power particle beams, Karlsruhe, Germany.
2. Electrical Breakdown study of De-ionized Water and Heavy water under Pulsed Power Conditions, **G.Veda Prakash**, R.Kumar, Saurabh.K, Nasir and A.Shyam, 5th

Euro Asian pulsed power conference (EAPPC 2014), Kumamoto University, Kumamoto, Japan.

3. Capacitive Voltage Sensors for Pulsed Power Applications, **G.Veda Prakash**, R Kumar, Saurabh Kumar, Nasir S Shah and A.Shyam, 5th Euro Asian pulsed power conference (EAPPC 2014), Kumamoto University, Kumamoto, Japan
4. Electrical breakdown study of water under nanosecond pulsed conditions using optical diagnostics, **G.Veda Prakash**, R Kumar, Saurabh Kumar and A.Shyam IEEE Pulsed Power Conference (PPC-2015) Co-located with IEEE Symposium on Fusion Engineering (SOFE).

National conferences

1. Dielectric breakdown study under pulsed power conditions" **G.Veda Prakash**, R.Kumar, J.Patel and A. Shyam, Page-109, PSSI-December, 2011, 26th National symposium on Plasma Science and Technology, Birla institute of technology Mesra, Patna campus
2. Liquid dielectrics breakdown study under nanosecond Pulsed power conditions", **G.Veda Prakash**, R.Kumar, J.Patel and A. Shyam, Page-31, PSSI-July, 2012, 1st PSSI scholars' colloquium, Institute for Plasma Research, Bhat, Gandhinagar
3. Electrical breakdown study of water under pulsed conditions", **G.Veda Prakash**, R.Kumar, J.Patel and A.Shyam, Page-187, PSSI-December 2012, 27th National Symposium on Plasma science and technology, Pondicherry University and Plasma Science Society of India (PSSI).

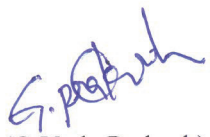

(G.Veda Prakash)

DEDICATED

TO

MY FAMILY

ACKNOWLEDGEMENTS

I would like to start by expressing my sincere gratitude to my thesis supervisor Prof. Anurag Shyam for the continuous support of my PhD study and research, for his patience, motivation, enthusiasm, and immense knowledge. His guidance helped me in all the time of research and writing of this thesis. I am deeply grateful to him for the discussions that helped me sort out the technical details of my work.

I am also thankful to Dr. Rajesh Kumar, for his help and discussion he gave, whose patience and support helped me overcome many crises and finish this thesis. He has been always there to listen and give advice. His insightful comments and constructive criticisms at different stages of my research were thought provoking and they helped me focus my ideas. I humbly appreciate his motivating ideas and fruitful discussions with him.

I would like to thank my committee Prof. Archana Sharma, Prof. S. Mukherjee and Dr. S. V. Kulkarni for their continuous support, encouragement and guidance throughout this thesis, which kept me on track.

I specially thank to Dr. Anitha V.P. and Ms. Priyavandana for allowing me to use their laboratory space and support in terms of experimental instruments. Without their help and patience, it was not possible to complete my work.

I am also thankful to Prof. P. K. Kaw, Prof. D. Bora for giving me this wonderful opportunity.

I am grateful for the support from everyone in the Pulsed Power laboratory, IPR. I would like to thank Bipin kaka, Jignesh, Ansari, Saurabh, Nasir, Manish, shailendra, Rahul, Naresh, Suresh, Jijo, Anup, Somesh, Subhnarayan and all the others for their assistance over the years.

I am also grateful to the staff members from Water-cooling department, workshop, computer center, library, stores, purchase section, administration, drafting section, canteen and security at Institute for Plasma Research for their co-operation and help during my entire duration of PhD.

I thank Saroj, Shravan, Smita, Shilpa, Pankaj, Amulya, Praveen lal, Jinto thomas, Purvi, Avdesh M, Aditya P, Pandya ji, Sanjay pandya, Rathod, Gaurav Bhatt, Parvez, Sudheer sharma, Vijay, Gandhi, Khanduri, Ramesh, Silel, Chirag, Subrat, Nitish, Dhaval, Arun, Anees Bano , Jeeva for their help.

I also thank my fellow researchers – Rana, Zuber, Prashant Prakash, Sandip, Dushyanth for their support during my PhD tenure. Thanks to my seniors Sanat, Sushil, Vikram, Deepak, Pravesh, Rameshwar, Shekar, Kshithish, Ujjwal, Gurdatt, Prabhal, Sita, Ashwin, Maya, Sharad, Jugal, Sayak, Manjit, Aditya, Soumen, Vikram dharodi, for their support, valuable inputs and guidance during PhD and providing friendly environment in scholar hall and hostel. I also would like to thank my juniors, Vara, Roopender, Chandra shekar, Bhibhu, Niraj, Mangilal, Deepa, Akanksha, Vidhi, Harish, Meghraj, Sameer, Arghya, Surbahi, Bhumika, Narayan, Ratan, Sonu, Modhu, Amit, Debraj, Umesh, Sagar, Atul, Jervis, Deepak, Prabhakar, Meenakshi, Pallavi, Alamgir, Sandeep, Harshita, Chetan Arun P and others for their support during the tenure, without their help and humor our hostel would have been a very dull place.

I would like to thank my parents and family members for being a constant source of love, concern, support, strength and patience all these years. I would like to express my heartfelt gratitude to my family.

CONTENTS

SYNOPSIS

In the pulsed power field, the energy is stored for a long duration at low power level in a temporary storage device and is delivered in a short period thus, increases the overall instantaneous power (GW) (voltage and currents in MV and MA respectively). In the recent past, the pulsed power machines have found its place in increasing number of applications like inertial confinement fusion, food processing, water treatment, medical treatment, industry and military applications etc. Many such applications require compact and low weight pulsed power systems with high voltage output (>100 kV). Research is open for studying and utilizing new dielectric materials, metals, techniques for designing the compact pulsed power systems. The portability and compactness of pulsed power systems can be achieved by having compact sub components, majorly energy storage devices. Conventionally, gases, liquids and solids serve as a dielectric medium for energy storage devices in pulsed power system components, such as capacitors, transmission lines and in high voltage switch medium. The properties of these components depend on electric breakdown strength and dielectric constant of material used. The ability to conform to complex geometries while maintaining the self-healing/recovery capabilities typical of gas systems makes liquids suitable for use as insulation for energy storage devices, particularly for nanosecond pulse generators. Study of pulsed breakdown in liquids, has received considerable attention in recent years due to the demands from the pulsed power field for the development of compact devices e.g. high power transmission lines, switching elements. Despite extensive research and theoretical studies, the understandings of electrical breakdown properties of liquids (like water) are far from complete. The aim of this work is to thorough understanding of liquid dielectrics including mechanisms of charge conduction, process leading to breakdown and characterizing the breakdown properties for optimizing the use of materials and attain the compact pulsed power systems. Identifying the failure modes or

critical conditions required for a liquid to fail is necessary to understand how breakdown will develop and successfully model the mechanisms involved in liquid breakdown. The area of research is focused on further understanding the breakdown properties of water in nanosecond time scales for developing the compact pulsed power systems. The analysis of breakdown in nanosecond regime may be of significance as it may aid in understanding the fundamental and inherent close packed features of liquid dielectrics breakdown properties. The study performed using various electrical and optical diagnostics with different experimental parameters. Further, the study extended to find the suitability of heavy water for developing compact pulsed power systems. Following chapters give brief introduction to work carried out in this thesis.

Chapter 1: Provides introductory description of pulsed power, necessity of compact pulsed power and motivation behind our studies. Pulse forming lines are often used as electrical storage units and high voltage pulse shapers in pulsed power applications. Increasing the power and energy capacity of such facilities by considering the compactness of the systems is an endless scientific requirement. Pulse forming lines are used as electrical storage units and high voltage pulse shapers in pulsed power applications. The operating efficiency of these pulse-forming lines depends on the electrical and chemical properties of the dielectric material used. The dielectric material should have high dielectric constant (ε_r) and good electrical breakdown strength (E_b) in order to optimize maximum efficiency and geometry. The efficacy of two characteristic features *viz.* ε_r & E_b of liquids make it more suitable for the energy storage in comparison to compressed gases. In addition, the freedom of circulation of liquid dielectrics makes it preferable over its solid counterparts concerning its applications involving complex geometries, thermal management and debris removal processing. The understanding of breakdown properties associated with dielectric medium may help in improving the geometry and breakdown concerns and certainly may improve the efficiency

of existing charge holding devices. Numerous experimental studies have been performed to understand the breakdown characteristics of liquid dielectrics (specifically water) but there is no comprehensive theory of breakdown in liquids is available in literature.

The compact pulsed power can be achieved by two ways. First one is to find the medium having good dielectric properties and use it to develop a compact system. Alternatively, the second option is to understand the breakdown properties of available dielectric materials and use the knowledge to avoid the breakdown for large extent. These techniques may be of help in achieving compact systems.

In this present work, the characteristic features of breakdown phenomenon have been analyzed and the possible approaches to improve the compactness of the storage system designing have been discussed.

In principle, there are varieties of liquids available, which can be used as dielectric in the high voltage environment. However, only few of them are found practically suitable for pulsed power applications for example, deionized water, which is characterized by high dielectric constant and moderate dielectric strength (in comparison to transformer oil). Its breakdown properties has been extensively been explored in microsecond regime while a little attention is paid in literature to nanosecond scale. The analysis of breakdown in nano-scale regime may be of significance as it may aid in understanding the inherent close packed features of water dielectrics. In this, further understanding the breakdown process in deionized water will lead to improvement in its breakdown strength.

Dielectric breakdown properties depend on many other parameters like electrode material, temperature, applied pulse duration and polarity, etc. Various studies have been made considering these parameters but the findings and conclusions are not very clear. To gain further knowledge of breakdown properties the experiments have been performed in nanosecond regime and the effect of electrode material, applied voltage polarity and distance

between the electrodes are analyzed. Further, the effect of electrode material on deionized water breakdown properties can also be visualized via emission spectra during discharge.

The compactness of the storage system can also be achieved by using alternative dielectric material with better dielectric properties than that of conventional dielectrics. The intuition is inspired from the fact that Deuterium is preferred choice in high voltage switching (Thyratron) applications than that of hydrogen. To examine this aspect, the breakdown study has been extended to heavy water (D_2O) and analyzed whether Deuterium oxide (D_2O) can be used in place of H_2O to enhance the efficacy of compact pulsed power systems.

The breakdown properties may also get influenced by modification in its chemical properties due to discharge; this feature can be analyzed by using Fourier Transform Infrared absorption spectroscopy. Analyzing the chemical behavior of dielectric medium due to discharge is other way, which leads to further understand the breakdown characteristic of medium. This can possible with Fourier Transform Infrared absorption spectroscopy.

Understanding the physical processes of initiating the pulsed breakdown of liquids and the basic laws of formation and propagation of discharges in liquid for nanosecond regime may further help in improving the system geometry. This can be realized by using fast optical ICCD camera.

Chapter 2: Includes the literature update on compact pulsed power technology and discusses the issues related to development of compact pulsed power system at dielectric and insulation level. It discusses the intermediate energy storage devices and its importance in development of compact pulsed power. It includes various dielectrics used for development of portable systems. This also covers the basic theories suggesting the breakdown behavior in liquids.

Chapter 3: Includes summary of the literature followed and describes the aim of the thesis. The chapter also outlines the way the thesis organized.

Chapter 4: Gives the details of the experimental set up developed for present studies. In the process of studying electrical breakdown properties of liquids under nanosecond (ns) time scales, a Tesla based pulse generator is developed. Use of Tesla transformer over conventional Marx generators makes the pulse generator very compact, cost effective (because less number of capacitors are used), and requires less maintenance. The designed pulse generator can deliver maximum output voltage of 350 kV and rise time of the order of tens of nanoseconds. The setup consists of primary energy source, Tesla transformer to step up the voltage, pulse forming line (PFL) to shape the pulse, high voltage spark gap switch to discharge the source voltage on to the load, voltage and current measurement chamber to measure the applied voltage and current profiles and finally the test chamber which is filled with test liquid. The test chamber consist pair of hemi spherical electrodes separated by a distance of several millimeter and has filled with liquid dielectric about to test. Pulse generator performance is validated by comparing the, experimental results with PSPICE (student version) simulation software results and both are well in agreement.

Chapter 5: describes the diagnostics, which have been used for our study. Measurement of high voltages short pulses in non-intrusive way is one of the challenging tasks in pulsed power. Insulation and geometrical restrictions in high voltage systems makes it difficult to access the high voltage points. A commercial available standard high voltage probe is limited to certain geometry and can measure up to few hundreds of kV. In this work, two capacitive voltage sensors are used, one is to monitor the source voltage (V_1) i.e. across Pulse forming Line, (i.e., before switching of SF_6 spark gap switch) and other is to measure voltage (V_2) across the test chamber electrodes. The output voltage of capacitive voltage sensor will be in differential form, which requires further integration to get the actual voltage. We have used computational software to further integrate the output of the voltage sensor. Both sensors have been calibrated by using a commercially available Tektronix (P 6015 A) voltage probe.

The current measurements have been made by using Rogowski coil. In this work, self-integrating Rogowski coil is developed. The designed Rogowski coil is calibrated with standard current transformer made of Bergoz instrumentations (model no FCT-016-20:1).

Optical diagnostics: We have used optical diagnostics for further understanding of our experimental results. Emission spectroscopy is used for understanding the discharge properties. In this work, 0.5 m visible spectrometer (Princeton Instruments, model no. SP 2500 i) is used.

Fourier transform infrared spectroscopy (FTIR) is used to identify the signatures of chemical compounds and substantial groups in the sample after the discharge in the test liquid. Thermo scientific, Nicolet-6700 model FTIR spectrometer has been used for this purpose. Data for Pre and post breakdown liquid samples were recorded which are further compared to find the formation of chemical combinations.

In order to understand the discharge breakdown characteristics, conductivity measurements were carried out on the original and post treated liquid samples for specific experiments. Eutech Cyber scan PC 300 model conductivity meter was used for this purpose.

Chapter 6: This chapter presents one of the experimental works carried out in the thesis. Electrical breakdown properties of pure water ($\varepsilon_r \sim 78$) under nanosecond scales have been studied. The experiments are performed using Tesla based pulse generator under uniform field electrodes. In this, effect of electrode material (brass and stainless steel (SS)) and distance between the electrodes (6 mm, 8 mm) are analyzed. Hemisphere electrodes of diameter 44, 42 mm, which builds the gap between the electrodes as 6 mm, 8 mm respectively. Conductivity is maintained at 0.45 μS/cm with continuous circulation of water through deionizer plant. Voltage is applied in incremental steps in terms of tens of kilo volts until breakdown occur in the water. Then the breakdown strength (E_B) is defined as the maximum stress experienced without breakdown for a series of tests (around fifteen). Initially

the experiments performed with pair of stainless steel (SS) electrodes, with 6, 8 mm gap between the electrodes. The same tests repeated with pair of brass electrodes for the same gap between the electrodes. Based on the experimental results, it is observed that water show better breakdown strength, with the stainless steel (SS) as electrode material compared to the brass material. It is also observed that, in case of SS electrode material charge hold for long duration compared to brass electrode material. Our observations are further supported by emission spectra, which we have performed during the experiments for both cases of electrode material. In case of brass, the spectra show the presence of Cu and Zn ions in the test sample whereas iron (Fe) ions with SS electrodes during discharge. In this, the prominent visible lines are identified with the help of NIST database. Zahn et al. have observed that, Cu is the probable injector of positive ions and Zn injects negative charges in to the test sample under micro second discharges and the same observed in our very small-applied pulse durations (i.e. nanosecond scales). It is assumed that, the presence of charges increases the conductivity that leads to early breakdown in case of brass compared to stainless steel. It is further observed that keeping negative polarity of the electrode gives slightly (~ 7-8%) enhanced discharge breakdown voltage when compared with discharges with positive polarity. Although the field distribution is uniform in the present case, how the electrode surface irregularities in the realistic experimental situation contribute to the breakdown is matters.

Chapter 7: This includes the heavy water breakdown properties under nanosecond time scales. We have also studied the electrical breakdown properties of heavy water(D_2O) and the results are compared with the water (H_2O) breakdown properties. The motivation behind the study is, in high voltage switching applicatons (Thyrotron), deuterium(D) is used as switching medium than hydrogen due to its higher voltage withstand. Similarly, it has been tried to understand whether D_2O is having high electrical breakdown strength compared to

H_2O. To our knowledge, we have not found any literature reporting the heavy water (D_2O) breakdown strength. In this process, we have studied electrical breakdown properties of heavy water(D_2O) and results obtained are compared with the water (H_2O). Heavy water, though chemically similar to normal water, is not identical with the later due to the presence of an additional neutron in the nucleus. Deuterium is unique among heavy stable isotopes in being twice as heavy as the lightest isotope. This doubled mass increases the strength of D-O bonds in heavy water, as a result of which D_2O less self-ionizes compared to H_2O. The number of hydrogen bonds per molecule of water is higher in heavy water (D_2O), giving its molecule a definite tetrahedral shape as compared to the broader structure of normal water molecule. D_2O has higher (~11%) density, dynamic viscosity, heat of fusion and heat of vaporization as compared to normal water, whereas H_2O has higher surface tension and refractive index. Considering all these properties, it is expected to result in different dielectric and breakdown characteristics of D_2O as compared to H_2O, an area where experimental studies are highly incomplete. In this work deionized water of conductivity ~ 0.65 μS/cm, dielectric constant (ε_r ~ 78), density 0.999 g/ml and heavy water (Nuclear grade), of conductivity 0.9 μS/cm , dielectric constant (ε_r ~78), density 1.10199 g/ml, Isotopic purity %D_2O 99.96 (obtained from Heavy water plant, Vadodara, Government of India) has been used.

The experiments have been performed with two different electrode materials (SS and Brass) and polarity (positive, negative) combinations. It is observed that, breakdown occurred in D_2O at lesser voltage and in short duration compared to H_2O deionized water irrespective of the electrode material and applied voltage polarity chosen. In addition to this, conductivity measurements carried out on all the original and post treated samples are supporting our observations on the breakdown behavior. For all the parametric combinations, the conductivity of the post-treated liquid is higher as compared to the original sample. However,

the relative enhancement in conductivity is considerably higher in case of Heavy water as compared to deionized water. Further, FTIR spectroscopy is performed on pre and post treated samples to understand the chemical changes in liquids due to discharge. There is a change in intensities of spectra is noticed for both D_2O and H_2O, however, the variation in intensity found is high in case of D_2O compared to H_2O (almost negligible). In case of D_2O, the significant change in intensity has been observed particularly for positive polarity of both stainless steel and brass electrode materials. This indicates possibility of chemical reactions during the discharge. Deuterium is known to react more slowly compared to ordinary hydrogen, and hence the D^+ and OD^- ions in D_2O would have remained for longer durations compared to the corresponding ions in H_2O. This could be the possible reason for increase in conductivity and reduced charge holding capability of D_2O. The overall experimental observations show that H_2O is suitable for nanosecond pulsed power applications compared to D_2O.

Chapter 8: Presents, the studies realted to anode breakdown initiation in water with nanosecond time scales under uniform electric fields. Electrical and optical diagnostics are used for this purpose. The experiments are performed in deionized water (0.6 μS/cm) for discharge gap of 6 mm, at room temperature (~ 26^o C). The voltage pulse had amplitude of ~100-150 kV with pulse durations ~120-140 ns. A high-speed photo recording in frame regime with exposure time of 3 ns and inter frame delay of 20 ns are reported. It is observed that, in nanosecond time scales under uniform electric field conditions for positive applied voltage, breakdown initiated at single point on the electrode surface. The discharge propagated as single stem for some duration and after that, the discharge split into branches, after that it further increased to sub branches in the one of the branch. All the branch channels emerge from a central channel called stem, which is connected to the anode electrode surface. The streamer increases in diameter and intensity with decrease in distance to the opposite

electrode. The first stage, is due to the local release of energy near electrode surface. As the field strength increased with respect to time, the growth of the streamers increased and at particular, the streamer split into branches and propagates to opposite electrode. The intensity of the discharge is increased up to 80 ns duration, after that the intensity fall in consequence propagation. The streamer velocity in the initial stage until the branches formed was high. Once the initiation of branches started, the velocity of streamer propagation started reduced, this might be the ion current density distributed in to the branches.

Chapter 9: provides the conclusions, findings and summarizes the future work. Following are the summary of the work carried out in this thesis.

As mentioned earlier, one way of achieving the compact pulsed power systems is to control the breakdown condition, which can be achieved by understanding the breakdown properties of dielectrics and finding the stimulating conditions for the discharge. The experiments based on motivation has been performed and the outcome of the studies are as follows

1. Tesla based pulse generator has been developed for studying the electrical breakdown properties of liquid dielectrics for developing the compact pulsed power systems. The system is designed to deliver maximum voltage up to 300 kV and pulse duration of several tens of nanoseconds. Calculated system parameters are verified experimentally. Overall, experimental setup is characterized by using PSPICE (student version 9.1) simulation software and the simulation results are in good agreement with experimental results. In order to understand the electrical breakdown properties of liquids, electrical diagnostics *viz.* capacitive voltage sensor and self-integrating Rogowski coil are developed and calibrated using standard commercial probes.
2. Electrical breakdown properties of deionized water are studied in nanosecond time scale with uniform electric field conditions. The effect of electrode material, and

distance between the inter electrode gap (6, 8 mm) are examined at room temperature (~26^{o}C). The observations indicate the discharge with SS electrodes occur at higher voltage and sustain for longer duration in comparison to those with brass electrodes. The variation in inter electrode gap shows the nonlinear behavior of breakdown characteristics for water.

3. Observed dependence of the breakdown properties of water on the electrode material are further analyzed using optical emission spectroscopy for nanosecond discharges. Based on the electrical results and spectra, it is observed that SS material is advantageous for the nanosecond compact pulsed power applications than that case of Brass.
4. The suitability of Heavy water (D_2O) as an alternative dielectric material for developing compact pulsed power has been examined by studying its electrical breakdown properties under nanosecond pulsed conditions. The experimental results obtained are compared with the results obtained with water (H_2O) under same experimental conditions. The effect of electrode material and voltage polarity are also examined with ~3 mm inter electrode gap. It is observed that irrespective of the combination of electrodes or polarity adopted, discharges with D_2O exhibit less breakdown voltage and time as compared to the discharges with deionized water. Further, in order to validate the above experimental observations conductivity measurements are carried out on pre and post breakdown test samples, for all the combinations of parameters (i.e. dielectric liquid, polarity, electrode material). The conductivity measurements are consistent with the observed breakdown behavior.
5. An attempt is made to understand the change in chemical behavior due to discharge in the liquids by using optical Fourier transform infrared (FTIR) absorption spectroscopy. The tests are performed on pre and post breakdown test samples

covering all the typical parametric combinations. The observations clearly reveal evidence of chemical reactions during breakdown and found more prominent in case of D_2O as compared to H_2O samples, enabling a qualitative interpretation of the superior performance exhibited by H_2O as a dielectric for compact pulsed power applications.

6. To understand the physical processes initiating the pulsed breakdown of liquids and the basic laws of formation and propagation of discharges in liquids a high speed fast optical photo recording(Stanford computer optics, 4 Picos, ICCD) camera has been used. The optical images are taken in frame regime with exposure time of 3 ns and inter frame delay of 20 ns. It is observed that, in nanosecond time scales and uniform electric field conditions for positive applied voltage, the breakdown is initiated at single point on the electrode surface and the discharge propagate as a single stem for a finite duration (~80 ns) and after that, the discharge split into branches. The optical images of breakdown initiation from anode, formation of streamers, branches, sub-branches and multiple discharge initiation from electrode surface are studied.

The understanding of breakdown properties can be carried out by theoretical modeling or using computational software. The research issues are still open on studying and utilizing new dielectric materials, metals, and interface in the design of compact pulsed power systems. Further, the breakdown characteristics can be understood visually by using optical diagnostics *viz.,* ICCD camera, spectroscopy, etc., which gives in-depth understanding of breakdown mechanism. Alternative topologies and novel engineering techniques must be investigated for developing the compact pulsed power systems.

List of Figures

List of Tables

List of symbols

ε_o	Permittivity of free space	8.854×10^{-12} F/m
ε_r	Dielectric constant	
μ_o	permeability of free space	$4\pi \times 10^{-7}$ H/m
σ	Conductivity of medium	S/m
ρ	Resistivity	Ωm
F	Farad	Farad
J	Joule	
E_b	Breakdown strength	V/m
c	Velocity of light	3×10^8 m/s

Chapter 1
Introduction

1 Pulsed power

In the pulsed power field, the energy is stored for a long duration at low power level in a temporary storage device and delivered in a short period thus, increases the overall instantaneous power (voltage and current in MV and MA respectively and power in several Giga watts (GW)) although the total energy remains same.

Energy is typically stored within electrostatic fields (capacitors), magnetic fields (inductors), in form of as mechanical energy (using large flywheels connected to special purpose high current generators), or as chemical energy (high-current lead-acid batteries, or explosives). By releasing the stored energy over a very short interval, a large peak power can be delivered to a load. For example, as shown in Figure 1.1, if one joule of energy is stored within a capacitor and released over one second, the peak power delivered to the load is only one watt. However, if all of the stored energy released within one microsecond, the peak power is one megawatt, a million times greater, this defines the Pulsed Power.

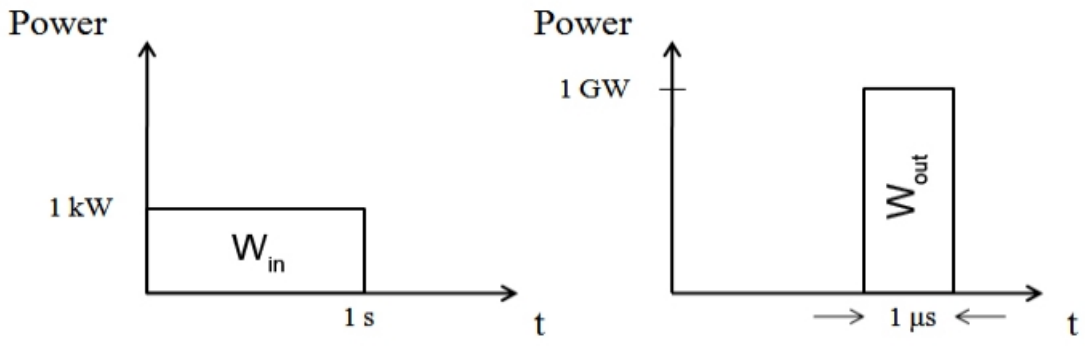

Figure 1.1 Concept of Pulsed power systems

Pulsed power involves the electrical generation of very short pulses of nanoseconds to milliseconds with the possibilities of

- Voltage up to several megavolts(MV)
- Current up to several hundreds of mega amperes (MA)
- Energy releases up to several millions Joules per second
- Power densities of up to Giga watts or more per square centimeter

1.1 History of pulsed power

The roots of pulsed power can be traced to the development of high voltage technology and nuclear physics prior to World War II. Pulsed power itself was first developed during World War II for use in radar technology. A massive development program was undertaken to develop pulsed radar, requiring very short high power pulses. After the war, development in pulsed power technology continued for various other applications that led to the development of novel pulsed power machines[1][2]. Since the security and the reliability of nuclear weapons has to be maintained without nuclear tests, one important use of pulsed power is in the simulation of the effects of fusion reactions in small volume, which has helped to push forward their civil applications.

1.2 General scheme of pulsed power systems

The pulse power system converts a low power long duration pulse to high power short duration pulse. The block diagram of pulsed power system is shown in Figure 1.2. In this, the primary energy source (in general DC source) is used to charge the energy storage device (viz. capacitor) for very long duration at low power level. The stored energy is discharged to intermediate energy storage or pulse forming line (PFL) unit through a switch (S_1) in micro second durations. The PFL further discharges these micro second pulse charges in

nanosecond time scale through a high voltage switch (S_2) to load which results into very high power output.

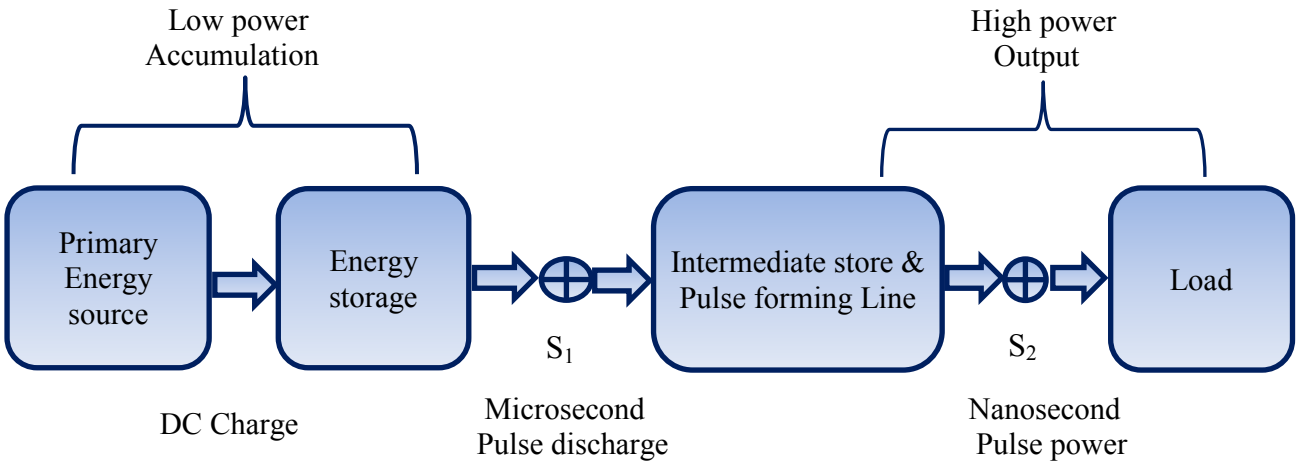

Figure 1.2 General scheme of pulsed power

1.2.1 Applications of Pulsed Power Technology

Pulsed power had many practical applications[3][4] in that few of them may be categorized as follows.

1.2.1.1 Industrial applications

Typical industrial application that are becoming widespread include

a) **Food processing/pasteurization** [5] Pulsed electric field (PEF) processing has been shown by multiple researchers being equivalent to pasteurization in terms of pathogen reduction for a wide range of liquid foods[6]. For foods, those are heat sensitive; it offers considerable benefits in taste, color and nutritional value above the other process.

b) **Production of nano-powders** [7] with the advent of nano-technology there is a great demand for a mass production process for the manufacturing of nano-sized powder for various industrial applications such as cosmetics, the electrodes for MLCC (Multi-Layer Ceramic Capacitors) and the production of silver fiber for anti-bacterial

products. A pulsed power based electric wire explosion[8] can be used to produce these Nano particles. The wires are exploded in a vessel that can be filled with gas at pressures between 50 and 150 kPa. Depending on the gas, metal oxide, nitride, or carbide powders can be produced.

c) **Medical waste treatment**[9] Pyrolysis is a pulsed power based process, where the waste is heated in an oxygen deficit that results in the gasification of organic components (a so-called synthesis gas is formed) and the melting of mineral components.

d) **Sludge treatment** [7] Sewage sludge is composed of organic materials, bacteria and mostly water. The bacteria contain digested organic materials and the objective of the sewage sludge treatment is to destroy the bacteria cell membrane. High voltage pulse power can be used to generate an arc discharge in the sewage sludge, which will ensure that this happens.

e) **Other industrial applications**[10] this technology can further utilized as for Bioelectric applications[11] viz. cancer treatment and induction of apoptosis treatment of exhaust gases; sterilization of microorganism; removal of biological wastes; fragmentation of rocks; recycling of concrete and electrical appliances; and surface treatments of material. The application of electric fields with a short pulse width allows direct interaction with biological cells substructure without heating the tissue, which has essence of medical application and may utilize to dissolve kidney stones (lithotripsy). Pulsed electrical discharges can be designed to create so-called streamers[12]. This non-thermal plasma has the ability to attack biological and chemical agents alike and is in particular promising for decontamination and purification of water (both fresh water and wastewater). The pulsed high power laser systems [13]used for example in car manufacturing. Another emerging application is

the manipulation of mammalian cells with pulsed electric fields. 'Longer' pulses (in the microsecond range) are a widely successful tool to bring large molecules into cells, as it is for example need in gene therapies. 'Shorter' pulses have demonstrated an ability to affect cells on a subcellular level. One of the most appealing results so far is that they can trigger apoptosis in cancer cells. By reminding cancer cells to undergo this 'programmed cell death', which these cells have forgotten, pulsed electric fields can be used to fight tumors.

1.2.1.2 Research and development

a) **Inertial confinement fusion** [14] Pulsed Power is also a key technology in the research on inertial confinement fusion reactors, such as the Z-Machine at Sandia National Laboratories or the National Ignition Facility operated by Lawrence Livermore National Laboratory. Inertial confinement fusion (ICF) [14][15] is a process in which nuclear fusion reactions are initiated by heating and compressing a fuel target, typically in the form of a pellet that most often contains a mixture of deuterium and tritium. The heating can be achieved using laser or high X-ray radiation.

   The extremely large output of pulsed power energy can be transferred into a wire array mounted in (say) the *z*-direction. A high current flowing in the *z* direction will produce a magnetic field $B(\theta)$, resulting in a $J(z) * B(\theta)$ force in the *r* direction. This phenomenon is called z-pinch[14] and implodes the wire array, thereby releasing a huge burst of X-ray radiation suitable for heating an ICF process.

b) **Transmutation of nuclear waste** [16] Nuclear transmutation is the conversion of one chemical element or isotope into another, which occurs often through nuclear reactions. Natural transmutation occurs when radioactive elements spontaneously decay over a long period and transform into other more stable elements. Artificial transmutation occurs in machinery that has sufficient energy to cause changes in the

nuclear structure of the elements. Pulsed power systems can be used to generate such a high power needed to achieve transmutation.

1.2.1.3 Military applications

Beside these civilian applications, the technology is also used in many military programs[17], for example radars (the birthplace of pulsed power), high power microwave generators, and electromagnetic launchers ("rail guns")[18].

1.2.2 Important requirements of pulsed power applications

The requirements of typical pulsed power devices for different applications are given in Table 1.1 Pulse requirement for various applications cover a wide range, from kilo-ampere to mega-ampere currents, kilovolts to megavolts voltage, nanosecond to millisecond pulse duration and pulse repetition rates of 1 to 30,000 pulses per second[19].

Table 1.1 Typical pulsed power applications and requirements

Applications	Voltage MV	Current MA	Repetition rate(kpps)	Load type	Pulsed energy MJ
Advanced test Accelerator	0.1-1	0.01-0.1	10	Capacitive	0.002-0.5
Modified betatron	0.5	0.2	0.001-10	Inductive	100
Lasers	0.01-0.1	0.001-0.03	0.01-0.1	Resistive/ Capacitive	0.001-0.04
EM guns	0.002-0.02	0.1-5	0.001-0.05	Resistive and Inductive	5-500
Inertial fusion	3	0.1	0.01	Capacitive	0.1-3
EMP simulator	1-5	0.01	0.1	Capacitive	0.1-0.5

1.3 Compact pulsed power

In addition to the above-mentioned requirements, many pulsed power applications require compact and low weight[20] pulsed power systems with high voltage output (>100 kV).

The portability and compactness of pulsed power systems can be achieved by having compact sub components, majorly intermediate energy storage devices or pulse forming lines. Research is open for studying and utilizing new dielectric materials, metals, techniques for designing the compact pulsed power systems.

Chapter 2
Literature review

2 Introduction

Pulsed power is a technology that is used to drive the loads requiring very large power (MW to several GW) pulses in short. Various pulsed power applications viz. inertial confinement fusion, food processing, water treatment, medical treatment, industry and military applications[21][2] etc., require technology that can be deployed in small spaces under stressful environments. Several areas of applications like medical, military and industrial applications require compact, portable pulsed power in order to operate on mobile platforms. These requirements enable the search for compact pulsed power systems.

Since the World War II, the pulsed power research increased to many areas viz. industrial medical and military[23]. Still many applications today await the availability of compact pulsed power systems.

In general, a pulsed power system consists of primary energy storage, pulse shaping, transmission and load matching components as shown in Figure 2.1. Each of these sub elements of the pulsed power system must also be efficient to achieve the overall objective of compactness.

To achieve compactness of overall system one may focus on (i) introducing the new materials for use in pulsed power systems (ii) examining the alternative topologies for compact pulse generation (iii) investigate the basic physics related to the generation of pulsed power, such as the behavior of dielectrics under intense electric field conditions.

Essential to these studies is a better understanding of the basic electrical properties of dielectrics viz. solids, liquids, and gaseous dielectrics for intermediate storage or pulse forming lines.

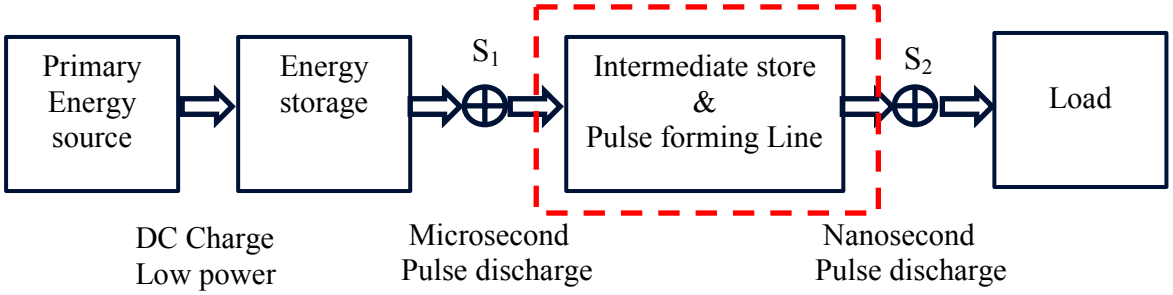

Figure 2.1 Pulsed power systems

In general, many pulsed power systems use capacitive storage systems, either as primary energy storage or as intermediate storage. The tradeoff between high dielectric constant and large hold off voltage has been identified as a major issue in the search for suitable dielectric materials with high energy density storage device. Understanding the breakdown mechanisms of these dielectrics has the potential of enabling the engineering of superior materials for use in pulse forming lines as well as advanced capacitor design.

The key requirements for developing the efficient energy storage for developing the compact pulse power system are either finding new dielectric medium having a high permittivity and a high breakdown strength[24] result in compact and increased stored energy density or by understanding the conventional dielectric mediums for smaller volume and higher voltage operations.

2.1 Research issues in compact pulsed power technology

The technical areas for compact geometry of pulsed power are its architecture, switching, increased energy density storage, and thermal management. By architecture, it means the overall properties of the system that allow it to be compact, lightweight, and efficient[20].

In order to minimize the volume and weight of a pulsed power system, efficiency of the system is of prime importance. Thus, any architecture study must start with consideration of efficiency of the system. The system efficiency further requires that the components, each taken individually, also be efficient. The combination of energy storage and switching must be optimized for efficiency in the context of reasonable component count for reliability.

When developing pulsed power systems, a primary factor in identifying directions for component and materials development is the system architecture. In order to minimize the volume and weight of a pulsed power system, efficiency of the system is of prime importance. Thus, any architecture study must start with consideration of efficiency of the system. The system efficiency further requires that the components, each taken individually, also be efficient. The combination of energy storage and switching must be optimized for efficiency in the context of reasonable component count for reliability[25].

In common pulsed power systems, energy is initially delivered from a primary energy source (in general DC source) power device, stored in an energy storage device, transferred to a pulse forming and voltage–current scaling device and then transferred to a load using multiple switches.

From a volume, weight, and complexity point of view, it is always better to store the energy only once in a single storage device that also serves to form the pulse and scale the voltage current to the parameters required by the load. Furthermore, the pulse-shaping device should also provide a relatively “square” pulse and be matched to the load such that the ratio of delivered pulse energy to stored energy approaches unity.

In a repetitive pulsed power system, component efficiency is of even greater importance than in a single-shot system. In that, energy dissipated in the storage and switching components is additional energy, generated repeatedly must be supplied by the prime power system, stored

by the energy storage system and removed by an auxiliary cooling system, increasing the overall mass.

The energy density (in joules per cubic meter)

$$Energy\ density\ (W_E) = \frac{1}{2} E^2 \varepsilon_o \varepsilon_r \qquad \textbf{(2.1)}$$

Considering the equation (2.1), the energy density of storage device depends on dielectric strength and permittivity of material selected.

The compact pulsed power research is more application specific nature than an organized effort[26]. Many historic examples of compact pulsed power are available in the literature[20].

From the literature, it was found that the research on high voltage insulation material is one area, which can help in designing very compact systems[25]. This area of research also explores development of high relative permittivity material. The other reliable solution will be to use the best of the material available in this field and continue development of compact systems. The newer techniques for storing energy could be explored for making compact pulsed power system.

Some issues of fundamental importance are needed to be investigated for compact pulsed power system developments such as new materials for high dielectric strength and high dielectric constant, exploring alternate engineering topologies for compact systems, improvements in switches[27] etc. The research issues are still open on studying and utilizing new materials dielectrics, insulators, metals, and interface in the design of components of the compact pulsed power systems.

Fundamental studies on compact pulsed power system development with new materials and novel engineering techniques are needed to be investigated to reduce the size of the system. The energy density of pulsed power systems is often limited by the storage capabilities of the

dielectric subsystem. Advances in pulsed power switches, capacitors, and pulse-forming line are necessary to develop compact, reliable electrical power on directed energy systems as well as space platforms for military applications. Research is also underway by to gauge the future of compact pulsed power by investigating the fundamental limits of dielectric materials and pulsed power components.

The portability and compactness of pulsed power systems [2]can be achieved by having compact sub components, majorly energy storage devices. Conventionally, gases, liquids and solids serve as a dielectric medium for energy storage devices in pulsed power system components, such as capacitors, transmission lines and in high voltage switch medium. The properties of these components depend on electric breakdown strength and dielectric constant of material used.

2.1.1 Dielectric Strength:

The theoretical dielectric strength of a material is an intrinsic property of the bulk material and is dependent on the configuration of the material or the electrodes with which the field is applied.

The dielectric strength can be defined as The maximum electric field that a pure material can withstand under ideal conditions without breaking down i.e., without experiencing failure of its insulating properties[28].

The intrinsic dielectric strength is measured using pure materials under ideal laboratory conditions. At breakdown, the electric field frees bound electrons. If the applied electric field is sufficiently high, free electrons from the background radiation may become accelerated to velocities that can liberate additional electrons during collisions with neutral atoms or molecules in a process called avalanche breakdown. Breakdown occurs quite abruptly (typically in nanoseconds), resulting in the formation of an electrically conductive path and a disruptive discharge through the material.

2.2 Electrical breakdown

Electrical breakdown or dielectric breakdown refers to a rapid reduction in the resistance of an electrical insulator when the voltage applied across it exceeds the breakdown voltage. This results in a portion of the insulator becoming electrically conductive. Electrical breakdown may be a momentary event, or may lead to a continuous arc discharge if protective devices fail to interrupt the current in a high power circuit.

Under sufficient electrical stress, electrical breakdown can occur within solids, liquids, gases or vacuum. However, the specific breakdown mechanisms are significantly different for each, particularly in different kinds of dielectric medium. From the literature, some of the dielectric breakdown theories are discussed here.

2.2.1 Breakdown of solids

Solid insulating materials are used almost[29] in all electrical equipment viz., circuit breaker, generator or many house hold appliances. Solid insulation forms an integral part of all electrical equipment especially when the operating voltages are high. The solid insulation not only provides insulation to the live parts of the equipment from the grounded structures, it sometimes provides mechanical support to the equipment.

The breakdown of solid dielectrics not only depends upon the magnitude of voltage applied but also it is a function of time for which the voltage is applied[30]. The product of the breakdown voltage and the log of the time required for breakdown is almost a constant *i.e.,*

$$V(\text{breakdown})\ \mathbf{x}\ \ln t\ (\text{time to breakdown}) = constant \qquad (2.2)$$

Where **V** is breakdown strength of dielectric in kV/cm.
t is the total time

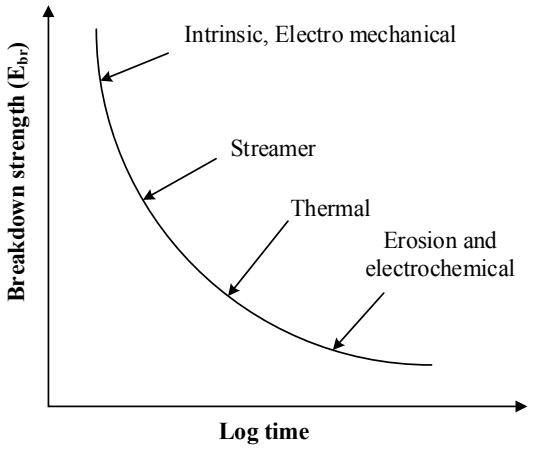

Figure 2.2 Breakdown strength Vs. time characteristics of solids

The dielectric strength of solid materials is affected by many factors viz. ambient temperature, humidity, duration of test, impurities or structural defects, whether a.c., d.c. or impulse voltages are being used, pressure applied to these electrodes etc. As said earlier the time of application plays an important role in breakdown process, for discussion purposes, it is convenient to divide the time scale of voltage application into regions in which different mechanisms operate[31].

The various mechanisms are:

a. Intrinsic or ionic breakdown

b. Electromechanical breakdown

c. Thermal breakdown

d. Electrochemical breakdown

e. Treeing and tracking

f. Internal discharges

2.2.2 Breakdown of gases

A gas in its normal state is almost a perfect insulator. However, when a high voltage is applied between the two electrodes immersed in a gaseous medium, the gas becomes a conductor and an electrical breakdown occurs.

The processes that are primarily responsible for the breakdown of a gas are ionization[32] by collision, photo-ionization, and the secondary ionization processes. In insulating gases (also called electron-attaching gases), the process of attachment also plays an important role.

1. **Ionization by Collision**

The process of ejecting an electron from a gas molecule with the simultaneous production of a positive ion is called ionization. In the process of ionization by collision, a free electron collides with a neutral gas molecule and gives rise to a new electron and a positive ion. If we consider a low pressure gas column in which an electric field (**E)** is applied across two plane parallel electrodes, then, any electron starting at the cathode will be accelerated more and more between collisions with other gas molecules during its travel towards the anode.[33]

A few of the electrons produced at the cathode by some external means, say by ultra-violet light falling on the cathode, ionize neutral gas particles producing positive ions and additional electrons. The additional electrons, then, themselves make `ionizing collisions' and thus the process repeats itself. This represents an increase in the electron current, since the number of electrons reaching the anode per unit time is greater than those liberated at the cathode. In addition, the positive ions also reach the cathode and on bombardment on the cathode give rise to secondary electrons.

2.2.2.1 Secondary Ionization Processes

Secondary ionization processes by which secondary electrons are produced are the one, which sustain a discharge after it, is established due to ionization by collision and photo-ionization. They are briefly described below.

(i) Electron Emission due to Positive Ion Impact

Positive ions are formed due to ionization by collision or by photo-ionization, and being positively charged, they travel towards the cathode.

A positive ion [34]approaching a metallic cathode can cause emission of electrons from the cathode by giving up its kinetic energy on impacts. If the total energy of the positive ion, namely, the sum of its kinetic energy and the ionization energy, is greater than twice the work function of the metal, then one electron will be ejected and a second electron will neutralize the ion. The probability of this process is measured as γ_i , which is called the Townsend's secondary ionization coefficient due to positive ions and is defined as the net yield of electrons per incident positive ion. γ_i increases with ion velocity and depends on the kind of gas and electrode material used.

(ii) Electron Emission due to Photons

To cause an electron to escape from a metal, it should be given enough energy to overcome the surface potential barrier. The energy can also be supplied in the form of a photon of ultraviolet light of suitable frequency. Electron emission from a metal surface occurs at the critical condition

$$h.\nu \geq \varphi$$

Where **φ** is the work function of the metallic electrode, frequency **(ν)** is given by the relationship

$$\nu = \frac{\varphi}{h}$$

iii) Electron Emission due to Metastable and Neutral Atoms

A metastable atom or molecule is an excited particle whose lifetime is very large (10^{-3} s) compared to the lifetime of an ordinary particle (10^{-8} s)[30]. Electrons can be ejected from the

metal surface by the impact of excited (metastable) atoms, provided that their total energy is sufficient to overcome the work function. This process is most easily observed with metastable atoms, because the lifetime of other excited states is too short for them to reach the cathode and cause electron emission, unless they originate very near to the cathode surface.

iv) Electron Attachment Process

The types of collisions in which electrons may become attached to atoms or molecules to form negative ions are called attachment collision. Electron attachment process depends on the energy of the electron arid the nature of the gas and is a very important process from the engineering point of view. All electrically insulating gases, such as O_2, CO_2, $C1_2$, F_2, $.C_2F_6$, C_3F_8, C_4F_{10}, $CC1_2F_2$, and SF_6 exhibit this property[30]. An electron attachment process can be represented as:

$$\text{Atom} + e^- \longrightarrow \text{negative atomic ion} + (E_a + K)$$

The energy liberated as a result of this process is the kinetic energy K plus the electron affinity E_a. In the attaching or insulating gases, the atoms or molecules have vacancies in their outermost shells and, therefore, have an affinity for electrons. The attachment process plays a very important role in the removal of free electrons from an ionized gas when arc interruption occurs in gas-insulated Switchgear.

2.2.3 Breakdown of vacuum

In principle, a vacuum should have infinite dielectric strength, because there are no charge carriers to carry current. However, in practice, we can have an 'arc' or breakdown in a vacuum.

If we have two metal plates separated by a vacuum, and apply a high enough voltage, you will get current flowing[35]. The charge carriers do not come from the vacuum, like they do

in other dielectrics, but from the metal plates themselves. Initially, the high electric field will pull electrons from one plate and accelerate them to the other plate, which constitutes a current. Then through heating, some positive ions can leave the other plate surface and move the other way. So you can have a current in a vacuum, but generally a high vacuum will have a high breakdown voltage, which does depend strongly on the electrode shape and spacing (pointed electrodes will have a lower breakdown, just as in air). It also depends strongly on the electrode material. Basically, there is a point where reducing the pressure causes the breakdown to be more dependent on the electrode material or temperature etc., than the gas pressure, since now most of the charge carriers come from the electrode material. Also, any imperfections in the vacuum will lower the breakdown[36].

A vacuum is sometimes used as a dielectric in large circuit breakers (which has to interrupt currents of tens of thousands of amperes at thousands of volts). The two arcing contacts are drawn apart quickly in a vacuum. As they separate, some of the material vaporizes and forms an arc though the metal vapour. The heat of the arc and the low pressure of the vacuum cause the metal vapour to be blown away and cooled rapidly so the arc goes out. Once this has happened the contacts are far enough apart so the electric field cannot cause the arc to re-strike between the electrodes. Even through the vacuum this could happen, electrons can be emitted from the hot electrode surface, and are accelerated, they heat the electrode when they strike it and heat and vaporize some of it, so eventually we have a metal vapour arc forming once again in the vacuum.

2.2.4 Liquid dielectric breakdown

Geometrical suitability and self-healing property of liquids makes the liquid dielectrics suitable for use as insulation for energy storage devices, particularly nanosecond pulse generators. Study of pulsed breakdown in liquids[24], has received considerable attention in recent years due to the demands from the pulsed power field for the development of compact

devices e.g. high power transmission lines, switching elements. Although many aspects of liquid breakdown have been studied in the past, the findings and conclusions are not yet clear[24].

In principle, there are varieties of liquids available, which can be used as dielectric in the high voltage environment. However, only few of them are found practically suitable for pulsed power applications[37] for example, deionized water, which is characterized by high dielectric constant and moderate dielectric strength (in comparison to transformer oil). Dielectric breakdown properties of liquids depend on many other parameters like electrode material, temperature, applied pulse duration and polarity, etc.[38] Various studies have been made considering these parameters but the findings and conclusions are not very clear.

In principle, breakdown in liquids are referred as two different thoughts, the first assumes the development of an initial gaseous phase, which then serves as the medium for avalanche development. Consequently, electrical breakdown in liquids is considered a gas discharge'.

In other approach, it has been postulated that the suspended particles are polarizable and are of higher permittivity than the liquid. As a result, they experience an electrical force directed towards the place of maximum stress. With uniform field electrodes, the movement of particles is presumed to be initiated by surface irregularities on the electrodes, which give rise to local field gradients. The accumulation of particles continues and tends to form a bridge across the gap, which leads to initiation of breakdown.

2.2.4.1 Polar liquids

The use of polar liquids as an attractive switching media due to their high dielectric strength and flow properties for the design of small, low inductance, and, therefore, fast high power switches[39] The fact that the liquid can be flowed within the switch volume allows for effective thermal management and easy removal of debris after switch breakdown.

Research on conduction in liquid dielectrics, especially transformer oil, began many years ago because of its high breakdown strength. Others[40] have conducted studies of the effects of age, contamination, and gas content on the overall quality of the oil, affecting the conduction and breakdown mechanisms. Characterizing breakdown of liquids is important for optimizing the use of materials. Identifying the failure modes or critical conditions required for a liquid to fail is necessary to understand how breakdown will develop and successfully model the mechanisms involved in liquid breakdown.

Establishment of a clear and effective model is difficult in part due to various characteristics of liquid dielectrics. Liquids combine some of the best features of both gas and solid dielectric breakdown. The physical nature of liquids, high density, viscosity, quality, thermal and electrical properties etc., compared to gases adds multiple dimensions to problems associated with developing a comprehensive model. Since liquids tend to have higher breakdown strengths and permittivity than most gases they are ideal for compact pulsed power applications where increased energy densities and decreased physical dimensions are very important. In addition, the ability to recover from breakdown events is a useful trait for use as a switching medium.

Several models of liquid breakdown have been proposed over the years[41], each explaining possible mechanisms, usually for specific cases, but do not explain all behavior observed or there are more than one method/mechanism to achieve a similar result. W. G. Chadband focused his research efforts on comparing liquids to amorphous solids for both positive and negative discharges. The goal was to test various liquids with increasing viscosity, approaching a solid dielectric. His studies showed that “under certain conditions electrical breakdowns in viscous liquids and plastics show similarities.” He established a link between solids and liquids by choosing liquids that were physically similar to solids. Many models begin with some form of charge injection at the electrode/liquid interface, where current

injection at an area of high field leads to the formation of a “bubble” or low-density region. Inside the bubble, electron avalanches occur producing current pulses, if they fail to completely cross the gap, multiple pulses eventually lead to final breakdown. Current pulses have been observed in many experiments [17, 18]. In this case, the presence of a low-density region such as a “bubble” is a critical component for the initiation of breakdown.

2.3 Theories of Liquid Breakdown

Liquid breakdown does not consist of a single comprehensive theory for breakdown that is unanimously accepted for describing dielectric liquid breakdown phenomena. There are several reasons for lack of a single theory. The complex nature of liquids makes the theoretical analysis more difficult than with gases. Liquid quality is a critical issue. It is very difficult to create a pure liquid compared to a pure gas. It is generally accepted that liquid purity plays a very important role in the development of final breakdown [41][42].

Pure liquids:

Pure liquids are those, which are chemically pure, do not contain any impurity. In case of pure liquids, at very low field, the current is due to the self-dissociation of ions. At moderate fields, this current reaches saturation, whereas at very high fields, the current generated because of the field aided electron emission from the cathode and further multiplication in the liquids as given by Townsend mechanism. This current multiplication also occurs from the electrons generated by the interface of liquid and impurities.

Commercial liquids

Commercially available liquids are not chemically pure and have impurities like gas bubbles, suspended particles. These impurities may be having different permittivity values due to which the variation in electric field causes the breakdown in the commercial liquids. Due to

the breakdown, an additional gases and gas bubbles will generate and solid components will form.

The predominant theories of liquid breakdown are the bubble theory, suspended particle and electronic theories.

2.3.1 Bubble theory

The bubble theory is based on the gas pockets present on the electrode surface of the liquids.

In general, it requires the formation of a bubble near the electrode tip. Once the bubble present it will lead to trigger the avalanche, either by injecting the more charges into the low-density region (vapor). Due to the difference in permittivity of bubble and liquid, the field enhancement creates at low-density regions. The bubble formation may occur due to the local heating, electrical stress or cavitation.

The primary mechanism discussed is localized energy injection [7-12]. Partial discharges inject “hot” electrons into the liquid and cause local heating and vaporization. Hot electrons are electrons with energy in excess of the thermal energy. The vaporization phase change consumes most of the energy of the pulse.

2.3.2 Suspended particle mechanism

The impurities in the liquids may present in the form of fibers or dispersed solid particles. However, the permittivity of this particle (ε_2) will be different form the permittivity of the liquid (ε_1). If it is considered that particle as spherical of radius r, the particle experiences the force F as give n by [43]

$$F = \frac{1}{2r^3}\frac{\varepsilon_2 - \varepsilon_1}{2\varepsilon_1 + \varepsilon_2}\, grad\, E^2 \tag{2.3}$$

This force is directed towards the areas of maximum stress.

If the voltage applied is continuous (d.c.) or the duration of the voltage is long (a.c.) then this force drives the particles towards the areas of maximum stress. If the number of particles present are large, they becomes aligned the inter electrode gap causing a breakdown between the electrodes.

However, if it is only a single particle then it will give rise to local field enhancement depending on the shape.

2.3.3 Electronic Breakdown Theory:

In general, it is unlikely for electrons injected into the liquid to produce significant ionization[44] in the liquid state to develop an amplification process. Cathode initiation assumes that electrons are injected into the liquid as a column of electrons emitted from a micro-protrusion on the cathode. The electrons will collide with molecules locally heating the liquid through collisional impacts. The heating of the liquid reduces the density allowing future electrons to obtain more energy from the field before colliding with another molecule. The impacts that ionize a molecule will leave two slow electrons to drift in the field. The buildup of low energy electrons at the front of the streamer "marks the onset of spherical expansion under the columbic forces of the consequent cloud of negative charge".

The streamer will[45][46] expand and appear thick and bushy as it propagates across the gap. The lower the density of the region the faster electron amplification will occur. The obvious extreme of this process is the formation of an avalanche within a bubble. Anode initiation[47] of breakdown requires a rapid charge development mechanism[48]. Assuming that holes emitted from the anode via resonance tunneling, or tunneling from molecule to molecule[49], requires that the intermolecular distance be as small as possible to achieve high probabilities for tunneling. For this, high-density regions are required to maintain minimal intermolecular spacing.

Tunneling establishes a hole propagation[50] pathway through the liquid. These pathways will trace the path of a hole through the liquid to the electrode, and should appear as thin filamentary structures in the liquid. The path left by the propagation of the hole through the liquid will be an ideal return path for an electron to propagate in the opposite direction. The electrons prefer the lower density region created by the passing of a hole through the liquid. Energy transfer via collisions that heat the fluid will be detrimental to hole propagation since the density of the liquid will be reduced, reducing the tunneling probabilities.

Conventionally, gases, liquids and solids serve as a dielectric medium for energy storage devices[51] in pulsed power system components, such as capacitors, transmission lines and in high voltage switch medium. The properties of these components depend on the electric breakdown strength (E_b) and dielectric constant of material used. The ability to conform to complex geometries while maintaining the self-healing/recovery capabilities typical of gas systems make liquids suitable for use as insulation for energy storage devices, particularly for nanosecond pulse generators.

Study of pulsed breakdown in liquids, has received considerable attention in recent years due to the demands from the pulsed power field for the development of compact devices e.g. high power transmission lines, switching elements[24]. Despite extensive research and theoretical studies, the understandings of electrical breakdown properties of liquids (like water) are far from complete. Therefore, considering the advantage of suitability of liquid dielectrics for high voltage pulsed power applications, in this work, an attempt has been made to understand the liquid dielectric breakdown properties for the development of compact and efficient intermediate storage devices. Earlier many researchers have studied the liquid dielectric breakdown properties towards the efficient energy storage devices. Few of their works are discussed as follows.

J.Pace Vandevender et al.[52] have realized the development of relatively simple, ultra-low impedance, short pulse, relativistic electron beam generators by using synchronous untriggered multichannel switching in water. Their experiments resulted in the delivery of a 1.5 MV, 0.75 MA, and 15 ns pulse into a 2 Ω line with a current rise time of 2 x 10^{14} A/sec. Their results shows, when the knife-edge electrode is negatively charged, the breakdown fields for 1 MV<V<3 MV are adequately described by the empirical relation based on data for V<1 MV for short charging time. When the knife electrode is charged positively, the corresponding relation overestimates the breakdown voltage by as much as 100 percent. They presented alternate empirical relations. Their results further indicate a better switching performance is obtained with a knife edge electrode charged negatively and they have shown the achievement of current rise times excess of 2 x 10^{14} A/Sec are achieved. R.P.Joshi et al.[53] have developed a time dependent model containing several new features for treating the breakdown of water under nanosecond pulsed conditions. The simulations show a breakdown within about 200 ns for and applied pulse of 20 kV for a 200 μm water filled switch. The simulation results and temperature profile evidenced that the bubble formation and thermal heating no longer apply for nanosecond breakdown conditions. Instead, the mechanism of breakdown is directed by the electric field behavior and subsequent injection of electrons at the interface. They have further concluded that the interface layer and the condition of the electrodes will begin to be far more important than the bulk liquid properties in determining breakdown and hold-off voltages. Dingjiu et al.[54] describe the breakdown studies on dielectrics of demineralized water (1 to 5 MΩ) and transformer oil(> 60 kV/cm for DC) for various electrode shapes like cone-cone, cone-plane and various spacing for 1/40 μs and 10-150 ns pulse duration having shapes of [1-cos(ωt)] and near rectangular pulse shapes obtained by cable discharge. The breakdown time for demineralized water can be changed from 55 ns to 155 ns under controlled conditions. In their experiments, they have

found the resistivity of demineralized water has no clear effect on breakdown voltage in 1 to 5 MΩ range, but lower resistivity leads to higher conduction currents. They have established relationship between breakdown strength and spacing for cone- cone and cone-plane electrodes. The polarity effect of breakdown strength in case of water is also established. Yamada et al.[55] have studied the positive streamer propagation, pre breakdown current and breakdown time lag in cyclohexane with point to plane electrode configuration under micro second rectangular voltage pulse (20 to 50 kV amplitude, 20 ns rise time and 4 μs pulse duration). They have performed experiments using an image converter camera and a photo optical current measuring technique. They have concluded that the positive streamer in cyclohexane has three propagation velocities viz. sub sonic, sonic and supersonic. The presented plots of time delay to total breakdown indicates the propagation velocities of 0.18 km/s and 1.3 km/s, whereas for 4 mm gap spacing show that the propagation velocity of positive streamer is 1.3 km/s and 2.8 km/s. The constancy of streamer propagation in cyclohexane would suggest that wave like propagation mechanism originating from the structures if liquid is responsible for the streamer development. Further, they have reported that the constancy of streamer propagation and the discrete change in the propagation velocity seems to indicate a wave like propagation in the liquid. Christophorou et al.[56] have provided the concept for a dielectric liquid as a medium in fast-pulsed power switches by employing flash lamps as a source for ionization of dielectric medium at room temperature. The photo injection of excess electrons makes a good dielectric liquid to a good conductor. The measurements of drift velocity, with reference to maximum electric field along with in tetramethylsilane (TMS), tetramethylin (TMT), tetramethylpentane (TMP) and neopentane (TMC) are provided. Further, they have discussed the method of reduction of work function to create excess electrons at low photon energy for fast switching applications. Auckland et al.[57] have investigated for agglomerative effects in liquids similar like solids under point to

plane and plane to plane electric field for the inter electrode gap of 5 mm. the majority of experiments were performed with 50 Hz alternating test voltage. They have devised the test arrangement to create optimum conditions in terms of water tree growth. The experiments investigated the effect of electrolytic ion content, the effect of viscosity (1000, 30000, 60000 cSt of fluids) to detect any possible correlation in liquids between tree development and mechanical characteristics similar like solid dielectrics. They have concluded that water can migrate through the silicon fluid and accumulate in a tree like form at points of high electric stress, under an applied alternating voltage. The alkali metal ions with large hydration factor are responsible for carrying the water molecules across the interface and into the silicon fluid under the applied electric field and found the relation that the tree growth decreases with decrease in hydration factor. They have showed under the asymmetric field ions which have larger hydration factor will form water tree structures more readily and of a greater size. Under direct voltage of either polarity was applied under uniform field conditions convections was observed but not tree growth and reported that this convection involves both dielectrophoresis and electrophoresis. The experimental conclude that the liquid insulation exhibits an ability to create regions of excessive water concentration when stressed asymmetrically and in the presence of aqueous solutions, which may enhance the deleterious effects accompanying the presence of water in transformer oil. T.J. Lewis et al[58], have experimentally studied the electrical breakdown in organic liquids. The experiments are performed on pure hydrocarbon liquids using direct voltage. Their results of experiments with n-hexane show that the breakdown is practically independent of both electrode material and external radiation in uniform fields but that is dependent on the cathode gradient when the field is non-uniform. Komin et al[59]. have investigated pre breakdown process in deionized water (ρ 18 MΩ cm) by Mach-Zehnder interferometry technique. They have performed experiments with two kinds of pulses. The first sequence of monopolar pulses and

pauses with t=800 ns, used to observe relaxation of medium after high voltage action, the second the pulse with t=10 ms that create a step rising of direct voltage on the test cell. They have analyzed the interferograms and their interpretation established following features. At some instant emission of electrons from cathode, take place, as a result, a negative space charge forms near the cathode. They have estimated the density by interferogram as 10^{11} l/cm^3 and electric intensity as 1000 kV/mm. They have reported that the moving of space charge by strong electric field leads to appearance of zones intensive perturbations developing towards the anode with sonic speed. These zones could be vapor- gas hollows may arrive due to result of shock boiling of water by moving the space charge through it. When these zones arrive at cathode region, an ionization of one of them takes place and a discharge channel begins to form from anode. Ekram Husain et al[60]. have investigated the effect of electrode shape, material and chemical structure on electric strength of liquid hydrocarbons. The experiments are carried out with power frequency (50 Hz) on n-pentane, n-hexane, benzene, toluene, xylene, 2, 2, 4 Trimethyl pentane which include straight (n-hexane), ring (benzene) and branched chain hydrocarbons. The electrode materials used are brass, copper, brass and aluminum. The shape of electrodes used are point to point, point to plane, point to sphere, sphere to sphere, sphere to plane and plane to plane. Their findings includes for chemical structure showed breakdown voltage increases with increasing molecular weight irrespective of chain length. Breakdown voltage of straight chain liquid shows increasing nonlinearity with increasing gap setting. On the contrary no nonlinearity with is observed with increasing gap setting for branched chain liquid. Benzene yields higher breakdown voltage compared to n- hexane for all electrode material whereas sphere to plane arrangement gives maximum breakdown voltage whereas the point-to-point arrangements yields minimum breakdown voltage of all combinations. I.M. Garilov et al[61]. have studied the pre breakdown events such as effect of heating and EHD in non-uniform field (point to

plane and knife to plane) in water. They have observed the ramified dendrites propagating with subsonic velocities and thin supersonic plasmic channels. Further, they have concluded that in deionized water heating has no influence on initiation and development of discharge channels. The EHD events, at the discharge time 10^{-4} to 10^{-3} s affect the development of slow dendrite without changing the discharge dynamics. E.O.Forster et al[62] have experimentally studied the effect of electrode gap on breakdown in liquid dielectrics. The experiments are performed on polyethers, hydrocarbon oils, perfluorinated polyehters. They have discussed that, in general, under non-uniform field dc conditions (point to plane) with gaps of 5 mm of larger, one find that typical transformer oils have higher breakdown voltages when the point is negative that when is positive. However, perfluorinated polyethers have found to produce opposite results when using average gap sizes of 5 to 10 mm. to elucidate the findings they have studied the effect of gap size on breakdown voltage. Their findings shows for polyethers at larger gaps the sequence is reversed. Their observations are explained in terms of streamer development in the particular liquids and relative stability of their negative ions. In their work, they presented the breakdown voltage (needle positive and negative voltage) vs gap for perfluoro polyether, transformer oil, silicon oil and perfluoro hydrocarbon are presented. In the case of two perfluoro polyethers the two lines representing the gap dependence of the breakdown voltage for positive and negative polarities are intersect. For gaps $\leq$ 1.25 cm, the breakdown voltages are higher when the needle is anode than when it is a cathode. Above the gap the reverse is true. For silicon fluid, the transformer oil and fluorinert FC 77, the breakdown voltage is always higher for all gaps tested when the needle is a cathode than when it is an anode. H. M.Jones et al.[63] have investigated the influence of hydrostatic pressure (atmospheric to 40MPa) and liquid conductivity on the pulsed breakdown of water. They have carried out experiments on de-ionized water (non-distilled, distilled and ultrasonically treated), sodium chloride solutions or magnesium sulfate solutions using 80

kV, 3 ns rise time, 100 ns duration pulse with 0.4 to 2.1 mm inter electrode gap. The findings include the time lag increases with increase in pressure, this suggesting a bubble mechanism is a factor for discharge in water. They have assessed the formation of bubble by considering the contributions of the ionic and electronic pre breakdown currents to the bubble formation time. They have found that the bulk and local heating by ionic pre breakdown currents contribute little to the initiation of the breakdown process. Further suggested that the field emission currents from asperities which can provide the necessary heating and free electrons for avalanches to develop in a bubble emerges as the most probable agent contributing to bubble nucleation. As a consequence of electron avalanche growth in the bubble, an ionizing front develops which subsequently bridges the gap. In particular they have concluded that the breakdown evolves via bubble formation by field emitted currents near asperities on the cathode, and that the time for the change in liquid conductivity as a result of breakdown is limited by process other than ionization growth(due to electron impact ionization of molecules in the bubble) of pre breakdown electron currents. T.J.Lewis [64] have reviewed the basic process of electrical conduction in liquids especially the similarities between conductive electrolytic polar liquids and insulating non-polar ones. In this, the role of the reorganization energy in determining electronic states is emphasized. Further, the electrode conditions, particularly the electrode double layer are explained for the process of control conduction and for electro hydrodynamic effects. T.J. Lewis et al.[65] discussed a new model for electrical ageing and breakdown in dielectrics. They have come up with a simple but generally, applicable model for multi factor ageing in which thermally induced bond scission is a universal underlying physical process, which determines ageing. They have found the final destruction of the dielectric is assumed to occur by a Griffith crack treeing process and this will have a formative time, which is a part of the overall ageing time, whether it will be a significant part will depend on critical time to reach critical concentration and therefore on

the electric field. Martin Marci et al.[66] have attempted to verify the breakdown characteristics of insulating oils in the process of developing new and environment friendly alternative oils (organic oils). In this process, they have performed experiments and compared the results of electric breakdown strength of mineral oils (aged and new), silicone oil and vegetable oils for the inter electrode gaps of 0.6 mm to 3 mm with 0.3 mm incremental steps. They have summarized the experimental results as that the mineral oils are well considered to be the best choice. Further, they have experimentally showed that the Vegetable oils can compete with the mineral oils in addition to satisfy breakdown strength values, with oil stability even for repeated discharge activity. J.F,Kolb et al.[67] have discussed the nanosecond optical diagnostics for liquid dielectric breakdown study. For this, utilization of optical methods such as interferometry, schlieren photography and shadowgraphy for liquid dielectric breakdown study have been discussed. Kwan C Kao et al.[68] have proposed a new theoretical model for high filed electric conduction and breakdown in dielectric liquids based on theory of filamentary single injection. A.M. Sletten et al.[69] have extensively studied the characteristics of the trigatron spark gap for utilization as high voltage controlled switching purpose. Their observations show that the voltage range over which it may be triggered satisfactorily depends not only on the polarities of the main gap and triggering voltages, but also in the energy of the discharge. The breakdown time lag is also determined by these same voltage polarities and by the time constant of the trigger discharge circuit. From the above characteristics and based on other relative observations, a theory of breakdown process is discussed involving the propagation from the trigger of a low-density easily ionized region. After characterizing the spark gap thoroughly, they have concluded that in their results most efficient overall operation is obtained when the main gap has negative voltage V and a negative trigger pulse is used, the trigger discharge energy being the maximum that can be conventionally obtained.

In general, it is accepted that, liquid purity plays a very important role in the development of final breakdown [132]. Since the start of the liquid dielectric breakdown properties study, there have been essentially two [42] different viewpoints on the phenomenon of electrical discharge in the liquids. According to one of them, discharge in gas which occur in gas bubbles that either are initially present in the liquid and on the electrodes or are formed under the action of voltage (electrolysis, boiling, degassing of the electrode surface, etc.). The second one, as a consequence of the avalanche multiplication of free charge carriers in the liquid itself and use a model which is in fact a version of gas discharge as applied to the liquid phase.

Most of the theories [133] suggest that, in strong fields, electrons may be accelerated in liquid and ionize molecules in atoms. Gennady et al. [29] reported that during a long-term application of voltage, four processes occur in the electric discharges in liquid: formation of filaments from weighed particles, the motion of the liquid, the formation and motion of gas bubbles, and finally a spark discharge. theories [8] suggest that, the breakdown in liquids as electron avalanche ionization and streamer mechanisms as like in gases[47][134]. According to them, the first possible assumption was development of gas phase first which then serves as the medium for avalanche development. Streamers are likely to be initiated by photons emitted from the primary avalanche tip in the high-field region in front of the primary avalanche.

Peek et al. [135] are suggested an alternate possibility that, a gaseous phase is not required and impact ionization in the liquid itself will result in a charge carrier multiplication, which is responsible for breakdown. The conflict between bubble theory and the direct impact ionization model is not cleared until days. The bubble theory is based on a combination of gaseous and liquid components for breakdown. In general, it requires the formation of a bubble near the electrode tip then after a bubble is present, an electron avalanche or

amplification process begins. The avalanche is triggered either by the injection of more charges into the vapor phase or by field ionization occurring in the bubble due to the field enhancement caused by a region of lower permittivity. Several of the methods of bubble formation such as local heating, cavitation, or electrical stress may occur simultaneously to one degree or another in liquids.

Lewis [49] discusses a review of electronic breakdown theory. He discusses the conditions necessary for cathode and anode initiated processes. In general, it is unlikely for electrons injected into the liquid to produce significant ionization in the liquid state to develop an amplification process. Cathode initiation assumes that electrons are injected into the liquid as a column of electrons emitted from a micro-protrusion on the cathode. The electrons will collide with molecules locally heating the liquid through collisional impacts. The heating of the liquid reduces the density allowing future electrons to obtain more energy from the field before colliding with another molecule. The impacts that ionize a molecule will leave two slow electrons to drift in the field. The buildup of low energy electrons at the front of the streamer marks the onset of spherical expansion under the columbic forces of the consequent cloud of negative charge. The streamer will expand and appear thick and bushy as it propagates across the gap. The lower the density of the region the faster electron amplification will occur. The obvious extreme of this process is the formation of an avalanche within a bubble.

Anode initiation of breakdown requires a rapid charge development mechanism [11-12], which suggests the breakdown is due to holes emitted from the anode via resonance tunneling, or tunneling from molecule to molecule and it requires that the intermolecular distance to be as small as possible to achieve high probabilities for tunneling. High-density regions are required to maintain minimal intermolecular spacing. Tunneling establishes due to a hole propagation pathway through the liquid. These pathways will trace the path of a

hole through the liquid to the electrode, and should appear as thin filamentary structures in the liquid. The path left by the propagation of the hole through the liquid will be an ideal return path for a complementary electron to propagate in the opposite direction.

2.4 Summary

The literature review of liquid dielectric breakdown properties for development of compact pulsed power is discussed. The importance of dielectrics in the development of compact pulsed power is explored. Different types of conventional dielectrics used for intermediate storage and their advantages and limitations are reviewed. Types of breakdown theories of solids and gases are briefed. Breakdown theories of dielectric liquids are discussed. The understanding of breakdown characteristic of dielectrics may lead to the efficient energy storage devices by considering the geometry.

Chapter 3
Summary of literature and Aim of the thesis

3 Summary of literature

As discussed in chapter 1, increasing the power and energy capacity of the Pulse forming lines or intermediate energy storage by considering the compactness of the systems is an endless scientific requirement. The operating efficiency of these pulse-forming lines [2][29] depends on the electrical and chemical properties of the dielectric material. In order to optimize maximum efficiency and geometry the dielectric material should have high dielectric constant (ε_r) and good electrical breakdown strength (E_b)[73]. The understanding of breakdown properties associated with dielectric medium may help in improving the geometry and breakdown concerns and hence improve the efficiency of existing charge holding devices.

The advantage of reparability and self-healing properties of liquids and gases makes them suitable for pulsed power applications compared to solids (once breakdown occurs it is not reparable, one has to replace with new one).

The efficacy of two characteristic features *viz.* ε_r & E_{br} of liquids make it more suitable for the energy storage in comparison to the compressed gases. In addition, the freedom of circulation of liquid dielectrics[71] makes it preferable over its solid counterparts concerning its applications involving complex geometries, thermal management and debris removal processing[72].

Understanding the breakdown properties of dielectrics, leads to improve the breakdown strength and ultimately it pave the way to achieving the compactness of charge holding devices. As discussed in the chapter 2, many works have been devoted to understand the breakdown characteristics of liquids specially water (due to its satisfactory dielectric properties), but still there is no comprehensive theory[30] for breakdown that is unanimously accepted for describing the liquid dielectric breakdown phenomena. This may due to the peripheral conditions under which the experiments performed are different. There are also several other reasons for lack of a single theory viz. the complex nature of liquids makes the theoretical analysis more difficult than with gases and liquid quality is another critical issue. It is very difficult to create pure liquid compared to pure gas[129][130][131][45].

The understanding of breakdown properties associated with dielectric medium may help in improving the geometry and breakdown concerns and certainly may improve the efficiency of existing charge holding devices. Numerous experimental studies have been performed to understand the breakdown characteristics of liquid dielectrics (specifically water) but there is no comprehensive theory of breakdown in liquids [29] is available in literature.

The compact pulsed power may be achieved by two ways. First one is to find the medium having good dielectric properties and use it to develop a compact system[25]. Alternatively, the second option is to understand the breakdown properties of available dielectric materials and utilize the knowledge to avoid the breakdown for large extent. These techniques may be of help in achieving compact systems.

In this present work, the characteristic features of breakdown phenomenon have been analyzed and the possible approaches to improve the compactness of the storage system designing are discussed.

- In principle, there are varieties of liquids available, which can be used as dielectric in the high voltage environment. However, only few of them are found practically suitable for pulsed power applications [70]. For example, deionized water, which is characterized by high dielectric constant and moderate dielectric strength (in comparison to transformer oil). Its breakdown properties has been extensively been explored in microsecond regime while a little attention is paid in literature to short time (nanosecond) scale.
- The analysis of breakdown in nano-scale regime may be of significance[22] as it may aid in understanding the inherent close packed features of water dielectrics. In addition to this, further understanding of the breakdown process in deionized water will lead to improvement in its breakdown strength.
- Dielectric breakdown properties depend on many other parameters like electrode material, temperature, applied pulse duration and polarity[73], etc. Various studies have been made considering these parameters but the findings and conclusions are not very clear. To gain further knowledge of breakdown properties the experiments have been performed in nanosecond regime and the effect of electrode material, applied voltage polarity and distance between the electrodes are analyzed. Further, the effect of electrode material on deionized water breakdown properties can also be visualized via emission spectra during discharge.
- The compactness of the storage system can also be achieved by using alternative dielectric material with better dielectric properties than that of conventional dielectrics.
- The breakdown properties may also be influenced by modification in its chemical properties due to discharge; this feature can be analyzed by using Fourier Transform Infrared absorption spectroscopy. Analyzing the chemical behavior of dielectric

medium due to discharge is other way, which leads to further understand the breakdown characteristic of medium. This can possible with Fourier Transform Infrared absorption spectroscopy.

- Understanding the physical processes of initiating the pulsed breakdown of liquids and the basic laws of formation and propagation of discharges in liquid for nanosecond regime may further help in improving the system geometry. This can be realized by using fast optical ICCD camera.

3.1 Outline of the thesis:

Chapter 1 introduces the concept of pulsed power and general scheme of pulsed power. In addition, this chapter provides details of pulsed power applications such as industrial, medical and military applications.

Chapter 2 includes the literature update on compact pulsed power technology and discusses the issues related to development of compact pulsed power system at dielectric and insulation level. It analyzes the intermediate energy storage devices and its importance in development of compact pulsed power. It also includes various dielectrics used for development of portable systems. This also covers the basic theories suggesting the breakdown behavior in liquids.

Chapter 4 gives the details of the suitable experimental set up developed for the present studies. Design and development of individual components and their experimental verification are discussed. Validation of Pulse generator performance with PSPICE (student version) simulation software and their results are discussed.

Chapter 5 describes the various electrical diagnostics, which have been used for present study. Measurement of high voltages short pulses in non-intrusive way is one of the challenging tasks in pulsed power. Insulation and geometrical restrictions in high voltage

systems makes it difficult to access the high voltage points. In present work, a current sensor and two voltage sensors are used. One is used to monitor the source voltage (V_1) i.e. across Pulse forming Line, and other is to measure the voltage (V_2) across the test chamber electrodes. Working principle, theory, operating modes, design and calibration of electrical diagnostics with standard diagnostics are discussed. Further, the verification of calculated diagnostic parameters with PSPICE student version (9.1) simulation software is presented. Further, in this chapter utilization of optical diagnostics for further understanding of experimental results are discussed.

Chapter 6: this chapter presents experimental study of electrical breakdown properties of pure water ($\varepsilon_r \sim 78$) under nanosecond scales and uniform field conditions are discussed. The experimental procedure, effect of parameters viz., electrode material, applied voltage polarity and distance between the electrodes are presented. Also discusses observations made by using emission spectra diagnostic for analyzing the experimental results.

Chapter 7: This chapter includes motivation behind the study of electrical breakdown proerpties of D_2O and experimental procedure are discussed. It also includes the heavy water (D_2O) breakdown properties under nanosecond time scales and the results which are further compared with the water (H_2O) breakdown properties and their observations. It also includes effect of paramters like applied voltage polarity, electrode material on breakdown proerpties of D_2O. Further utilization of conductivity measurements, FTIR spectroscopy details in understanding the chemical changes in liquids due to discharge is reported.

Chapter 8: presents the understanding of the physical processes initiating the pulsed breakdown of water in nanosecond time scales under uniform electric fields by using high speed fast optical photo recording are reported. The basic laws of formation and propagation of discharges in liquid are presented.

The triggering method at low jitter is reported. The optical images of breakdown initiation from anode, formation of streamers, branches, sub-branches and multiple discharge initiation from electrode surface are studied.

Chapter 9: provides the conclusion of the work carried out and findings in the present work. This chapter also summarizes the future work

Chapter 4
Experimental setup

4 Introduction

The objective of development of present experimental setup is to study the electrical breakdown properties of the liquids in tens of nanosecond time scale applied voltage with inter electrode distances in millimeter. To meet this requirement a suitable voltage source capable of delivering voltages of few 100 kV is required. Conventionally there are many pulse voltage sources[72][33] are available and each of these have its own advantages and disadvantages. Few of those are capacitive energy storage, inductive energy storage and line-type pulse generators (e.g., transmission line pulse generator, pulse-forming networks).

In a practical system, the capacitor will typically be discharged into the load by means of closing switch, which is often a spark gap. The two major technical complexities encounter in inductive energy storage system[76] viz., one is charging circuit (it required very fast charging of the inductor) and other is opening switch (difficulty in its inbuilt complexities at the currents and voltage involved). However, simplest schemes like capacitive or inductive energy discharge circuits cannot be used in case where very high voltage (few 100 kV), due to lack of availability of commercial capacitors of such ratings. In that case, voltage multiplication is applicable like Marx, Tesla etc.

4.1 Conventional pulse generators

4.1.1 Marx generator

Marx is analogous to the capacitor bank, it also employ capacitors in parallel to store the energy. The main difference is that, when it discharges all the capacitors are momentarily converted into a configuration of series connection. Originally described by E. Marx in 1924[31]. If there is N stages, in principle the output voltage should be N time the original voltage. Therefore, the amount of output voltage depends on the number of stages. In this, as the required voltage amount increases, number of capacitors and switches required also increases. Therefore, the Marx generator not only can serve as energy storage but also can be used as a voltage multiplier. Proper working of Marx generator required regular maintenance of all these switches.

4.1.2 Tesla transformer/ Pulse transformers/Resonant transformer

The other method of generating high voltage pulse is by using Tesla (air core) transformers. These are very compact and simple systems, which can give voltage as high as million volts. However, this type of transformers can produce higher voltages but cannot be used directly for generating nanosecond pulses; even low. It required additional pulse forming lines to compress the micro second pulse to nanosecond pulse (which is our requirement).

Using a Tesla transformer instead of a Marx generator for a pulse charging application can offer a number of significant benefits, which in principle derived from two features:

1) Multiple numbers of primary storage capacitors are not required to operate at ultra-high output voltage
2) The complicated switching and dc charging components of the Marx circuit are not required.

The primary capacitor bank and transformer need not to be housed in a large tank of insulating oil and the resulting system is compact, requires substantially less floor space, and

may more readily accommodated in a laboratory. In addition, with fewer components, the possibility of failure and maintenance can be minimized. Finally, these simplifications yield a system that costs appreciably less than its Marx counterpart to both build costs and operate does.

Hence, considering the above advantages over the Marx, in this work the pulse transformer based high voltage generating method is adapted. In this, the pulse transformer technology is fulfilled by adopting the Tesla coil or transformer principles.

4.2 Experimental setup:

Present experimental work requires few 100 kV and tens of nanosecond (ns) pulse for studying the liquid dielectric breakdown properties. Considering the above advantages of Tesla transformer over the Marx, in this work Tesla transformer with pulse forming line (PFL) pulse generator is developed.

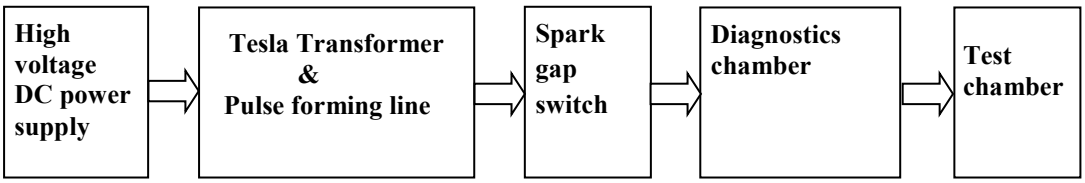

Figure 4.1 Main components of pulse generator

Present experimental setup consists of five sections as shown in Figure 4.1. The high voltage DC power supply to charge the capacitor, Tesla transformer to step up the voltage, pulse forming line (PFL) to shape the pulse, high voltage spark gap switch to discharge the stored pulse forming line voltage to the load, diagnostic chamber to incorporate the voltage and current sensors for measuring the applied voltage and current profiles and finally the test chamber. The test chamber consist a pair of uniform electric field electrodes separated by a distance in several millimeter and will be filled with liquid dielectric about to test.

4.2.1 High voltage DC power supply

Primary energy source is provided with high voltage (0-35 kV) DC power supply developed in our laboratory.

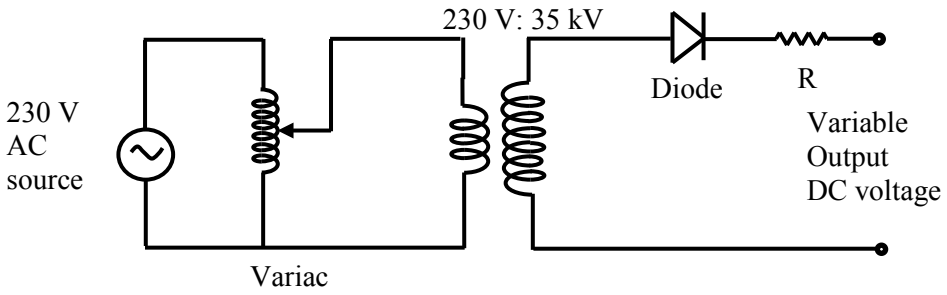

Figure 4.2 High voltage DC power supply electrical equivalent circuit

The electrical equivalent circuit of DC power supply shown in Figure 4.2. It is a single-phase half bridge rectifier circuit, used to charge the capacitor (C_1). The DC power supply includes the components viz. motorized variac transformer, Step up transformer (ratings 230 to 35 kV, 150 mA), High voltage diode (100 kV), and charging resistor (R), 50 kΩ.

4.2.2 Tesla transformer

4.2.2.1 History

Tesla transformer named after the inventor Nikola Tesla, the son of a Serbian Orthodox clergyman. He was born on 9 July 1856 in Croatia. [77]. Tesla paid his attention to investigation of the high frequency, high-voltage phenomena using what soon became known as the "Tesla coil," a resonant air-core transformer with a large turn's ratio between the primary and secondary windings. Tesla's pioneering works in the areas of electrical and mechanical engineering served to establish a number of prototype models those are available to be recreated and improved upon today. The Tesla coil is just one example.

4.2.2.2 Tesla coil

Tesla coil/transformer[78] is an electrical device capable of developing high potentials typically ranging from few hundred of kilovolt (kV) up to several megavolts (MV). The voltage produced is AC, being the frequency typically from hertz (HZ) to several megahertz

(MHZ). In its simple configuration, two air-cored coils, named primary and secondary coils, compose a Tesla Coil (TC). The output voltage of a TC is related to primary and secondary inductance ratio. A Tesla transformer differs significantly from a "normal" or conventional transformer and it may be termed as resonant transformer. Equivalent circuit of resonance transformer is shown in Figure 4.3. In this, the oscillating system is excited with a surge by the discharge of previously charged capacitor, into the primary circuit. Due to mutual coupling between primary and secondary circuits, voltage develops in the secondary. With the help of resonance transformers, voltage of the order of magnitude 10^6 V can be generated without difficulty, if the individual elements of the circuit are appropriately designed.

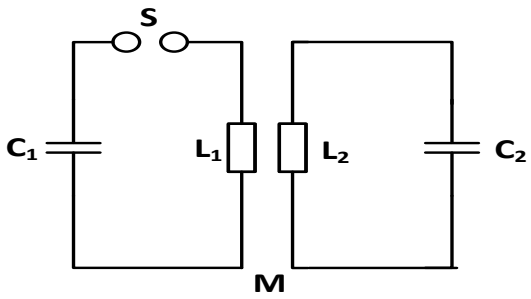

Figure 4.3 Resonant transformer

4.2.2.3 Working principle

The typical Tesla transformer is composed of two circuits. The primary circuit comprises a high-voltage capacitor that discharged through a switching device such as a spark gap, into a low inductance primary winding. The secondary winding simply features an air-wound coil with one side grounded, which forms a combination of inductance and its own stray capacitance. If the two coils are magnetically coupled, every discharge of the primary capacitor generates a magnified voltage in the secondary coil[77].

The working point of a Tesla transformer is influenced by the value of the capacitance (C) and inductance (L) of the primary and secondary windings, together with the coupling between them. Attempting to maximize the efficiency is not a trivial task, as these various

parameters all have a nonlinear effect on the transformer tuning and its magnification[79][80].

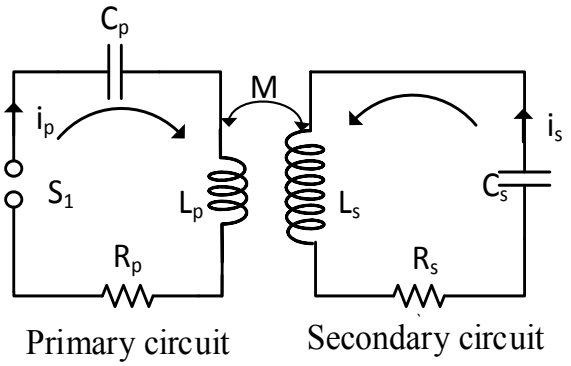

Figure 4.4 Primary and secondary circuit of a Tesla transformer

Figure 4.4 shows primary and secondary circuit of a Tesla transformer, with the resonant *LC* circuits (L_PC_P and L_sC_s) coupled through their mutual inductance *M*. Losses are represented by the resistances R_P in the primary and R_s in the secondary. The open circuit resonant frequencies of the two circuits are chosen to be equal for complete energy transfer from the primary circuit to the secondary circuit[81]. The primary capacitor C_P is initially charged, and discharge through the spark gap(*S*). Capacitor discharges the stored charge in to the inductor, oscillates forth and back in between L_P and C_P, and resonates. Due to mutual inductance (M) between primary and secondary, incremental voltage will appear at secondary inductance, which forms resonance circuit with secondary capacitance. The operation and working conditions of the transformer is described by solving the following equations.

For the primary circuit

$$R_P i_P + \frac{1}{C_P}\int i_P dt + L_P \frac{di_P}{dt} + M\frac{di_s}{dt} = 0 \tag{4.1}$$

And for the secondary circuit

$$R_s i_s + \frac{1}{C_s}\int i_s dt + L_s \frac{di_s}{dt} + M\frac{di_P}{dt} = 0 \tag{4.2}$$

If q_p and q_s, are the instantaneous charges on the capacitors C_p and C_s, then

$$i_i = \frac{dq_i}{dt} \qquad i = p, s \tag{4.3}$$

equations (4.1) and (4.2) may be rewritten as

$$R_P \frac{dq_p}{dt} + \frac{1}{C_P} q_P + L_P \frac{d^2 q_P}{dt^2} + M \frac{d^2 q_s}{dt^2} = 0 \tag{4.4}$$

$$R_P \frac{dq_p}{dt} + \frac{1}{C_P} q_P + L_P \frac{d^2 q_P}{dt^2} + M \frac{d^2 q_s}{dt^2} = 0 \tag{4.5}$$

Introducing the differential operator $D\left(=\frac{d}{dt}\right)$ and combining equation (4.4) and (4.5) [82][83] gives auxiliary equation.

$$\begin{aligned}(1-k^2)D^4 + \left(\frac{R_s}{L_s} + \frac{R_P}{L_P}\right)D^3 + \left(\omega_s^2 + \omega_P^2 + \frac{R_P}{L_P}\frac{R_s}{L_s}\right)D^2 \\ + \left(\frac{R_P}{L_P}\omega_s^2 + \frac{R_s}{L_s}\omega_P^2\right)D + \omega_P^2\omega_s^2 = 0\end{aligned} \tag{4.6}$$

Where $k = \frac{M}{\sqrt{L_P L_s}}$

$$\text{and } \omega_P = \frac{1}{\sqrt{L_P C_P}} \quad \text{and } \omega_s = \frac{1}{\sqrt{L_s C_s}} \tag{4.7}$$

Equation (4.6) has four complex roots E_i and its solution can be written in terms of the charge on the capacitors as shown in reference[83]

$$q_s = \sum_i A_i \exp(E_i t) \tag{4.8}$$

and

$$q_P = \sum_i B_i \exp(E_i t) \tag{4.9}$$

Where $\boldsymbol{A}_i$ and $\boldsymbol{B}_i$ are constants (and i=1...4), which can be evaluated by using the boundary conditions at

$$t = 0 \text{ of } q_s = 0,\ q_p = q \text{ (initial charge on } C_P) \text{ and } dq_P = dq_s = 0 \tag{4.10}$$

Subsequently, the primary and secondary capacitor voltages can be written as

$$V_P = \frac{q_P}{C_P} = \frac{1}{C_P}\sum_i B_i \exp(E_i t) \tag{4.11}$$

and

$$V_s = \frac{q_s}{C_s} = \frac{1}{C_s}\sum_i A_i \exp(E_i t) \tag{4.12}$$

Solution of equations (4.11) and (4.12), when the primary and secondary resistances are neglected [79] [84]gives the voltage developed across the secondary circuit capacitance C_s as

$$V_s = \frac{2kV_P}{\sqrt{(1-T)^2 + 4k^2T}}\sqrt{\frac{L_s}{L_P}}\sin\left(\frac{\omega_2 + \omega_1}{2}t\right)\sin\left(\frac{\omega_2 - \omega_1}{2}t\right) \tag{4.13}$$

Where for a transformer operating in the Tesla mode

$$T = \left(\frac{\omega_P}{\omega_s}\right)^2 = \frac{L_s C_s}{L_P C_P} = 1 \tag{4.14}$$

$$\omega_1 = \omega_s\sqrt{\frac{(1+T) - \sqrt{(1+T)^2 + 4k^2T}}{2(1-k^2)}} \tag{4.15}$$

$$\omega_2 = \omega_s\sqrt{\frac{(1+T) - \sqrt{(1+T)^2 + 4k^2T}}{2(1-k^2)}} \tag{4.16}$$

T is the tuning ratio, defined as the square of the ratio of the uncoupled resonance frequencies (ω_p and ω_s), while V_p is the initial voltage across C_p. ω_1 and ω_2 are the resonant frequencies of the primary and secondary circuits when magnetically coupled.

4.2.2.4 Condition for maximum voltage gain

From equation (4.13), one obvious way to optimize a Tesla transformer is to obtain the maximum achievable secondary voltage at a given primary voltage[85]. The maximum secondary voltage gain over the primary voltage can be written from equation (4.13) as

$$G = \left(\frac{V_s(t)}{V_P}\right)_{max} = \frac{2k}{\sqrt{(1-T)^2 + 4k^2T}}G_L \tag{4.17}$$

Where

$$G_L = \sqrt{\frac{L_S}{L_P}} \tag{4.18}$$

The gain G from equation (4.17) can be achieved only if the sine terms in equation (4.13) are simultaneously equal to ±1, i.e.

$$\frac{\omega_2-\omega_1}{2}t = \frac{\pi}{2} + n\pi \text{ and } \frac{\omega_2+\omega_1}{2}t = \frac{\pi}{2} + m\pi \tag{4.19}$$

Where "n" and "m" are positive integers. Without losing generality, n can be set to zero, thereby changing the requirement to

$$\frac{\omega_2}{\omega_1} = \frac{m+1}{m} \tag{4.20}$$

To make t as small as possible so that the maximum voltage occurs in the shortest time from *t = 0*, we take *m = 1*, which yields the condition:

$$\omega_2 = 2\omega_1 \tag{4.21}$$

In addition, if *Z* is the impedance operator[81] for the circuit shown in Figure 4.4, it can be written as

$$Z = \begin{bmatrix} j\omega L_P + {}^{1}/_{j\omega C_P} & j\omega M \\ j\omega M & j\omega L_P + {}^{1}/_{j\omega C_P} \end{bmatrix} \tag{4.22}$$

From the characteristics equation $|z| = 0$, it follows that

$$\left(j\omega L_P + {}^{1}/_{j\omega C_P}\right)\left(\omega L_P + {}^{1}/_{j\omega C_P}\right) - (j\omega M)(j\omega M) = 0 \tag{4.23}$$

Introducing the substitutions $k = \frac{M}{\sqrt{L_P L_S}}$ $\omega_P = \frac{1}{\sqrt{L_P C_P}}$ $\omega_s = \frac{1}{\sqrt{L_S C_S}}$ enables equation (4.23) to be rewritten as

$$(1-k^2)\omega^4 - (\omega_P^2 + \omega_s^2)\omega^2 + \omega_P^2\omega_s^2 = 0 \tag{4.24}$$

For complete energy transfer, the resonant electrical circuits must have same frequency

i.e. at resonance condition

$$\omega_P = \omega_s \tag{4.25}$$

In that case, equation (4.24(4.24) becomes

$$(1-k^2)\omega^4 - 2\omega_P^2\omega^2 + \omega_P^4 = 0 \tag{4.26}$$

With roots ω_1 and ω_2, where

$$\omega_{1,2}^2 = \omega_P^2\left[\frac{(1 \pm k)}{(1-k^2)}\right] \tag{4.27}$$

Since $\omega_2 > \omega_1$ from equation (4.21)

Therefore,

$$\omega_1^2 = \omega_P^2\left[\frac{(1-k)}{(1-k^2)}\right] \text{ and } \omega_2^2 = \omega_P^2\left[\frac{(1+k)}{(1-k^2)}\right]$$

Now the ratio of the square of the frequencies is

$$\frac{\omega_1^2}{\omega_2^2} = \frac{1-k}{1+k} \tag{4.28}$$

Solving equation (4.21) and (4.28) we have

$$\frac{1-k}{1+k} = \frac{1}{4} \; or \; k = 0.6 \tag{4.29}$$

Equations (4.25) and (4.29) provide the criterion for selecting the Tesla parameters for maximum voltage gain and maximum energy transfer from the primary circuit to the secondary circuit[86]. When $\omega_P \neq \omega_s$ complete energy transfer does not take place as a result equation (4.25) cannot applied. The equation is solved for the chosen values of ω_P and ω_s.

Taking into consideration of above-mentioned conditions for efficient Tesla transformer designing, the required parameters are derived. As discussed in the (section 4.2.2.2) Tesla coil is a combination of primary capacitor (C_1) inductor (L_1) and secondary capacitor (C_2) and inductor (L_2). In the following sections, the parameters selection, theoretical calculation and experimental measurement of parameters are discussed.

4.2.3 Modeling of Tesla transformer

The modeling of Tesla transformer primary and secondary inductance are performed by the numerical methods mentioned in reference[87] [88]. The method discusses the filamentary modeling technique, which is used to derive the inductance values for present geometry. Filamentary modeling is a simple and accurate and general-purpose numerical technique that enables a full description of electromagnetic, thermal and dynamic interactions to be included in a model, while still preserving considerable mathematical simplicity.

In filamentary modeling, the given assembly of conductors is divided into an assembly of filaments in the direction of the current paths through the conductors. In this method by assuming a uniform current distribution across the cross section of the filaments, the self-inductances is calculated from well-known formulae [89], and the mutual inductance between every possible pair of filaments. This reduces the electromagnetic problem in to a simple circuit problem, in which an assembly of current filaments represents the solid conductors. The currents in each branch are defined as state variables, and the circuit equations are written as a set of linear first order differential equations that have to be solved for the circuit currents.

The self-inductance of the i_{th} filament can be written

$$\frac{d}{dt}\left(\sum_{j=1}^{N} M_{i,j}\, I_j\right) = V_i(i = 1 \ldots N) \tag{4.30}$$

where N is the number of filaments, I_i (i = 1....N) is the current in the i_{th} filament, V_i (i = 1....N) is the complete inductive voltage term in the circuit containing the i_{th} filament and $M_{i,j}$ (i, j =1...N) is the mutual inductance between the i_{th} and j_{th} filaments. When $i = j$, $M_{i,j}$ equal to L_i ,

In this method [88], the set of first order differential equations that corresponds to the filamentary circuit model are solved using numerical ordinary differential equation solvers such as the Runge-Kutta technique, with the filamentary currents thus calculated providing the current distribution in the conductors.

In the following sections, it is shown how the self and mutual inductance associated with coils are determined. With the turns divided into a number of filaments, their effective self and mutual inductances are calculated assuming individual circular coils.

Mutual inductance between two parallel circular loops

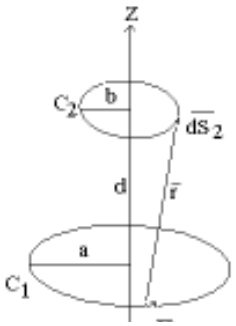

Figure 4.5 Schematic representation of two loops

The mutual inductance M between the two loops C_1 and C_2 shown in Figure 4.5 having radius of a and b respectively can be written

$$M = \frac{\mu_o}{4\pi} \iint_{C_1 C_2} \frac{dS_1 S_2}{r} \tag{4.31}$$

Where dS_1 and dS_2 are the differential vectors for each loop and r is the vector shown in Figure 4.5. Then M may be expressed in the form [89]

$$M = \mu_o \left\{ -\sqrt{(a+b)^2 + d^2}\; E\left(\frac{4ab}{(a+b)^2 + d^2}\right) + \frac{a^2 + b^2 + d^2}{\sqrt{(a+b)^2 + d^2}}\; K\left(\frac{4ab}{(a+b)^2 + d^2}\right) \right\} \quad (4.32)$$

Where d is the axial distance between the two loops and E and K are the elliptical integrals defined as

$$E(k^2) = \int_0^{\frac{\pi}{2}} \sqrt{1 - k^2 \sin^2\theta}\; d\theta \quad (4.33)$$

$$K(k^2) = \int_0^{\frac{\pi}{2}} \frac{d\theta}{\sqrt{1 - k^2 \sin^2\theta}} \quad (4.34)$$

Self-inductance of circular loops for finding the primary copper sheet inductance

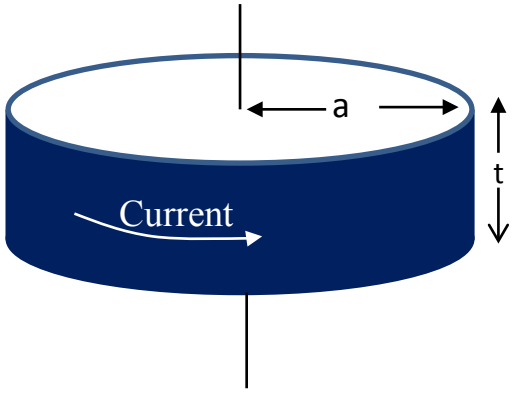

Figure 4.6 Circular ribbon

To calculate the self-inductance it is assumed[87] that a current is flowing along the circular ribbon of radius a and axial length t shown in Figure 4.6 [88]. The self-inductance L can be calculated from the magnetic flux produced when current flows with a uniform density in the ribbon, which is equivalent to taking an average of all the mutual inductances between the current loops in the ribbon [88]

then if t≪a

$$L = a\mu_o(0.386394 + 0.1730840q^2 - \ln q - 0.2538683q^2 \ln q) \qquad (4.35)$$

Where

$$q = \frac{t}{2a}$$

4.2.3.1 Self-inductance of a single loop

The self-inductance of a single loop with a circular cross section of finite radius r_c can be obtained as [89]

$$L = \mu_o R_c \left(\ln \frac{4\pi R_c}{2r_c} - \frac{3}{4}\right) \qquad (4.36)$$

The equations mentioned above are used to calculate the inductance of the transformer.

4.2.3.2 Inductance calculation of transformer

Once the filamentary currents are known, the magnetic energy stored in all the filamentary self and mutual inductances are calculated at any time during the discharge of the capacitor bank[88], [89]. The total energy stored in the winding can then be found directly by adding the magnetic energies associated with each filament, and the result obtained must be equal to the energy stored in the corresponding element of the lumped component model (i.e.$\frac{1}{2}\ LI^2$).

The self-inductance of the single turn primary winding can be written as:

$$L_P = \frac{\sum_{i=1}^{N_P}\sum_{j=1}^{N_P} M_{i,j}\ I_i I_j}{\left(\sum_{i=1}^{N_P}\ I_i\right)^2} \qquad (4.37)$$

where N_P is the total number of filaments in the primary winding.

The inductance of the multi-turn secondary winding (represented by N concentric cylinders) is given by

$$L_s = \frac{\sum_{i=1}^{N_S}\sum_{j=1}^{N_S} M_{i,j}\, I_i I_j}{\left(\frac{1}{N}\sum_{i=1}^{N_S} I_i\right)^2} \tag{4.38}$$

where N_S is the total number of filaments in the secondary winding.

Similarly, the mutual inductance between the primary and secondary windings can be written as

$$M_{P-S} = \frac{\sum_{i=1}^{N_P}\sum_{j=1}^{N_S} M_{i,j}\, I_i I_j}{\sum_{i=1}^{P} I_i \left(\frac{1}{N}\sum_{i=1}^{N_S} I_i\right)} \tag{4.39}$$

4.3 Requirement of present work:

The present work requires a generator capable of producing few 100 kVs and tens of nanosecond pulse at maximum charging voltage (V_P) of 30 kV. Since the primary capacitance is selected as 0.72 μF, which is made of three capacitors (NWL, UK made # 12723 model), arranged in parallel, each of 0.24 micro Farad (μF), 20 kA voltage and current respectively. Current from the total capacitor bank (rating 20 kA each) cumulatively 60 kA should not reach the maximum current limit of the capacitors i.e., 60 kA in present case.

$$I_{max} = V_P \sqrt{\frac{C_P}{L_P}} \tag{4.40}$$

For safe operation of the capacitor I should be < $I_{max.}$ If the maximum current is as given in equation (4.40), the primary inductance should not be lower than 200 nH, for the safety of the capacitors. To maintain the overall uniformity, the diameter of the primary coil should not exceed the diameter of the pulse forming line. Once the diameter of the primary is fixed, the length of the primary coil must be adjusted to give the primary inductance of 200 nH.

Once the inductance and capacitance of the primary circuit are known, the selection of secondary inductance and capacitance are made from the Tesla circuit conditions (equation

(4.14)and (4.29)) i.e., to work the transformer in Tesla mode, both the primary and secondary open circuit resonance frequency must be equal, i.e., the tuning ratio (T=1) should be equal to one and coupling coefficient k=0.6. This process provides values of the primary and secondary transformer parameters as mentioned in following Table 4.1.

Table 4.1 Calculated parameters for Tesla transformer

Primary capacitance	0.24 μF x 3 =0.72 μF
Primary Inductance	200 nH
Secondary capacitance	2.93 nF
Secondary winding	40 μH

4.3.1 Fabrication of Tesla primary and secondary winding

In the fabrication of Tesla transformer, an important aim is to make the primary winding inductance 200 nH and the secondary inductance 42 μH.

4.3.1.1 Selection of primary circuit for Tesla transformer

To maintain the overall system uniformity, the internal diameter of the primary coil should not exceed the diameter of the pulse forming line. Once the diameter of the primary is fixed, the length of the primary coil must be adjusted to give the primary inductance of 200 nH. A copper sheet of 200 μm thick, single turn copper sheet with 168 mm, 650 mm, width and length respectively is wrapped around a 240 mm diameter PVC (Polyvinyl chloride) mandrel to provide a inductance of 200 nH. Single turn primary of the Tesla transformer is shown in Figure 4.7 and Figure 4.9. However, internal inductance of capacitors ($L_{capacitor}$ 60 nH), inductance of spark gap switch (RE baverly III, model SG 101 E) ($L_{spark\ gap}$ 20 nH) and connections ($L_{connections}$ 20 nH) makes the total primary inductance as 340 nH.

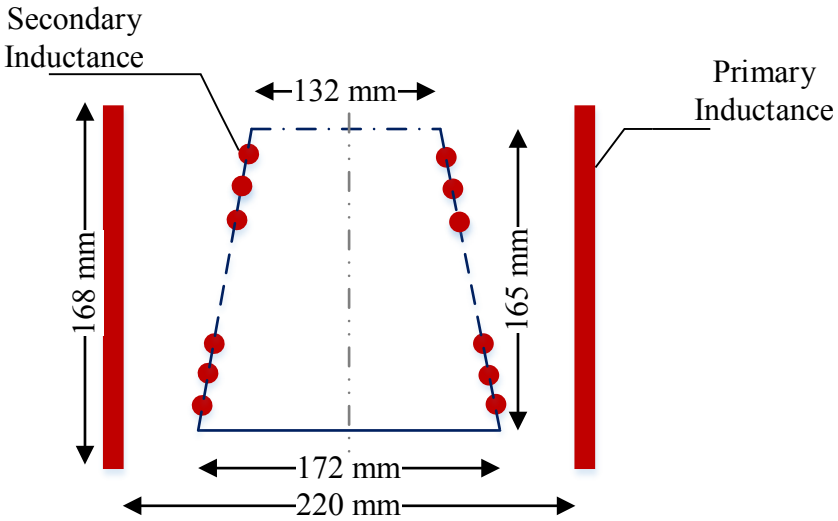

Figure 4.7 Primary and Secondary windings of Tesla transformer

4.3.1.2 Secondary winding:

4.3.1.3 Tapered secondary winding

When pulse transformers are to be operated at very high power levels or with large volt second (v.s) products, it is clear that to avoid core saturation large cores must be used with large number of turns. Eventually as the power levels are raised, a point is reached where the size of the core required becomes impractical. To tackle this problem, in general air core will be used in pulse transformers [78] In this work, secondary core is made of Delrin material.

A tapered construction (with the larger diameter at the bottom) as shown in Figure 4.11 is used for the secondary coils to avoid any breakdown at the high voltage end of the secondary winding. The high voltage will appear at the upper end (as the lower end is grounded) and the greater space around the high voltage terminal will prevent the possibility of any high-voltage break down.

4.3.1.4 Secondary winding

The secondary coil is placed inside the PVC cylinder, on which the primary winding is wrapped as shown in Figure 4.14. In this case, the maximum diameter and height of the secondary coil must not exceed the internal dimensions of the PVC mandrel (which not only

works as a support for the primary coil but also retains the insulating oil for the secondary windings.)

Once the height and diameter for the secondary winding is fixed, the remainder of the parameters for the secondary winding is calculated as discussed in section 4.2.3.2. The secondary winding was formed by 16 turns of commercially available copper wire 3 mm in diameter wrapped around a tapered mandrel with 8 mm inter turn pitch. The secondary core is made of delrin with dimensions are lower diameter 220 mm, and upper diameter 132 mm and height 165 mm as shown in Figure 4.11. The number of turns is determined by the required secondary inductance. The selection of the wire diameter is a tradeoff between the required low resistance of secondary windings and the higher inter-turn distance of the secondary windings to prevent any inter turn high voltage breakdown. The secondary of transformer after winding is shown in Figure 4.11. The calculated inductance of secondary windings is 40 μH, and the mutual inductance (M) between primary and secondary inductance is 1.85 μH.

4.3.2 Experimental measurement of Tesla parameter

4.3.2.1 Primary inductance (L_1)

The electrical equivalent circuit for experimentally verifying the inductance of the copper sheet is shown in Figure 4.8. In this, a capacitor of 0.24 μF charged to 1000 V and discharged through a switch to the copper sheet whose inductance is to be measured as shown in Figure 4.9. In this, the current of the circuit is measured through the current transformer (Pearson CT, model number 101). The entire circuit considered as RLC circuit and oscillations of resonant circuit are recorded in the oscilloscope.

Inductance value is obtained by solving the RLC equation (4.41) and (4.42) for current (i), an oscillating current waveform is plotted by using computational software for particular R, L, C and applied voltage (V). Comparing the computational waveform with the experimental

waveform by varying the R, L values in the equations (4.42) until both the waveforms match together in terms of amplitude and frequency. The compared experimental and theoretical waveforms are shown in Figure 4.10. With this, the value of inductance obtained is 240 nH. However, the total inductance of primary including inductance of capacitor bank, spark gap switch, connections makes the total inductance as 340 nH.

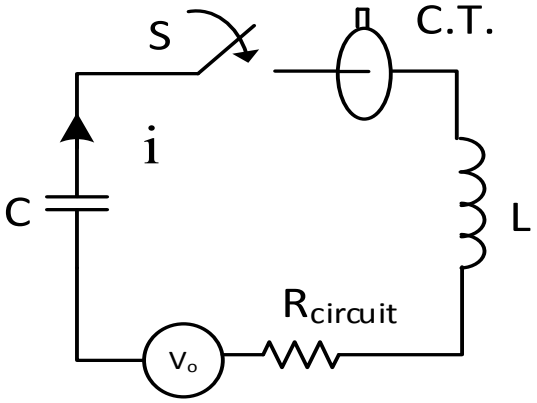

Figure 4.8 Electrical equivalent circuit of experimental setup used for inductance measurement

$$V_R + V_C + V_L = V_o \tag{4.41}$$

$$iR + \frac{1}{C}\int idt + L\frac{di}{dt} = V_o \tag{4.42}$$

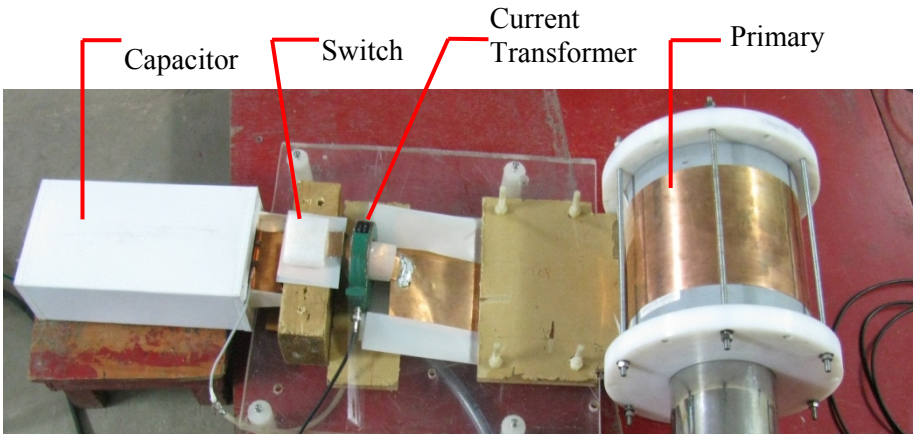

Figure 4.9 Experimental measurement of Primary Inductance

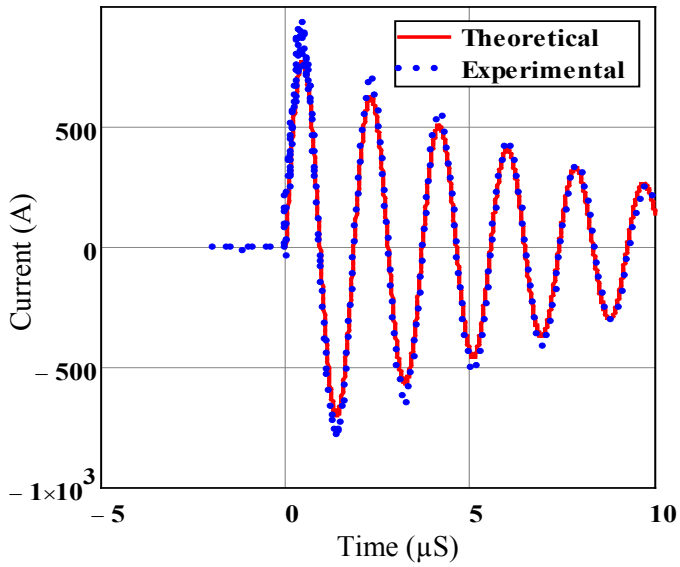

Figure 4.10 Experimental waveform for measuring primary inductance

4.3.2.2 Secondary inductance (L_2)

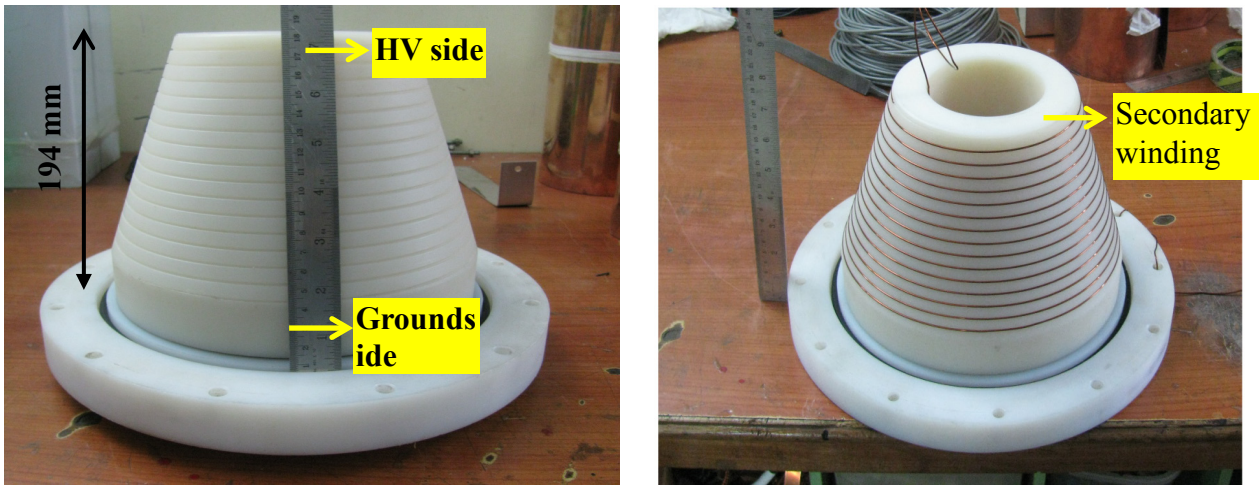

Figure 4.11 Secondary core of tesla coil made of Delrin, Secondary winding made on tapered shape Delrin material

The secondary inductance (L_2) is experimentally verified by charging the known capacitance (0.24 μF) with 1 kV and it discharged on to the secondary inductance (L_2). The resonance waveform of RLC circuit is recorded with a current transformer. By using computational software the RLC circuit equations are solved. A waveform is generated for particular values of R, L, C and voltage. The theoretical waveform has been compared with experimental

waveform. As capacitance and applied voltage are known, by changing the values of R and L both the waveforms are compared. The experimental setup used to obtain the secondary inductance is shown in Figure 4.12. The compared experimental and theoretical waveforms are shown in Figure 4.13, which give the secondary inductance value as 39 µH.

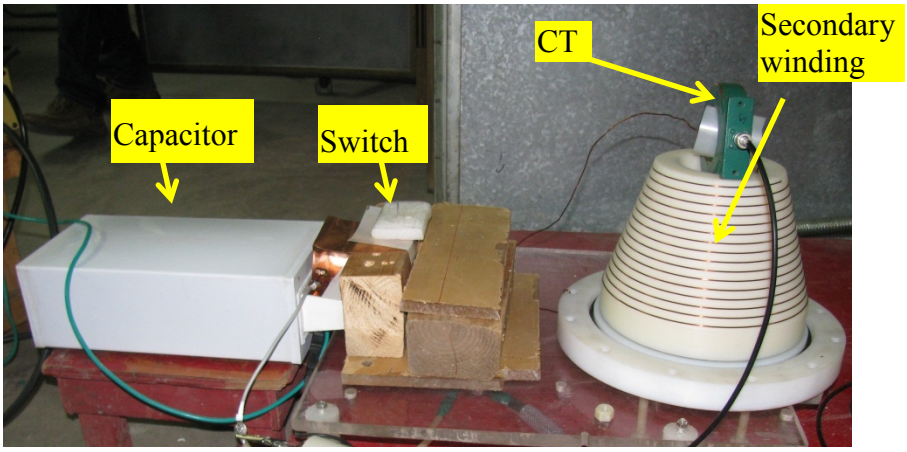

Figure 4.12 Experimental verification of secondary inductance

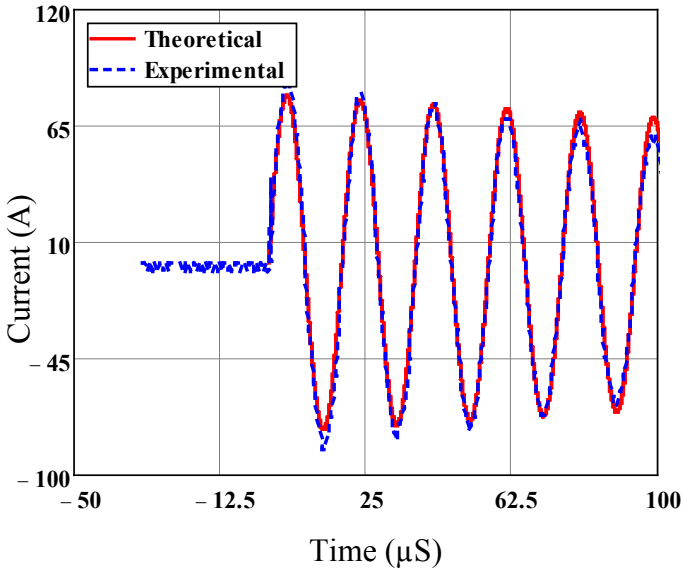

Figure 4.13 Experimental waveform for measuring secondary winding inductance

The secondary coil of Tesla transformer is placed inside the PVC mandrel (around which primary copper sheet is wrapped) as shown in Figure 4.14. The PVC mandrel is used as mechanical support for primary inductance and also retains the transformer oil to insulate the

secondary winding to avoid the electrical breakdown between primary and secondary windings.

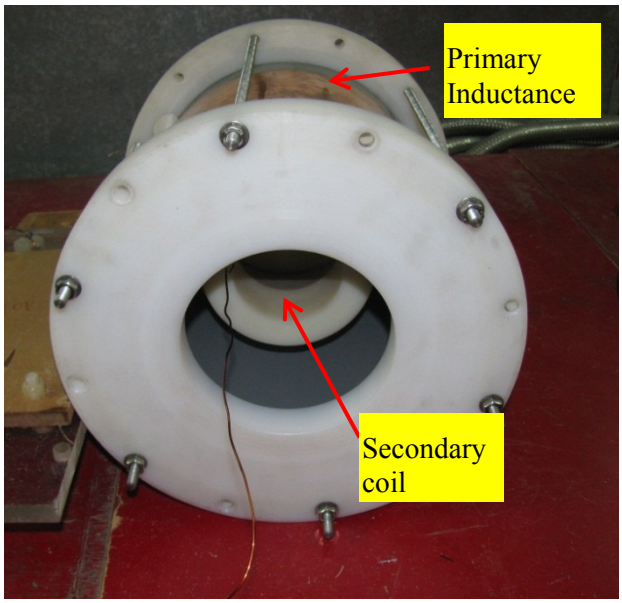

Figure 4.14 Tesla transformer with secondary placed in PVC mandrel

4.3.3 Secondary capacitance of tesla coil (C_2)

4.3.3.1 Pulse forming line

In the present work, fast rising high voltage pulse is required at the load (test chamber). The Tesla transformer can generate micro second pulse, but our experiments require nanosecond pulse. This can be achieved by using pulse-forming line (PFL). The PFL compresses the micro second pulse developed by Tesla transformer into nanosecond pulses. Pulse forming line is a transmission line (in present case a waterline), is charged as a lumped capacitor (also acts as a secondary capacitance (C_2) of the Tesla transformer) to store electrical energy and discharges this stored energy in it to the load. A coaxial pulse forming line is selected on the basis that it could easily be connected to a spark gap chamber (which is a cylinder same as outer diameter of PFL), explained in section 4.3.4. The coaxial structure as shown in Figure 4.15 is extremely suitable for a water capacitor, as it not only provides the capacitance but it also holds the water without any additional support. Since, this PFL acts like a secondary

circuit capacitance (C_2), it must satisfy the Tesla condition for resonance as per equation (4.14), $L_C C_S = L_P C_P$ must be satisfied.

$$\text{Capacitance} \quad C = \frac{2\pi\varepsilon_r}{\ln\frac{b}{a}} \quad (\text{F/m}) \tag{4.43}$$

$$\text{Inductance} \quad L = \frac{\mu_r \ln\frac{b}{a}}{2\pi} \quad (\text{H/m}) \tag{4.44}$$

$$\text{Characteristic impedance } Z_o = \frac{60\ln(\frac{b}{a})}{\sqrt{\varepsilon_r}} \quad (\Omega) \tag{4.45}$$

Where,

ε_r = dielectric constant value of medium used in PFL

μ_r = relative permeability of dielectric material used in PFL

l = length of the PFL in meters

b= inner dia of outer cylinder in meters

a= outer dia of inner cylinder meters

Outer cylinder inner diameter (b) =236 mm

Inner cylinder outer diameter (a) =136 mm

Length (l) =350 mm

Figure 4.15 Coaxial cylinder Pulse forming

Diameters of inner and outer cylinders are 136.8 mm, 236 mm respectively and length is 350 mm. In this work de-ionized water (at room temperature 26°C, $\varepsilon_r \sim 78$) have been used as a dielectric medium in PFL, which provides secondary capacitance (C_s) of 2.961(nF) and impedance of 3.658 ohms. The water used in the PFL is continuously circulated to maintain the purity of water (conductivity < 1 µS/cm) and to avoid the breakdown in the PFL. Designed PFL can easily withstand 300 kV, however our operating voltages are less than 200

kV. The chamber is made of stainless steel (SS 304) material with 3 delta finishing and ensured that no sharp edges present.

Calculated and experimental values of Primary and secondary parameters of tesla coil are presented in Table 4.2.

Table 4.2 Tesla coil calculated and experimental parameters:

Parameter	Calculated values	Experimental values
Primary capacitance	0.72 μF	0.7 μF
Primary inductance	240 nH	340 nH
Primary resistance	50 mΩ	60 mΩ
Secondary inductance	40 μH	39 μH
Secondary capacitance	2.961 nF	3.02 nF
Secondary resistance	2 Ω	2 Ω

4.3.4 Spark gap chamber

Spark gap chamber is a high voltage switch, used to transfer the voltage (developed by Tesla transformer) to the load. The chamber is of width 97 mm and length 210 mm. Each hemi spherical electrode is of diameter 65 mm and inter electrode distance is 5 mm which make the switch to operate at 15 kV at one atmospheric (1 ATM) pressure of air. The required high voltage (a few 100 kVs) can be achieved by pressurizing the chamber with sulfur hexafluoride (SF_6) gas whose breakdown strength is 90 kV/cm. The spark gap chamber and electrodes are made of stainless steel (SS 304).

4.3.5 Diagnostic chamber

Measuring the fast rising high voltage and current in non-intrusive way is not a trivial task. Limitations in standard probe operating voltage levels and geometrical difficulties lead to find alternate methods. In this work, to measure the applied voltage across test chamber and current through it, a suitable voltage and current sensors are developed.

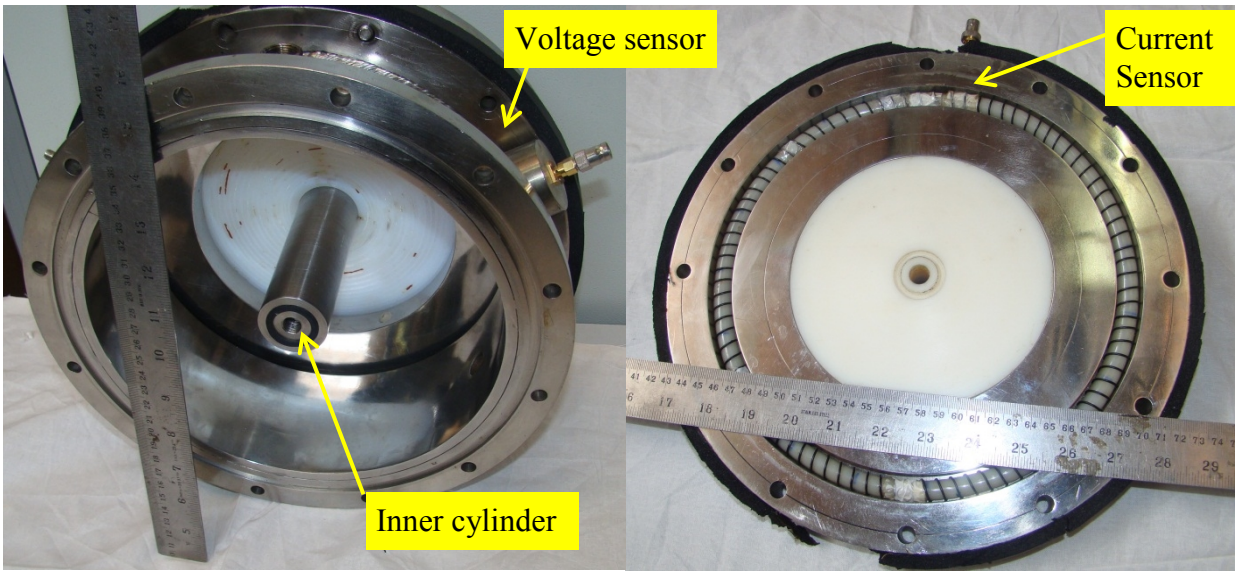

(a) (b)

Figure 4.16 Diagnostics chamber. (a) Coaxial cylinder showing voltage sensor, (b) current sensor inserted in flange

As the operating voltages are very high (few 100 kVs), the standard sensors or probes cannot be placed in open environment to avoid the insulation breakdown. So in this work capacitive voltage sensor and Rogowski current sensor are developed (will be discussed in chapter 5).

The chamber is a coaxial cylinder shown in Figure 4.16 is of dimensions of 95 mm width, inner and outer diameter as 40 mm and 210 mm respectively. The chamber is filled with deionized water (ε_r=78 and conductivity (σ) = 0.45 µS/cm) and is continuously circulated through deionized water plant to maintain the water purity (conductivity < 1µS/cm) to avoid the change in sensitivity (due to variation in conductivity) of the sensor. The voltage sensor is fixed in the chamber itself and current sensor is placed in one of the chamber flange which will be discussed in the chapter 5

4.3.6 Test chamber

The dimensions of test chamber are 160 mm width and 210 mm height. As mentioned in the chapter 2, our area of interest of study is in uniform field. So in this work, hemispherical electrodes of different dimensions (44, 46, 50 mm) are used which makes the inter electrode distances 8, 6, 3 mm respectively. As mentioned in the chapter 1, out major interest of study is to understand the breakdown mechanism in intermediate energy storage device or peaking capacitors. Hence, the end flange of the chamber is directly grounded without keeping termination or load at the end of chamber. The chamber also has the provision of optical window (50 mm diameter) to view the breakdown. The inlet and outlet valves make the provision to fill the test liquid into the chamber and remove it from the chamber. The entire chamber is made of stainless steel (304) material with 3 delta finishing. Utmost, care has been taken to avoid the sharp edges on the test chamber.

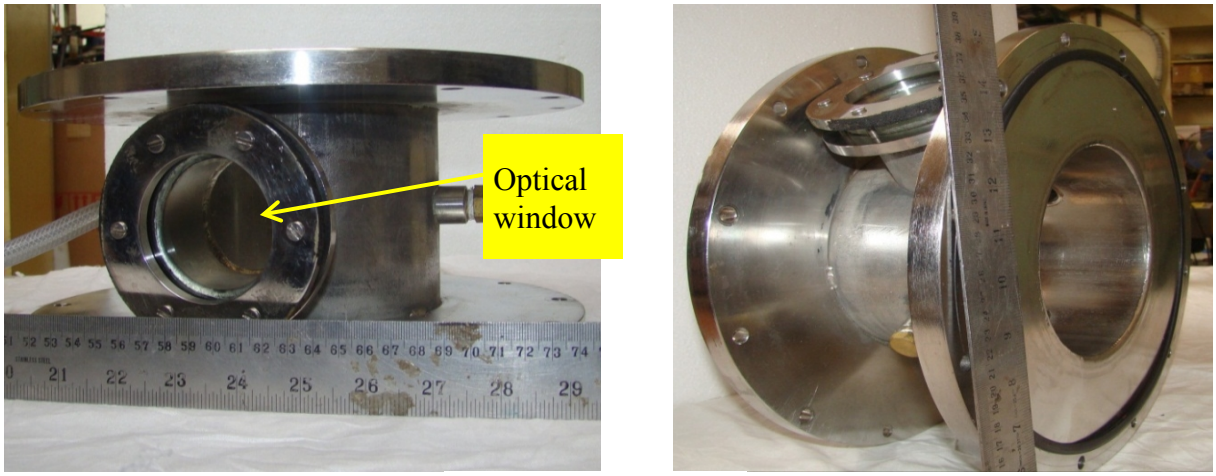

Figure 4.17 Test chamber

Sample images of electrodes used in the experiments are presented as below. In the Figure 4.18 (a) shows the stainless steel electrode, (b) shows the brass electrode, (c) shows the pair of brass electrode arrangement in test chamber. The surface roughness for tall the electrodes used are 3 Delta (0.025 µm). The contents of the electrode material are given in tabular column in Appendix-I

at the end of the thesis.

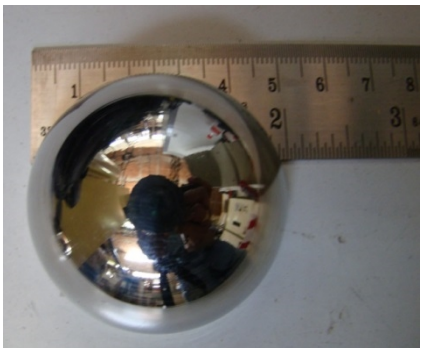

(a) Stainless steel (304)

(b) Brass electrodes

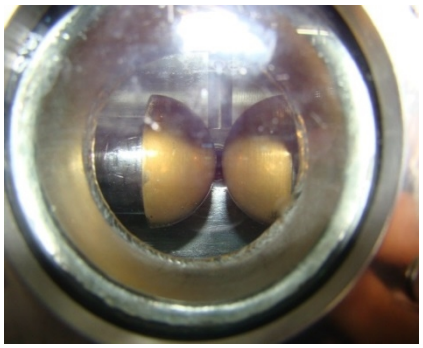

(c) Electrodes arrangement in the test chamber

Figure 4.18 Sample images of electrodes images used in the experiments

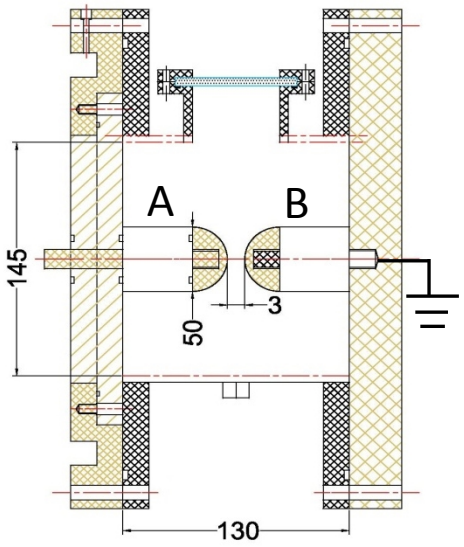

Figure 4.19 Geometrical view of test chamber in experimental setup (all dimensions are in mm)

4.3.7 PSPICE simulation using experimental parameters

The pulse generator is simulated using PSPICE student version (9.1) software. Experimentally determined parameter values are used for in simulation. The electrical equivalent circuit of tesla transformer simulation is shown in Figure 4.20. The output voltage waveform across secondary capacitance (C_2) (i.e. PFL) is shown in Figure 4.21 which is further compared with theoretical (by using transformer equations) and experimentally obtained output voltage waveforms. The comparative waveforms are shown in Figure 4.22.

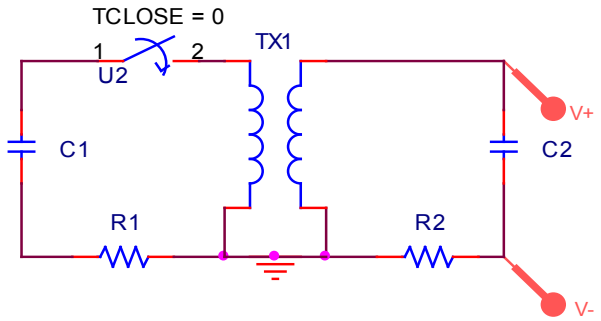

Figure 4.20 PSPICE simulation circuit of Tesla transformer

All the output waveforms are well in agreement with each other, which further resembles the calculated and experimental parameters.

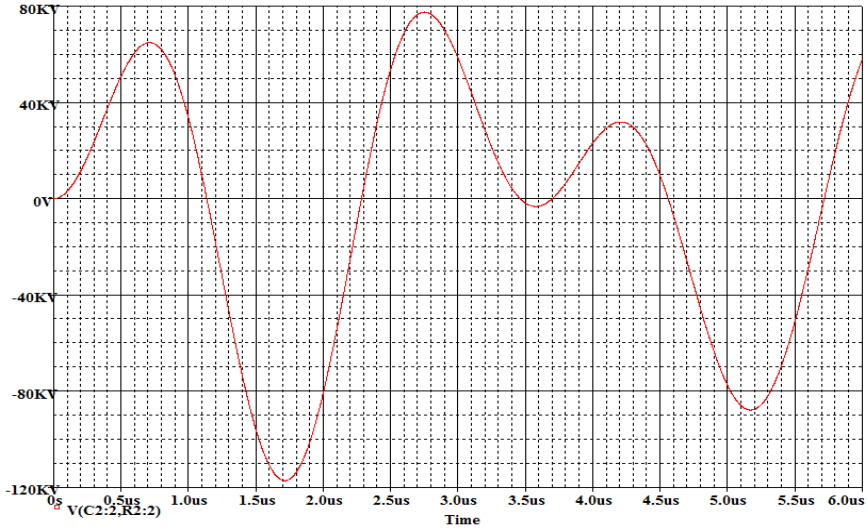

Figure 4.21 Output result of PSPICE simulation circuit

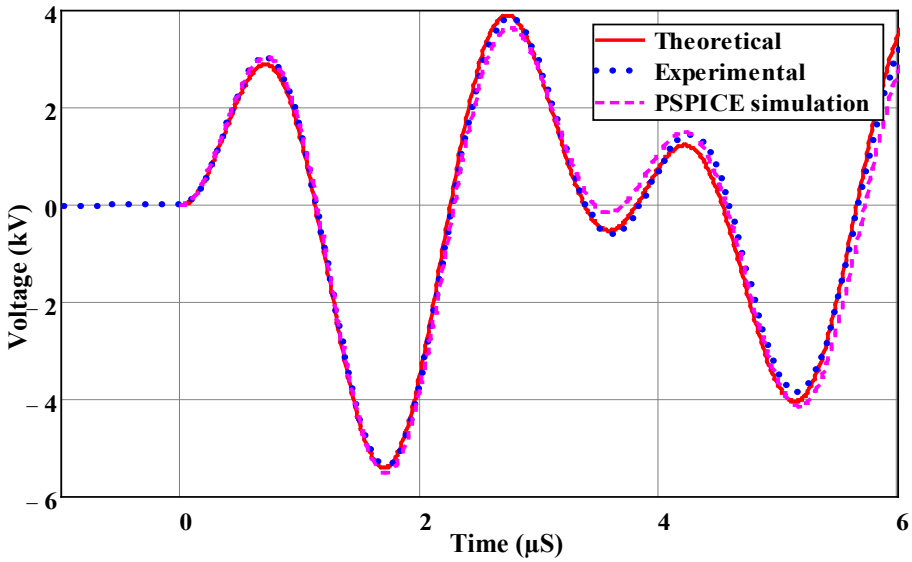

Figure 4.22 Voltage output across pulse forming line with water as dielectric medium

4.4 Pulse generator working procedure

Initial charging of primary capacitor bank (C_p) facilitated through a 0-35 kV laboratory developed variable DC power supply shown in Figure 4.2. Charged primary capacitor (C_P) is discharged to primary inductance (L_P) through triggered spark gap (RE Beverly made 101E model).switch (S_1).

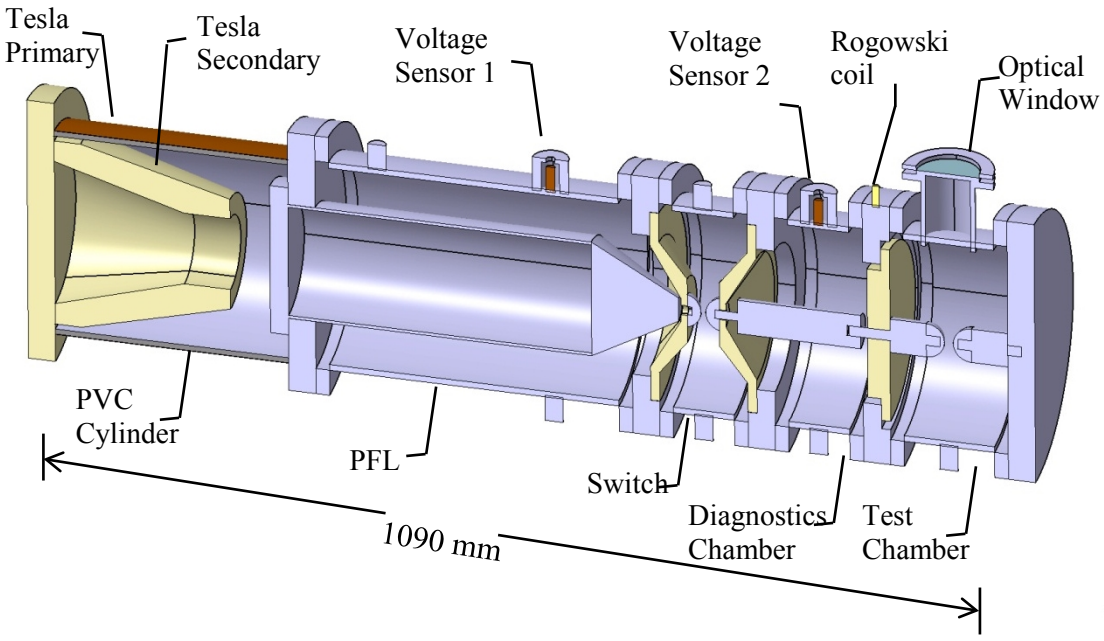

Figure 4.23 Section view of Experimental setup

Due to the mutual inductance between primary and secondary windings, the voltage induces in secondary winding and forms an oscillatory circuit with PFL capacitance (C_S).The voltage developed by tesla transformer is transferred to the load by spark gap switch (S_2). The switching voltage of designed spark gap (S_2) is 15 kV (at atmospheric pressure), which could be raised up to various levels (say 150 kV in present case) by pressurizing the spark gap chamber by Sulfur hexafluoride (SF_6) gas. Once SF_6 spark gap switch (S_2) turned on, the entire source voltage will appear at the test chamber (i.e. Load) in tens of nanosecond duration with a few nanosecond rise times. The sectional view of pulse generator is shown in Figure 4.23. The overall view of arrangement of experimental setup developed is shown in Figure 4.24. It comprises high voltage DC power supply, over which pulse generator is installed and also shows the Deionizer purifier unit, water tank, water circulation pump. The overall system occupies the size of 1.5 m x 1.5 m.

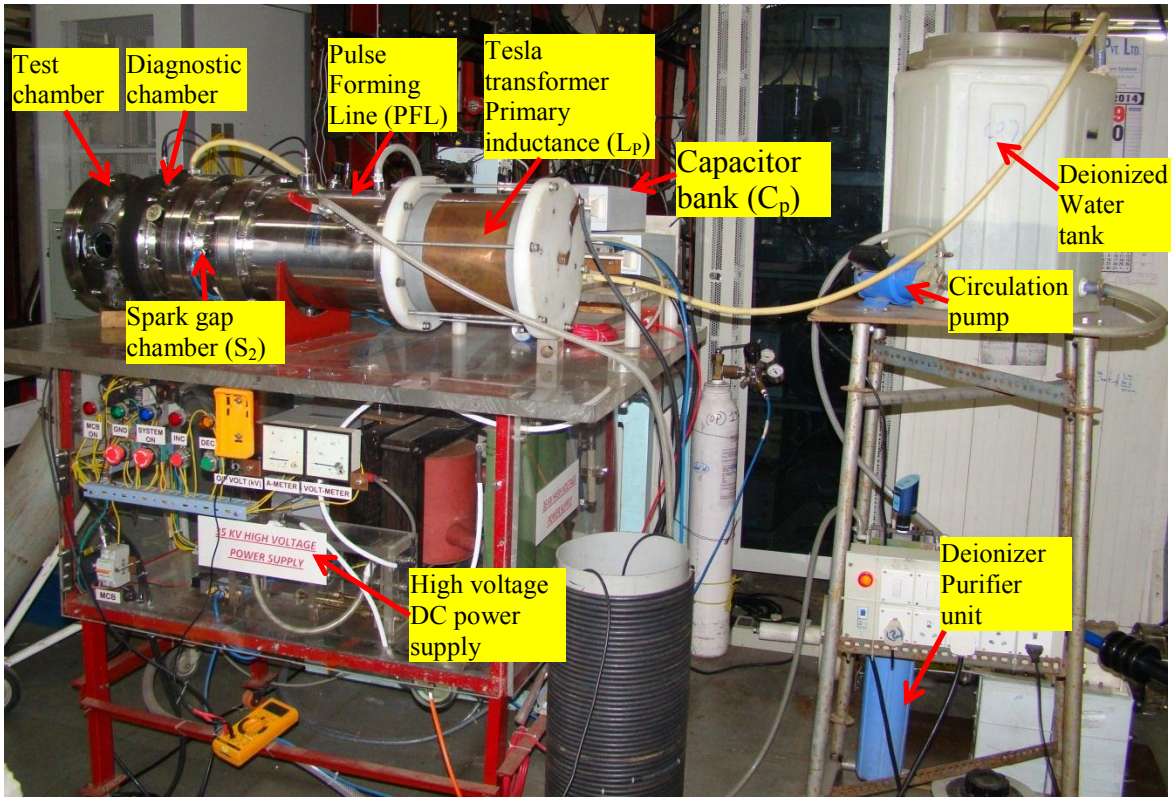

Figure 4.24 Complete view of arrangement of experimental setup

4.5 Summary

In the process of studying the electrical breakdown properties of liquids under nanosecond (ns) time scales, a Tesla based pulse generator[90] is developed. It is a combination of Tesla transformer, pulse forming line, a fast closing switch, and test chamber. The designed system component values are experimentally verified which are well in agreement with the calculated parameters.

The pulse generator is designed to deliver maximum output voltage of 300 kV and rise time of the order of few nanoseconds with pulse duration of tens of nanoseconds. To validate the pulse generator performance, experimental results are compared with theoretically calculated values, PSPICE simulation software and are in good agreement with simulation results.

Chapter 5
Diagnostics

5 Introduction

In the previous chapter, the design and development of Tesla based nanosecond pulse generator and its individual components are discussed in detail. The entire system can be said ready to use only when it is able to measure the desired voltage and current with significant accuracy. The measurement of transient electromagnetic field is important for pulsed power systems. An appropriate sensor has to be constructed and positioned such that it does not perturb the fields are to be measured. In this chapter we discuss various electrical sensors in order to obtain the desired signals precisely.

Our objective is to study the electrical breakdown properties in nanosecond time scale. For this, certain diagnostics, having fast response of the order of nanoseconds and which can measure high currents (kA) and voltage levels (of the order of a few 100 kV) are required. Estimation of fast transient high current and high voltage is required for understanding the electrical breakdown properties of liquids. Because of large magnitude and fast temporal behavior of these quantities, ordinary methods cannot be employed. Therefore, a Rogowski coil and a V-dot sensor are developed to measure the current and voltage respectively and have been used. The objective of developing suitable Rogowski coil is to measure pre and post breakdown currents, whereas V-dot sensor is to measure the applied voltage across the electrodes. based on data obtained from diagnostics, breakdown properties have been analyzed.

In the following sections, the working principle, design, fabrication, modes of operation etc., of current and voltage sensor are discussed.

5.1.1 Conventional current measurement methods

The commonly used methods to sense current are

a. Resistive shunt

b. Hall effect current sensor

c. Current transformer(CT)

d. Rogowski coil.

The comparison of these sensors is shown in Table 5.1. It is noticed that, in comparison to Resistive shunt and Hall effect current sensors, current transformer is a better option for measuring such fast transient high currents. Current transformer exhibits following operating features.

Advantages:

i. Provides voltage isolation

ii. Provides output voltage, ideal for noisy environment and easily convertibility to current

iii. Reliable

iv. No external power requirements.

Limitations:

i. Measures AC current only

ii. Output is frequency dependent

iii. Weight increases as the measured current increases

iv. Higher susceptibility to stray AC magnetic fields

Table 5.1 A comparison of four current measuring methods

Parameter	Resistive Shunt	Hall Sensor	Current Transformer	Rogowski Coil
Isolation	☹	☺	☺	☺
Light Weight	☹	😐	😐	☺
DC Response	☺	☺	☹	☹
Fast Current Change	☺	😐	☺/😐	☺
Ease Of Installation	☹	😐	😐	☺
Cost	☹	😐	😐	☺
Output	**Voltage**	**Current**	**Voltage**	**Voltage**

Where the emoticon indicate ☹ **No,** 😐 **Medium,** ☺ **Yes**

Concerning frequency dependent and weight increases as the measured current increases and susceptibility to AC stray magnetic fields, etc., for most of the pulsed power applications Rogowski is preferred over the current transformer. The Rogowski coil is a kind of current transformer it does not have toroidal magnetic core and hence relatively easy to design for high frequencies. The structure is a spiral winding on a toroidal insulating material. simplicity in structure and safety features (since there will be no contact between the Rogowski coil and the conductor where the target current flows) associated with Rogowski coil makes it preferred choice for current sensing experiments

Rogowski coil has following advantageous features over current transformers

- The coil is flexible and allows user to easily install it at any place.
- Very low price as compared to CT of same rating.

- Rogowski coil has air core, which removes the possibility of saturation thus giving linear B-H curve.
- The full-scale output of a properly designed Rogowski coil is typically a few hundred millivolts. So, determination of high current becomes easy, it effectively senses, as low induced voltages.

Limitations of Rogowski coil are as follows

- It cannot be used for constant current measurement.
- It requires external integrator circuit when working in differentiating mode.

Considering the above mentioned advantages viz. fast response, geometrical suitability and ease of measurement of high currents (kA), in this work, Rogowski coil is used.

5.2 Rogowski coil

A Rogowski coil(named after Walter Rogowski), is a toroidal solenoid [91][92]wound on a non-magnetic core and behave as a specially designed mutual inductor. It is an electrical device for which measures the alternating current (AC) or high-speed current pulses. It consists of a helical coil with the lead from one end returning through the center of the coil to the other end, so that both terminals of the coil are at the same end. The whole assembly is wrapped around the straight conductor whose current is to be measured, since the voltage induced in the coil is proportional to the rate of change (derivative) of current in the straight conductor.

5.2.1 Working Principle

Two main aspects that govern the basic principle of a Rogowski coil are

- **Amperes Circuital Law**
- **Faradays Law of Electromagnetic Induction**

Rogowski coil is very well embodiment of **Ampere's Law**, which provides a relationship between the current flowing through and the magnetic field around it.

If a line is drawn in a loop, which totally encircles the current then, according to Ampere's Law, the line integral of the magnetic field around the loop is equal to the net current enclosed by it, no matter what path the loop takes. If the loop encloses no net current, the line integral is zero[93].

Mathematically this is expressed as

$$\oint H.dl = \iint_S J_f.dS = I_f\ (enclosed) \tag{5.1}$$

Where,

$\oint$ is the closed line integral around the closed curve ***C***

dℓ is a differential element of the curve ***C***

dS is the vector area of an infinitesimal element of surface ***S***

J is the current density

Hence, by using Amperes Law, Rogowski coil can easily measure the current that a wire carries.

Figure 5.1 shows a long, thin helical coil, with n turns per meter and cross-sectional area (A) which encircles a conductor carrying a current I. In a section of length dl, the number of turns is "**ndl**" and the magnetic flux linking the section is ϕ

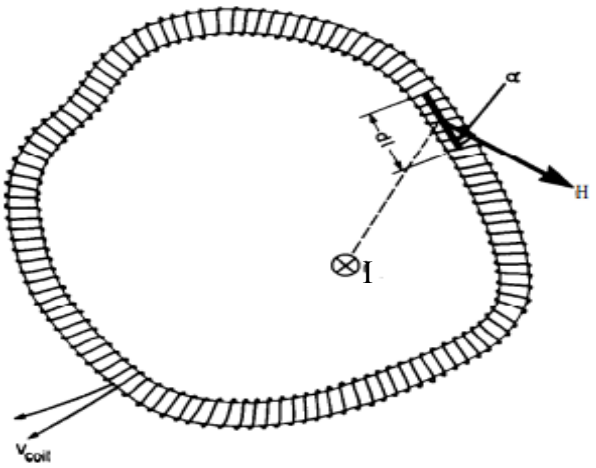

Figure 5.1 Amperes circuit law

$$d\phi = \mu HAn\, dl \cos(a) \tag{5.2}$$

where,

H is the magnetic field and

a is the angle between the direction of **H** and the axis of the coil section.

The flux linking the entire coil is given by integrating along the coil as

$$\phi = \int d\phi = \mu nA \int H \cos(a)\, dl = \mu nAi \tag{5.3}$$

For an alternating current, the voltage output from the coil is given by the rate of change of flux i.e.

$$V_{coil} = -\left(\frac{d\phi}{dt}\right) = -\mu nA\left(\frac{di}{dt}\right) \tag{5.4}$$

A thin, flexible, Rogowski coil can be used because, according to equation (5.4), the voltage output from the coil is independent of the way that the coil is placed around the conductor; provided only the ends of the coil is to be brought together. Ampere's Law makes a thin Rogowski coil ideal for use as a transducer for alternating currents since it responds only to the currents, which thread the loop, and reject currents and fields from the external sources.

In addition, the output of the transducer does not depend on the exact path taken by the loop. It can be shown that similar considerations apply to coils with a large cross-section, provided that they are circular. For practical purposes, the coupling between a coil and the conductors threading is described in terms of a mutual inductance M,

$$\text{where } M = \mu_o nA \tag{5.5}$$

μ_o is air permeability, A is the turn area and n is the number of turns per unit length.

5.2.1.1 Electrical equivalent circuit

The electrical equivalent circuit of Rogowski coil is shown in Figure 5.2. Here R_C is the coil resistance, L_C is its inductance, C_C is the stray capacitance, and Z is the terminating impedance [94].

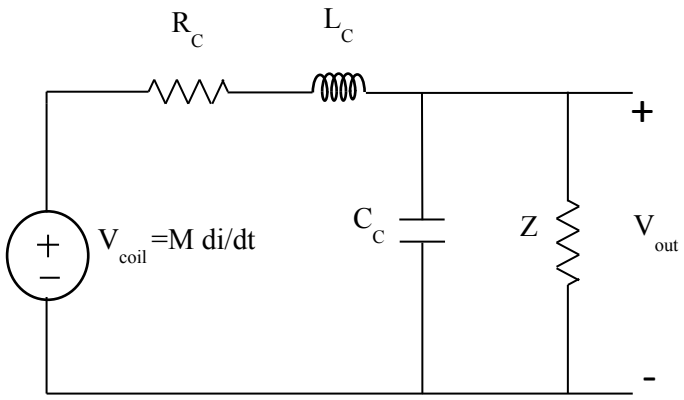

Figure 5.2 Electrical equivalent circuit diagram of Rogowski coil

If this impedance Z is placed in the coil terminals, the transfer function of the model is

$$\frac{V_{out}}{V_{in}} = \frac{Z}{L_c Z C_c S^2 + (L_c + R_c Z C_c)S + R_c + Z} \tag{5.6}$$

Neglecting stray capacitance in the transfer function, (5.6) can be modified as

$$\frac{V_{out}}{V_{in}} = \frac{Z}{L_c S + R_c + Z} \tag{5.7}$$

5.2.1.2 Modes of operation

Rogowski coil can be designed for two modes of operation[91] viz.

1. Self-Integrating mode
2. Differentiating mode

Let ϕ be the flux induced by the current I in the cross section of the Rogowski coil, the circuit equation for the Rogowski coil can be written as

$$I_c R = N\left(\frac{d\phi}{dt}\right) - L\left(\frac{dI_c}{dt}\right) \tag{5.8}$$

OR

$$\frac{1}{L} n\left(\frac{d\phi}{dt}\right) = \frac{dI_c}{dt} + \frac{R}{L} I_c \tag{5.9}$$

Based on equation (5.9) the mode of operation of Rogowski coil can be determined as follows.

Case 1 : Self-integrating mode

If $\frac{R}{L} I_C \ll \frac{dI_c}{dt}$

Then,

$$\frac{1}{L} n\left(\frac{d\phi}{dt}\right) = \frac{dI_c}{dt} \tag{5.10}$$

Since the system is linear, the equation can be re-written as

$$\frac{n\phi}{L} = I_c \tag{5.11}$$

This is called self-integrating mode where we automatically obtain the voltage directly proportional to the current that is to be measured.

Case 2 : Differentiating mode

If $\frac{R}{L} I_c \gg \frac{dI_c}{dt}$

Then
$$\frac{1}{R} n \left(\frac{d\phi}{dt}\right) = I_c \tag{5.12}$$

It is clear that in **Case 1**, the current produced in the Rogowski coil is proportional to the induced magnetic flux due to the current *I*. Therefore, the condition on case 1 is the criteria for the Rogowski coil to work in a self-integrating mode.

In **Case 2,** the current produced in the Rogowski coil is proportional to the rate of change of the magnetic flux. The condition in case (2) is therefore the criterion for a differentiating mode.

5.2.1.3 Advantages

The advantage of self-integrating Rogowski coil over its differential counterpart is as follows

- A differentiating coil can generate dangerously high voltages and currents if dI/dt is high whereas former generates fairly lower voltage levels.
- Moreover, an external integrator is also required in case of a differentiating mode.

Eventually, the values of R and L determine that a Rogowski coil is whether in Self-Integrating mode or Differentiating mode.

The self-integrating Rogowski coil also had several other advantages over its differentiating counterpart, including the output voltage being essentially independent of frequency, and hence of the rise-time of the measured current. It is also less sensitive to electron impact or photon induced currents and there is less cable attenuation of the signals from the coil, since the output is proportional to the current rather than to its derivate and is much lower than that from a differentiating coil. A differentiating coil can generate dangerously high voltages and currents if *dI/dt* is high. For these reasons, the self-integrating mode is selected and developed in present work. It is based on using a small resistance called current viewing resistor (R_{CVR})

as terminating impedance Z, there the voltage induced in the integrated Rogowski coil V_{Rogo} being given by

$$V_{Rogo} = I_c R_{cvr} \tag{5.13}$$

5.2.2 Designing of a Self-Integrating Rogowski Coil

Schematic diagram of self-integrating Rogowski coil is shown in Figure 5.3. It consists of a helical coil wound on air core material[94] (in general flexible plastic pipe) with the lead from one end returning through the center of the coil to the other end, so that both terminals

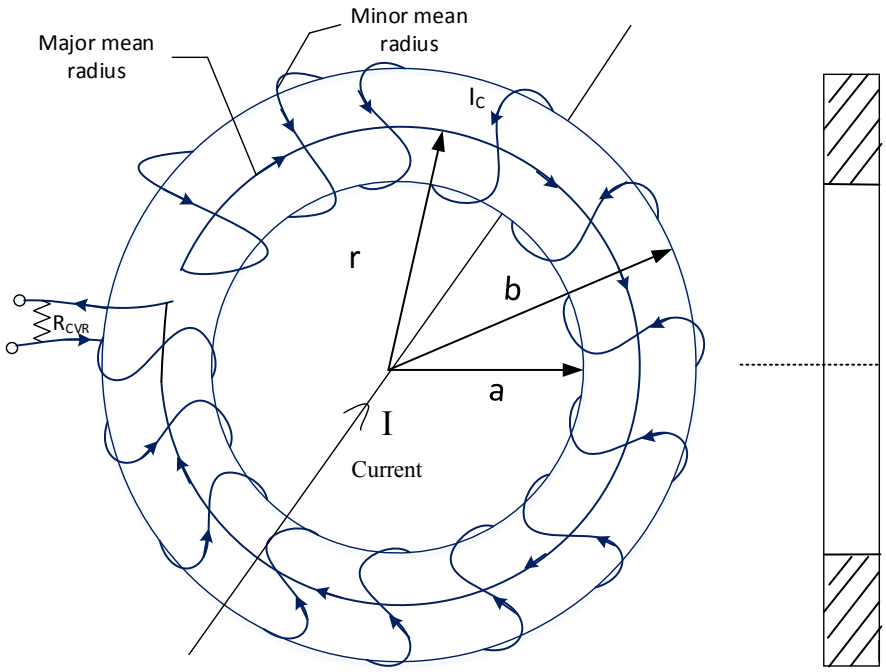

Figure 5.3 Schematic diagram of the Rogowski coil

are at the same end of the coil and terminated with a small resistor R_{CVR}.

List of parameters required for designing of a Rogowski coil[91]

r = major mean radius of the coil

a = minor mean radius of the coil (to center of winding)

d=wire diameter;

f = fundamental frequency of applied pulse

I= current threading the coil;

I_C= current flowing in the windings of the coil

R= total coil resistance = $R_{skin} + R_{cvr}$

R_{cvr}= current-viewing resistor

R_{skin}= skin effect resistance

L_S= coil self-inductance

ϕ = Magnetic flux linking the winding

N = Total no. of turns on the coil

ρ = resistivity of the conductor

μ = magnetic permeability

b = total mean major circumference

p =pitch of the winding

B = Magnetic field intensity

The value of R for any coil is given by

$$R = R_{cvr} + R_{skin} \tag{5.14}$$

where

$R_{skin} = \rho\left(\frac{l}{A}\right)$,

the length if the wire used in the coil is

$$l = n\sqrt{(P^2 + (2\pi a^2)} \tag{5.15}$$

moreover, the effective cross section of the wire is given by

$$A = \pi d \sqrt{\left(\frac{\rho}{\pi f \mu_o}\right)} \tag{5.16}$$

Therefore,
$$R_{skin} = \frac{n}{\pi d}\sqrt{\rho \pi f \mu_o (P^2 + (2\pi a)^2} \tag{5.17}$$

where

$$f = \frac{0.35}{t_r} \tag{5.18}$$

and t_r is the rise time of the current (I) pulse to be measured.

Number of turns for the present geometry can be written as

$$n = \frac{2\pi r}{P} \tag{5.19}$$

The self-inductance of the Rogowski coil plays an important role in determining the self-integration properties as shown in equation (5.9). According to Grover's formula [89] for calculating self-inductance of coil, inductance may be given as

$$L = \mu a \left(\frac{2\pi r}{P}\right)\left[\frac{\pi a}{P} + \ln\left(\frac{2P}{d}\right) - \frac{5}{4} - \sum_{i=0}^{3} a_i \ln\left(\frac{2\pi r}{P}\right)^i\right] \tag{5.20}$$

Where the constants a_i are:-

a0 = 0.00070,

a1 = 0.17730,

a2 = -0.03220 and

a3 = 0.00197.

Since, in theory the output voltage of an integrating Rogowski coil is directly proportional to the current viewing resistor R_{CVR}, this resistance should have a very low inductance

otherwise the induced voltage in the coil will see an additional term L_{CVR} dI/dt, where L_{CVR} is the inductance of the $R_{CVR.}$

Continuing with equation (5.7), R_{CVR} as the terminating impedance Z, so that the transfer function that relates the voltage induced in the coil V_{coil} and the voltage measured in the coil terminals V_{out} can be further simplified as

$$\frac{V_{out}}{V_{coil}} = \frac{(R_{CVR} \left\| \frac{1}{S_C} \right)}{R_c + sL_c} \quad = \frac{R_{CVR}}{R_c + sL_c} \tag{5.21}$$

In the case of high frequency current measurement, the term sL_C will be much higher compared to R_C .So the transfer function can reduced to

$$\frac{V_{out}}{V_{coil}} = \frac{R_{CVR}}{R_c + sL_c} = \frac{R_{CVR}}{sL_c} \tag{5.22}$$

Replacing the voltage induced in the coil (V_{coil}) from the equation (5.4), so that the measured voltage V_{out} can be related to the current (*I*) to be measured

$$V_{out} = \frac{R_{CVR}}{sL_c} V_{coil} = \frac{R_{CVR}}{sL_c} MsI \tag{5.23}$$

From equation (5.23)

$$V_{out} = \frac{R_{CVR}}{L} MI = KI \tag{5.24}$$

The sensitivity (*k*) of the Rogowski coil is defined as the voltage generated by the Rogowski coil in measuring 1 A of current. The relation shown in equation (5.24) gives the sensitivity as

$$Sensitivity = k = \frac{\mu n a^2 R_{CVR}}{2bL} \tag{5.25}$$

5.2.2.1 Designing of Current viewing resistor (R_{CVR})

As mentioned in equation (5.13), the voltage output of an integrating Rogowski coil is directly proportional to the current viewing resistor R_{CVR}. Therefore, the measurement of current relies upon the voltage developed when the circuit current flows across the resistor.[95]

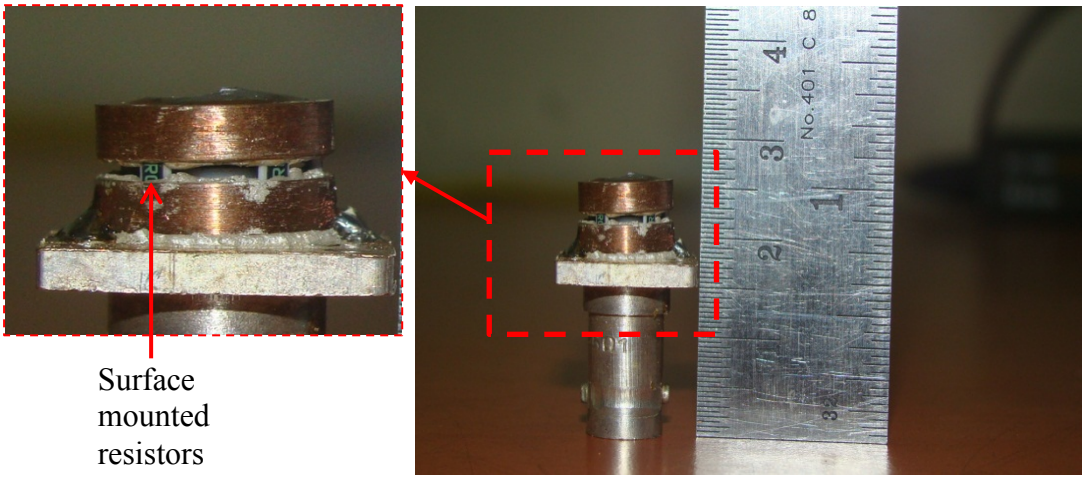

Figure 5.4 Geometrical view of Current viewing resistor

The arrangement of R_{CVR} is shown in Figure 5.4. This resistance should have a very low value to obtain the safe operating voltage at CRO end and low inductance to avoid the additional term L_{cvr} dI/dt in the induced voltage,. The low value of the R_{CVR} is achieved by placing the five surface mountable resistors in parallel to the central conductor of the BNC connector as shown in Figure 5.4. In the present case, two copper rings are used to hold the surface mount resistors. This provides the requisite resistance with a very low inductance.

In the present liquid dielectric breakdown characteristics study, it requires a self-integrating Rogowski for measuring the pre and post breakdown profiles. For this purpose, in the experimental setup (as discussed in chapter 4) the Rogowski coil is placed in a groove of the flange (shown in Figure 5.5 and Figure 5.6) between the diagnostic chamber and test chamber. The arrangement of Rogowski coil in experimental setup is shown in Figure 4.23

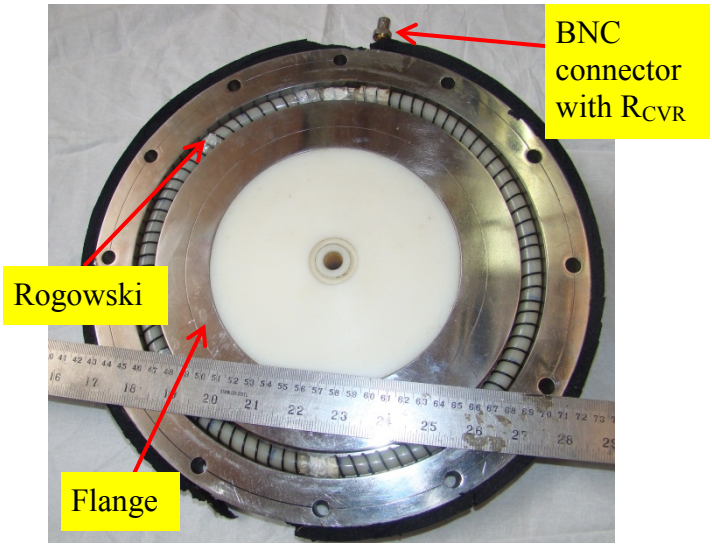

Figure 5.5 Arrangement of Rogowski coil in a flange

The calculated parameters of the present self-integrating Rogowski coil are listed in Table 5.2

Table 5.2 Design specifications of Rogowski coil

No. of turns	94
Pitch(P)	0.75 cm
Major radius(r)	11.5 cm
Minor radius(a)	0.75 cm
Wire diameter(0.1)	0.1 cm
Current viewing resistor(R_{CVR})	0.2 Ω
Inductance(L)	3.5 μH
Sensitivity (Theoretical)	1.62×10^{-3}
Sensitivity (Practical)	1.8×10^{-3}

5.3 Calibration of Rogowski coil

To calibrate the designed Rogowski coil, a capacitor of 1 nF is charged and discharged to the ground terminal through a conducting wire, which develops nanosecond oscillations. These

oscillations are measured with designed Rogowski and commercially available current transformer Bergoz instruments (model no FCT-016-20:1).sensitivity 1.25 V/A. The calibration waveforms are shown in Figure 5.7.

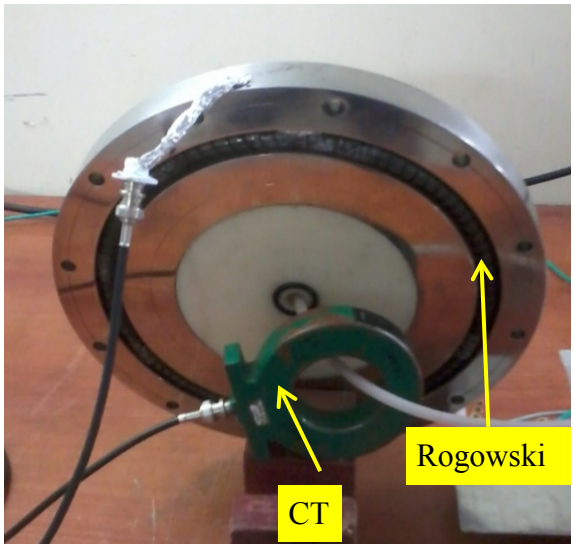

Figure 5.6 Rogowski coil experimental calibration using Pearson current transformer

Rogowski coil also has calibrated for micro second pulse using a commercially available current transformer (CT) (Pearson current monitor, model 101) having sensitivity of 0.01 V/A and rise time of 100 ns. The calibration waveform is shown in Figure 5.8

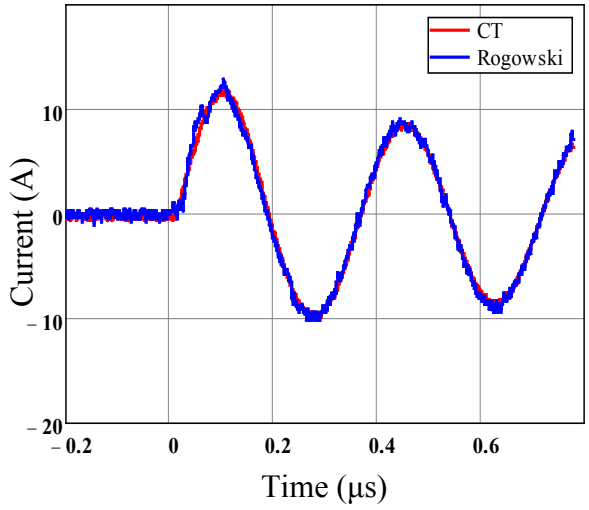

Figure 5.7 Rogowski calibration waveform for sub micro second pulse

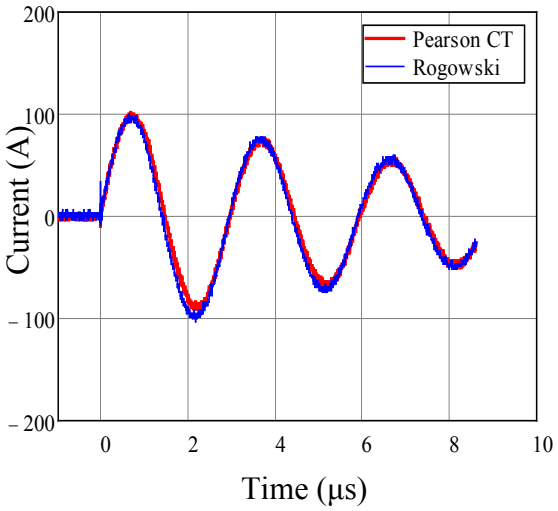

Figure 5.8 Rogowski calibration waveforms for micro second pulse

5.4 V-dot sensor

Owing to its structural simplicity and wide range of applicability, the resistive voltage divider is one of the widely used devices for the voltage measurements. In ideal case, it consists of two resistors, one acts as high voltage arm while other as low voltage arm from where output voltage is collected. However, in actual cases, circuit inductance and stray capacitance cannot totally be ignored. Therefore, it is essential that these components values must be as low as possible. In general, resistive voltage sensors are highly used for high voltage measurements by creating reference voltages, or by reducing the magnitude of a voltage and as attenuators at low frequencies. For direct and relatively low frequencies, a voltage divider may be sufficiently accurate if made only of resistors, whereas for frequency response over a wide range, a voltage divider may require capacitive elements[31][72].

The measurement of impulse voltage even of short duration present no difficulties, if the amplitudes are low or are in the kilovolt (kV) range. The tremendous development during last three decades in the technique of common CROs, digital scopes or transient recorders provide instruments with very high bandwidth and the possibility to capture nearly every kind of short-duration single phenomena. Although the usual input voltage range of these instruments is low, high voltage probes or attenuators for voltages up to some 10 kV are commercially available.

The problems arise with much higher voltage. It is well known that impulse voltages with magnitudes of the order of few megavolts (MV) are used for testing and research. The voltage dividers necessary to accommodate these voltages are specialized apparatus, and there are a few manufacturers throughout the world who are ready to produce such dividers with adequate accuracy. Self-provided constructions are often adequate if the problems are known.

Measurement of high voltage short pulse in non-intrusive way is one of the challenging tasks in pulsed power. Insulation and geometrical restrictions in high voltage systems make it difficult to access the high voltage points. A commercial available standard high voltage probe is limited to certain geometry and can measure up to few hundred of kVs. This necessitates a search for alternative measurement system for fast and high voltage pulses. The objective of the present work is to provide a lossless and convert high amplitude impulse voltage signal to a low voltage capable of being measure by oscilloscopes. Therefore, in order to measure fast and very high voltages, a V-dot sensor is developed. Its working principle, design, fabrication, etc., are explained in the following sections.

In this work, two capacitive voltage sensors are developed for measuring voltage at Pulse forming line (PFL) and applied voltage across test chamber. For this, suitable capacitive voltage sensors are designed and fabricated. In this, to measure the voltage across the pulse forming line, the sensor (Voltage sensor 1) is mounted on PFL itself, whereas to measure the voltage across the test chamber (voltage sensor 2) an additional chamber i.e. diagnostics chamber is used and placed before the test chamber.

5.4.1 Working principle

The sensors have a coaxial structure, with a central electrode and an outer case in cylindrical geometry. An insulator separates the electrodes and the sensor is mounted on the pulse forming line or coaxial cylinder, as shown in Figure 5.9. An equivalent electrical circuit is presented in Figure 5.10, where C_1 is the capacitance between the sensor and the high voltage point and C_2 is between the central electrode and the outer case of the sensor. R_1 is a resistor attached to the sensor (which is zero in this work due to directly shorting the sensor to the output terminal) and R_2 is the terminating resistance at the oscilloscope, which is 50 Ω in the present case.

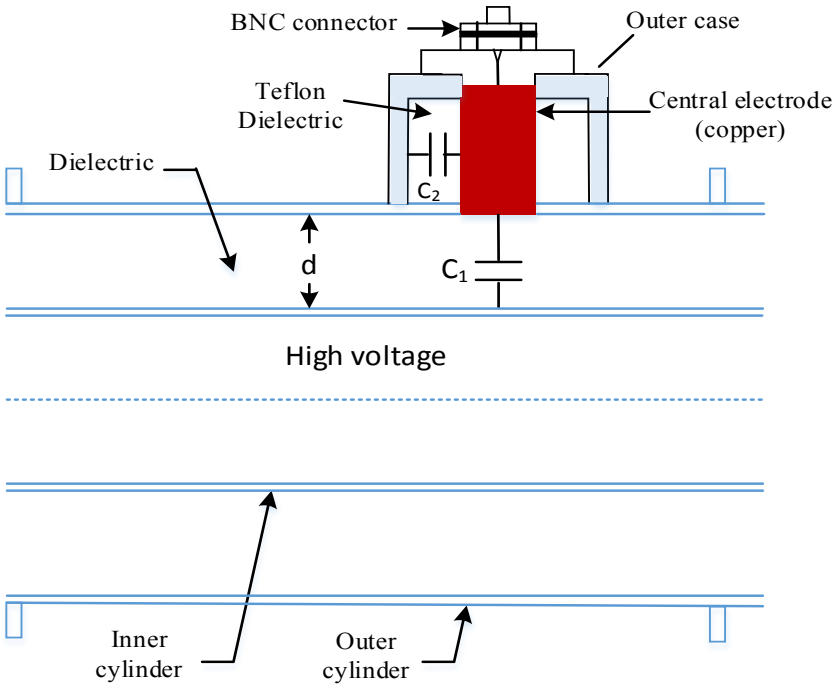

Figure 5.9 Capacitive voltage sensor geometrical arrangement on coaxial cylinder

5.4.2 V dot mode of operation

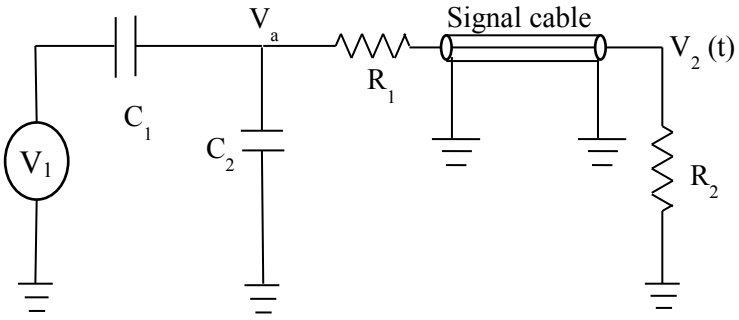

Figure 5.10 Electrical equivalent circuit of V dot sensor

If V_1 (t) is the input voltage and V_2 (t) is the output voltage of the sensor, then from Figure 5.10 it follows

$$C_1 \frac{d(V_1 - V_a)}{dt} = C_2 \frac{dV_a}{dt} + \frac{(V_a - V_{2)}}{R_1} \tag{5.26}$$

$$\frac{(V_a - V_2)}{R_1} = \frac{V_2}{R_2} \tag{5.27}$$

$$V_a = V_2 \frac{(R_1 + R_2)}{R_2} \tag{5.28}$$

$$C_1 \frac{dV_1}{dt} = \frac{V_2}{R_2} + (C_1 + C_2) \frac{R_1 + R_2}{R_2} \frac{dV_2}{dt} \tag{5.29}$$

If $R_1 + R_2 = R$

and

$C_1 + C_2 = C$

Then equation (5.29) can be written as

$$\frac{R_2 C_1}{RC} \frac{dv_1}{dt} = \frac{dV_2}{dt} + \frac{V_2}{RC} \tag{5.30}$$

If RC is very small in equation (5.30), then $\frac{dv_2}{dt}$ term can be neglected, then the output voltage V_2 becomes proportional to $\frac{dV_1}{dt}$, which means the sensor operates in the so-called 'V-dot' mode.

Thus, the equation (5.30) can be re-written as

$$\frac{dV_1}{dt} = \frac{V_2}{R_2 C_1} \tag{5.31}$$

If RC is $\gg \tau_{rise}$ then the sensor wil operate in capacitive divider mode as discussed in reference[96]

5.4.3 Criterion for the voltage sensor

Complete geometrical view of individual parts of the capacitive voltage sensor is shown in Figure 5.11. To explain in more detail, the criterion for a voltage sensor[97][24] to work

satisfactorily, the conditions that must be met are discussed in this section. In this voltage sensor is installed on a coaxial line.

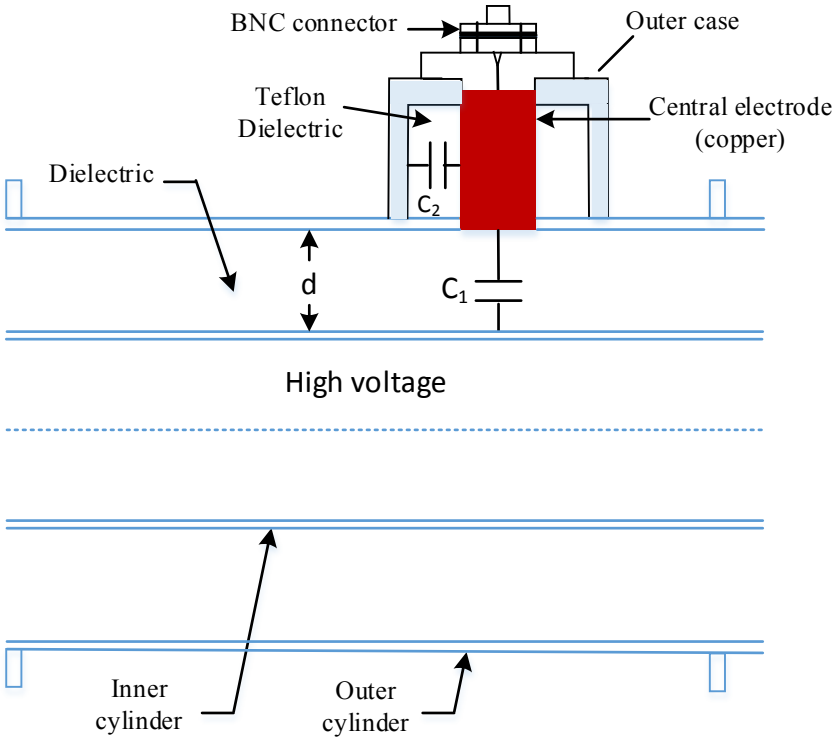

Figure 5.11 Capacitive Voltage sensor schematic

(i) The spatial variation of the field should be such that all information concerning voltage rise time, etc. reaches the sensor without distortion**,** i.e. $d \ll \frac{\tau_{rise} C}{\sqrt{\varepsilon_r}}$ where $\boldsymbol{\tau_{rise}}$ is the rise time of the high voltage pulse, ε_r is the dielectric constant of medium and d is the distance between high voltage surface and the voltage sensor.

(ii)The conductivity of the dielectric medium can be represented as a resistance shunting the coupling capacitance C_1 and therefore the sensor gives an accurate measurement only for a time less than RC product for the medium, where R is the effective resistance offered by the medium from sensor to high voltage point and $C = C_1$. This time alternatively can be

written as $\tau_{medium} = \varepsilon_r \varepsilon_o \rho$, where ε_r is the dielectric constant and ρ is the resistivity of the dielectric material. In present case water ($\varepsilon_r = 78$), having resistivity (ρ) of 2 MΩ cm is used as a dielectric medium

(iii) $(R_1 + R_2).(C_1 + C_2) << \tau_{rise}$ for the probe to work in a differential mode.

The voltage sensors are designed by considering the above-mentioned criteria to work in V-dot mode. The main parameters for the voltage sensors at pulse forming line (voltage sensor 1) and diagnostic chamber (voltage sensor 2) are as mentioned in Table 5.3

Table 5.3 Electrical parameters of the voltage sensors used in the experiments

Voltage sensor parameters	**Voltage sensor-1 at Pulse forming line**	**Voltage sensor-2 at Diagnostics chamber**
C1	1.122×10^{-12}	5.677×10^{-13}
C2	5.474×10^{-12}	5.225×10^{-12}
Calibration factor	1.197×10^{10}	6.4×10^{10}

5.4.4 Calibration of V-dot probe

The designed capacitive voltage sensors are calibrated by using two different commercially available standard probes (i) Tektronix voltage probe, P6015A model, 75 MHZ bandwidth and voltage attenuation ratio 1000X, 40 kV rating (ii) Tektronix Tek P5100A, 500MHz bandwidth, 100X voltage attenuation, 2.5 kV rating.

The output voltage across the pulse forming line of the Tesla based pulse generator is measured with commercially available voltage probe P6015A and designed voltage sensor. The oscilloscope screen shot for voltage waveform is shown in Figure 5.12. It can be

observed that the voltage waveform of sensor is 90^{o} out of phase with standard probe waveform, indicates the V-dot mode of operation of the sensor.

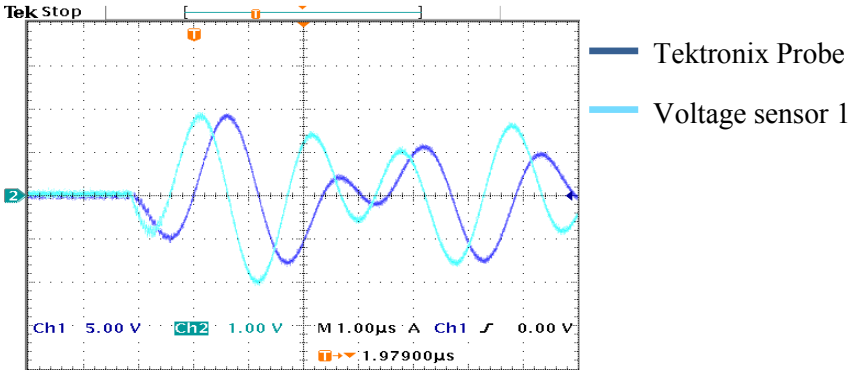

Figure 5.12 Voltage (dv/dt) across Voltage sensor 1

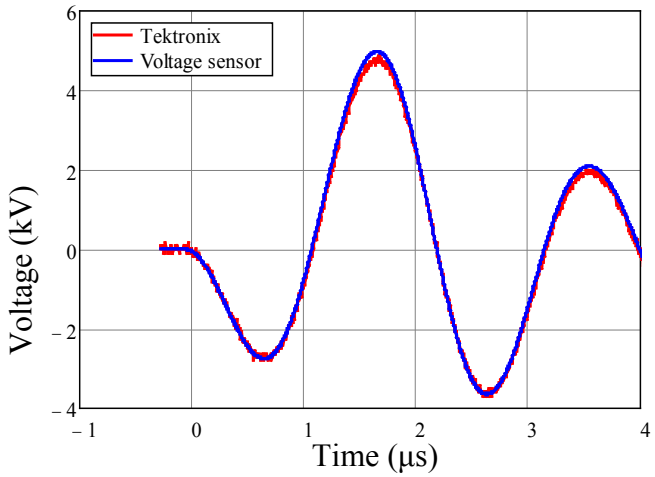

Figure 5.13 Original waveform of voltage sensor after integration

In this, differential signal is integrated by using computational software to get the actual voltage. The integrated voltage waveform for V-dot sensor 1 is shown in Figure 5.13.

Further, the voltage sensor-2 is calibrated for various voltage pulse duration, rise time and amplitudes as shown in Figure 5.14. The calibration results from the Figure 5.14 confirm reliable working of voltage sensor-2 for various pulse durations.

The performance of voltage sensor is further verified using PSPICE simulation software.

Figure 5.15 shows the electrical equivalent circuit used for simulation and results. The calculated electrical parameters for voltage sensor-2 are used in the simulation. The dv/dt output is further integrated and multiplied by the calibration factor to reproduce the voltage. The simulation results further confirms the reliable performance of voltage sensors.

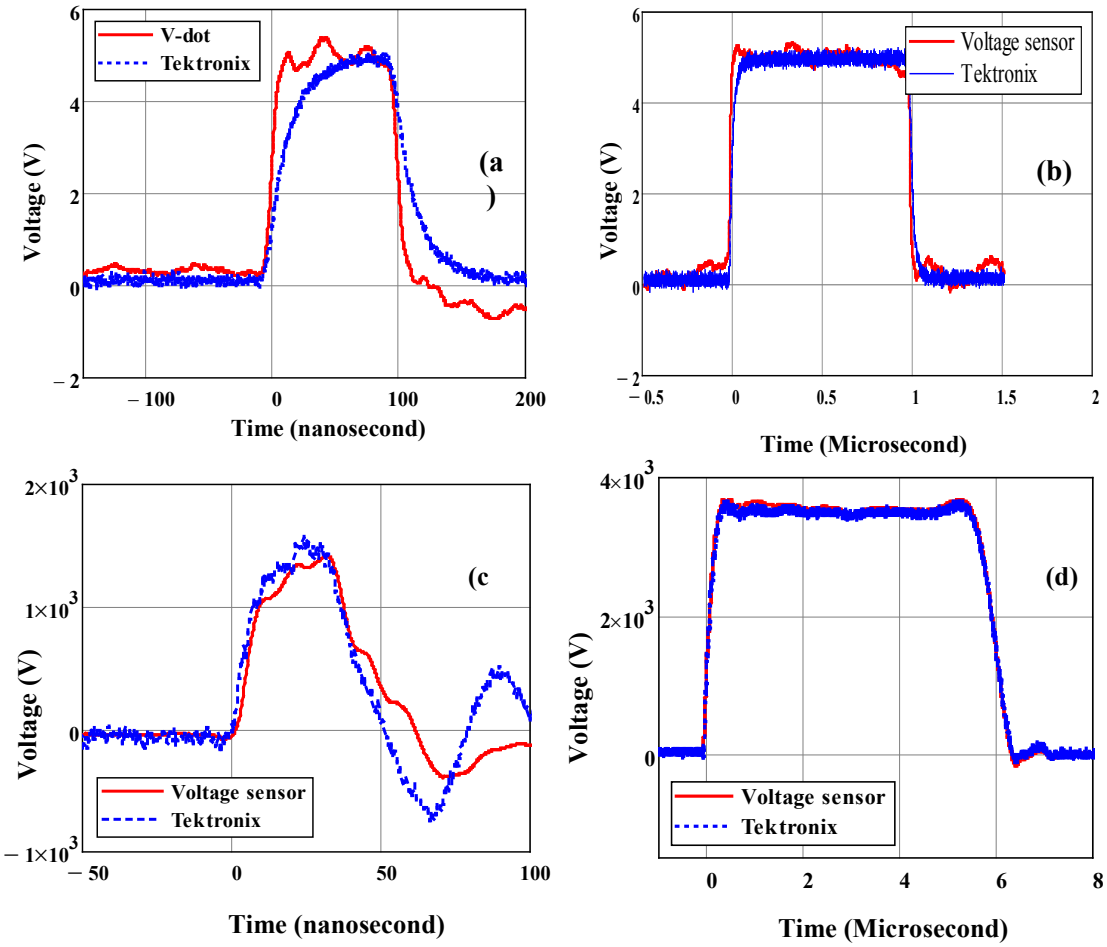

Figure 5.14 Calibration of voltage sensor -2 with various pulse duration, amplitude and rise times. (a) and (b) for 5 V TTL pulse for nanosecond and microsecond pulse durations respectively. (c) and (d) for 1.5 kV and 3.5 kV for nanosecond and microsecond pulse durations respectively.

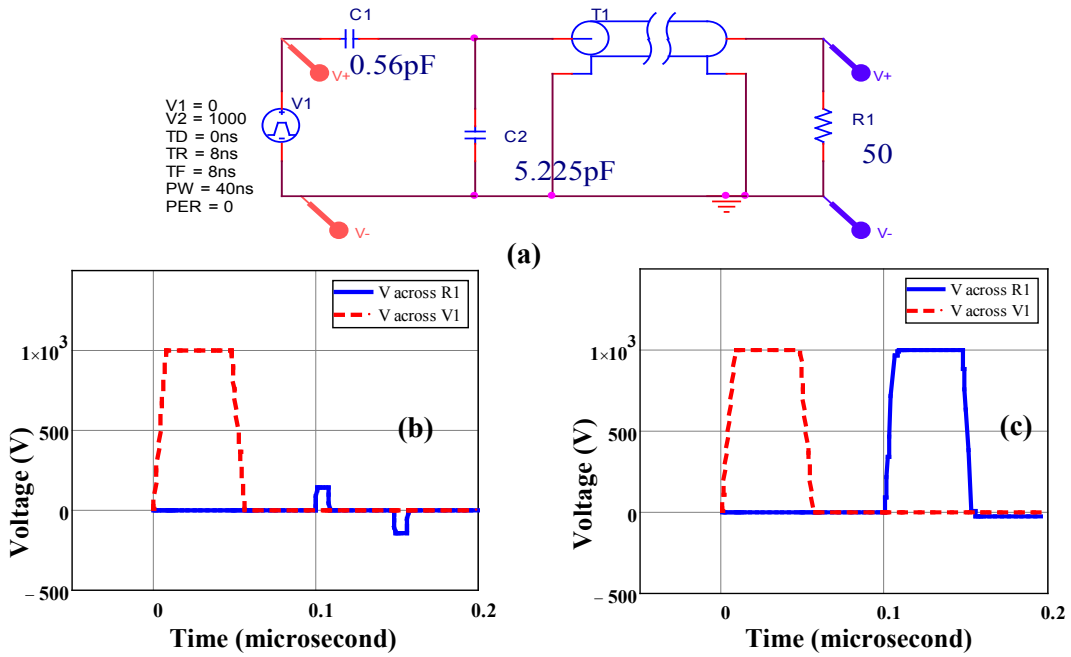

Figure 5.15 PSPICE simulation (a) Electrical circuit used for simulation (b) input and output (dv/dt) voltage and (c) Input and integrated output voltage

The geometrical views of diagnostics chamber used in the experimental setup is shown in Figure 5.16.

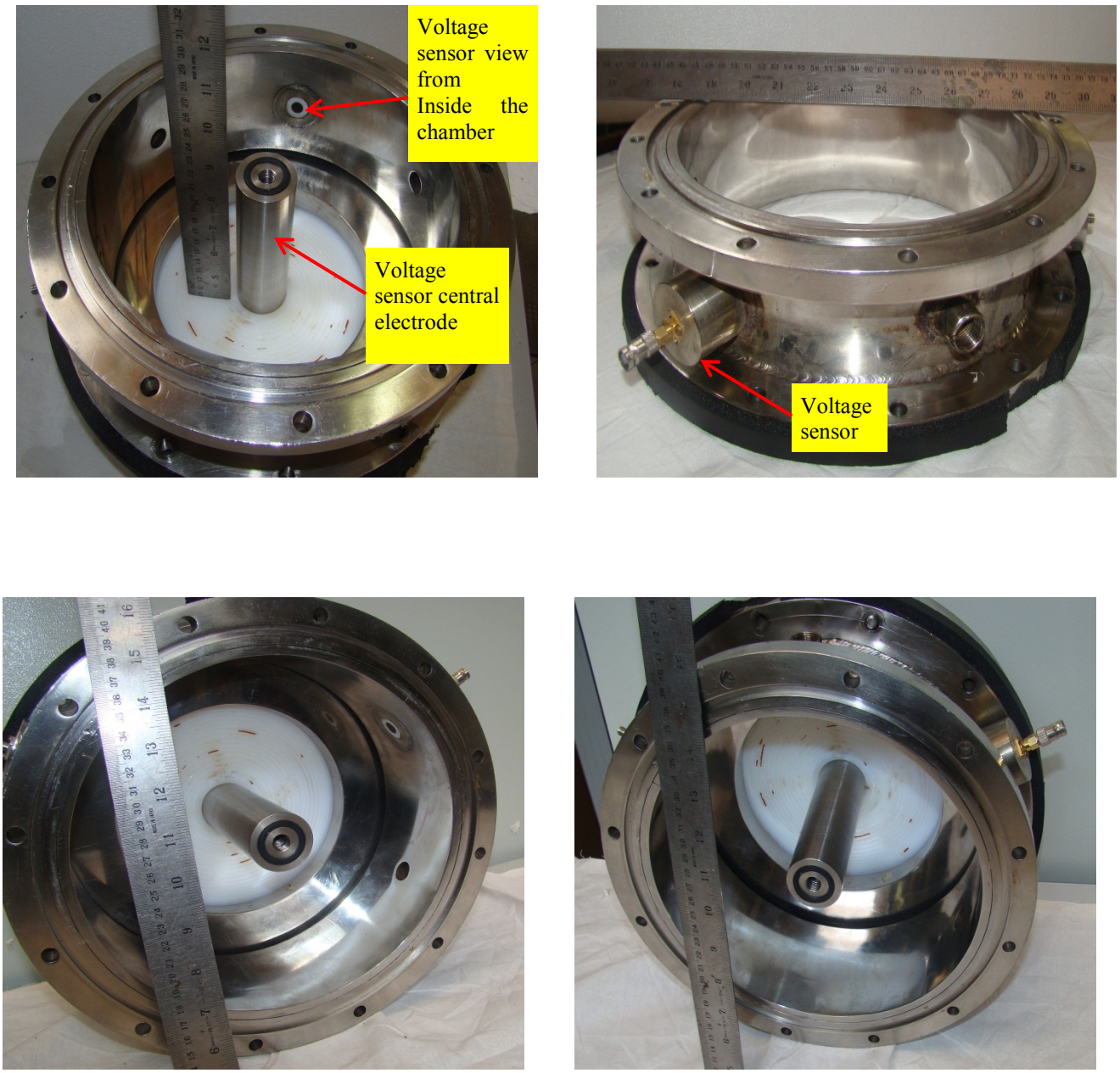

Figure 5.16 Geometrical views of diagnostics chamber

Arrangement of two voltage sensors, one is at PFL and other at diagnostics chamber is shown in Figure 5.17.

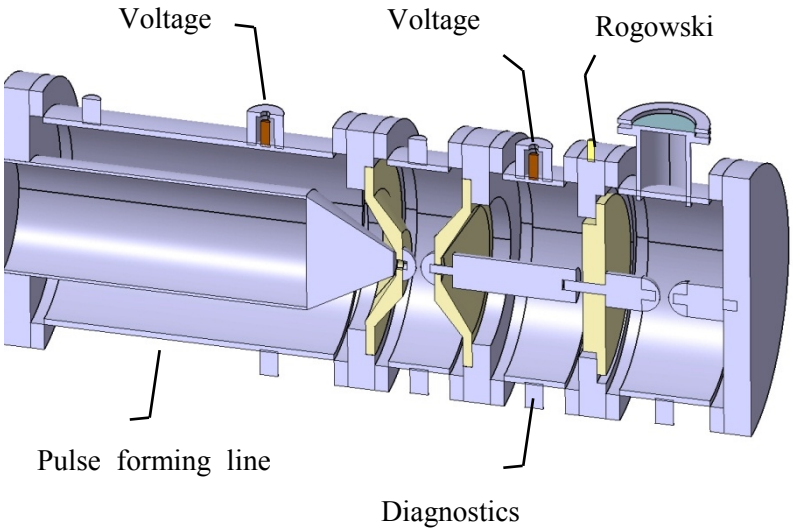

Figure 5.17 Section view of voltage sensors arrangement in Experimental

5.4.5 Analysis of experimental voltage and current profiles

Figure 5.18 shows the comparison of experimental waveform across the PFL (with electrical breakdown in the water (ε_r =80) filled test chamber) and the theoretical simulated output voltage of Tesla parameters. This confirms the experimental results are well in agreement with those of simulation outcome.

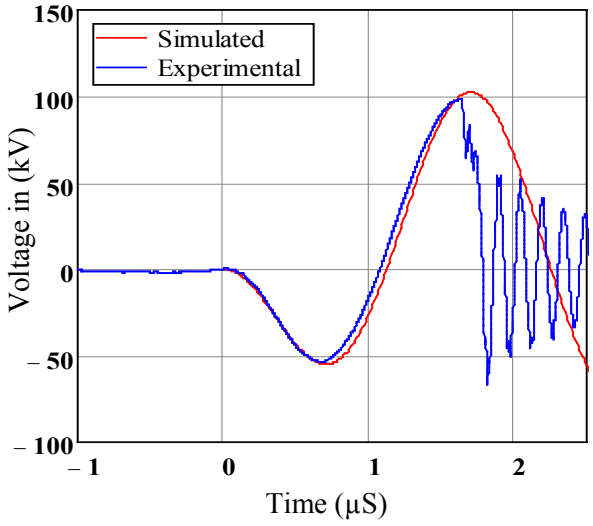

Figure 5.18 Comparison of experimental and theoretical output voltage across PFL

Figure 5.19 shows the combined plot of experimental output voltage waveforms obtained at Voltage sensor 1 and 2, during electrical breakdown in deionized water filled test chamber.

Individual plots for voltage sensor 1 and 2 are in shown in Figure 5.20 . The oscillations in the voltage waveform are due to two capacitances formed across the electrodes of spark gap switch and the test chamber electrodes.

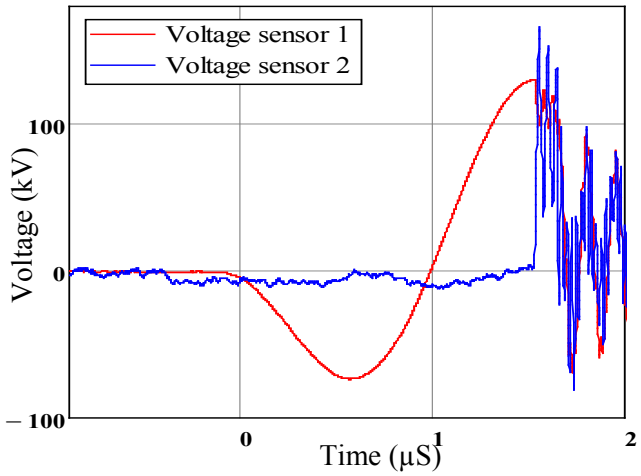

Figure 5.19 Experimental voltage waveforms with water breakdown in the test chamber

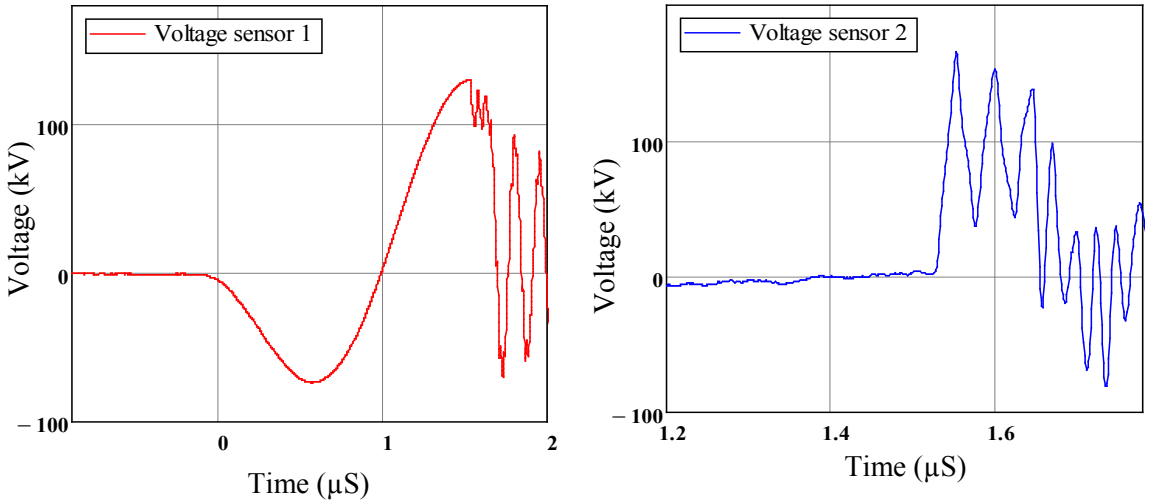

Figure 5.20 Typical voltage profiles across voltage sensor 1 and 2 during electrical breakdown in the deionized water filled test chamber

Figure 5.21 shows the typical voltage and current waveforms at test chamber during electrical breakdown of water. It is seen that the voltage is sustained for finite duration (t_P). The sudden sharp rise in the current waveform indicates the event of breakdown.

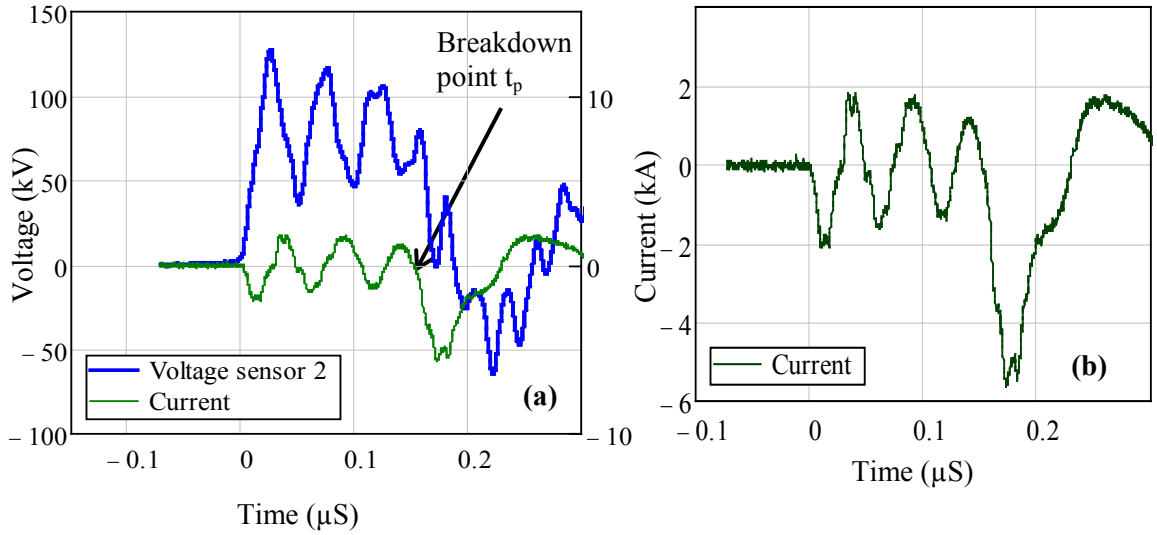

Figure 5.21 (a) Typical voltage and current profiles at test chamber during electrical breakdown of water in the test chamber, (b) current waveform

Figure 5.22 shows the typical voltage waveforms across the PFL (voltage sensor 1) and Test chamber (voltage sensor 2) for negative polarity voltage applied across the test chamber electrodes.

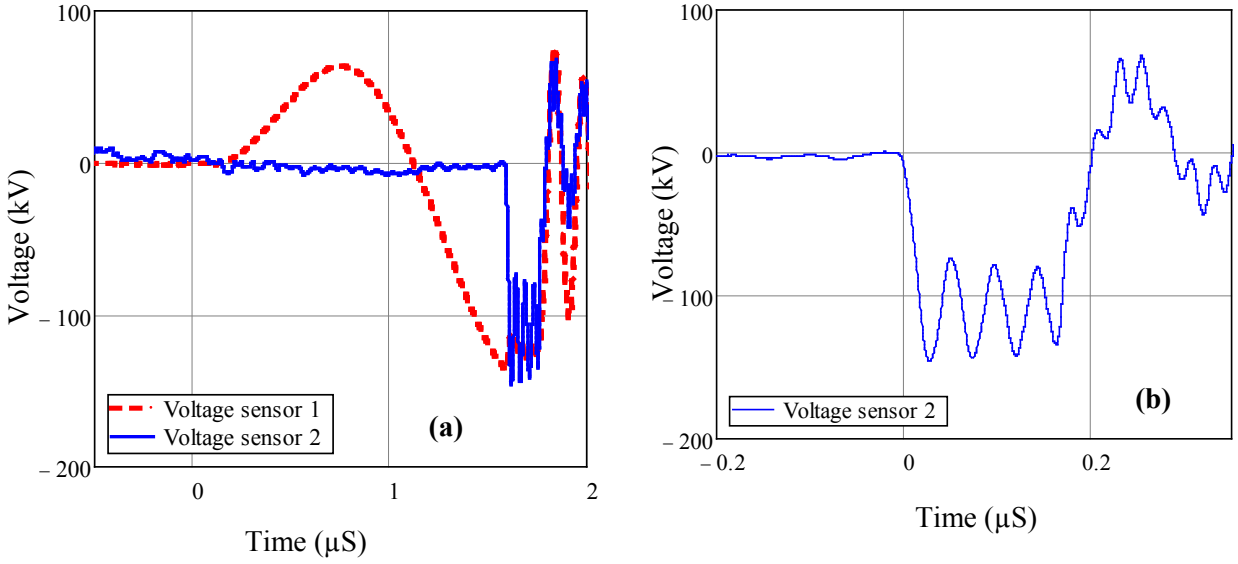

Figure 5.22 Typical experimental voltage profiles with water filled test chamber (a) Voltage profiles across the PFL (Voltage sensor 1) and at test chamber (Voltage sensor 2) on same time scale, (b) typical voltage profile across test chamber.

Further, the experimental voltage waveforms are verified by using PSPICE (student version 9.1) simulation software. The electrical equivalent circuit for the experimental setup is shown in Figure 5.24.

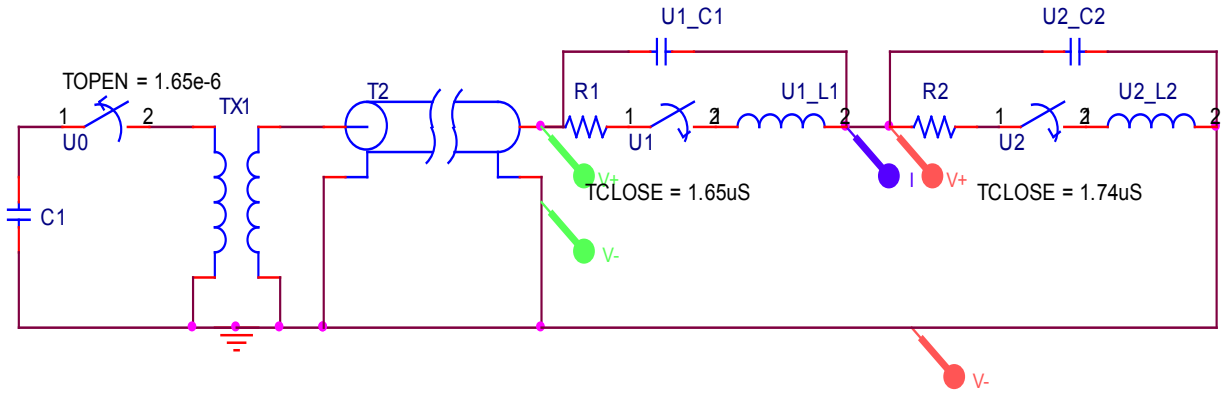

Figure 5.24 Electrical equivalent circuit of experimental setup used in PSPICE software

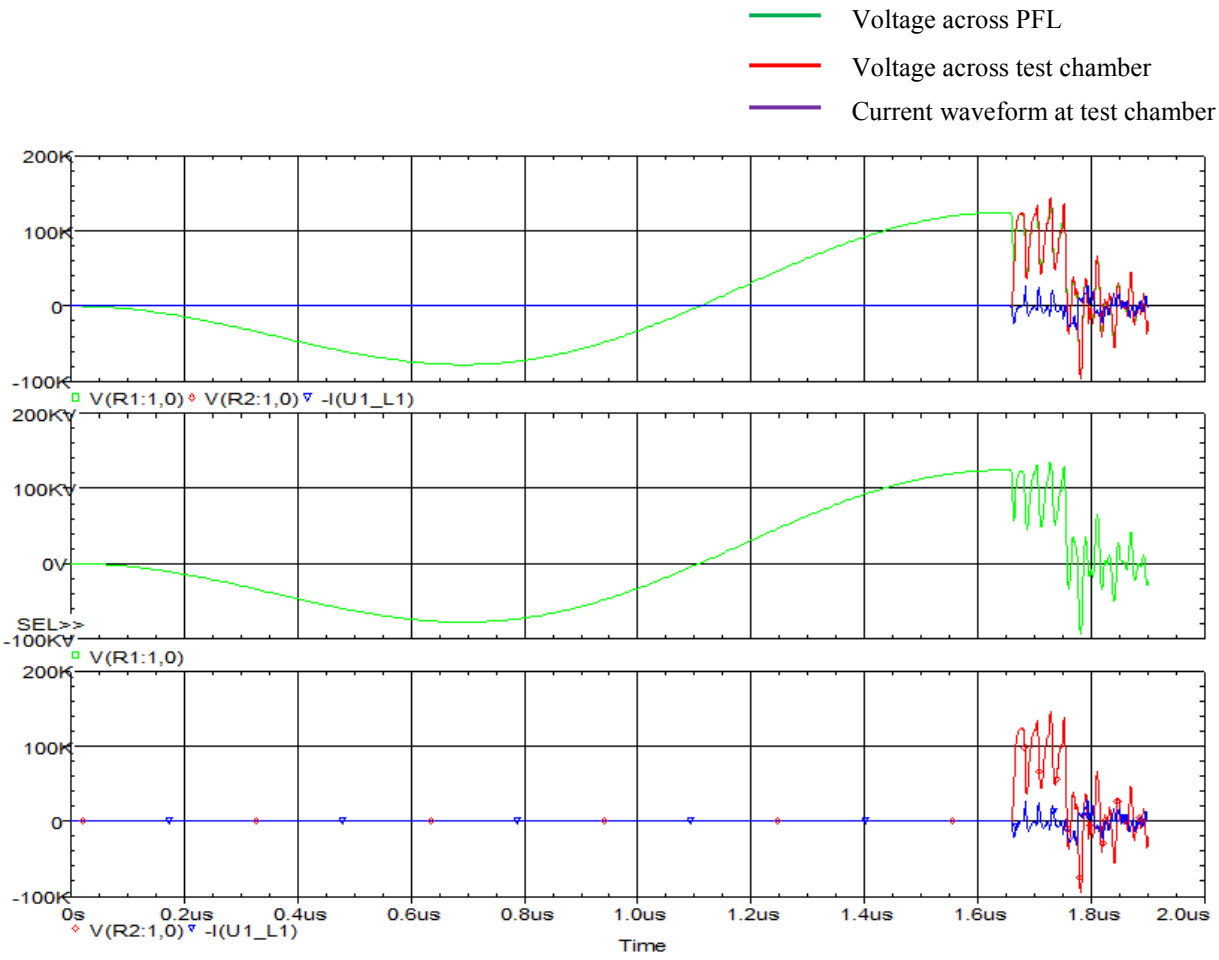

Figure 5.24 Simulation output voltage waveforms of voltage sensors and current waveforms

The switching time of spark gap switch and load (test chamber is modeled as a switch) are controlled by using voltage controlled switches. The capacitances of spark gap switch and test chamber electrodes estimated through Ansys 2D (student version) software. The voltage across PFL (transmission line in simulation) and across the test chamber are shown in Figure 5.24. All the simulation output voltage and current profiles are well in reasonable agreement with the experimental results. The oscillations in the voltage waveforms are due to the capacitances formed across the spark gap chamber and test chamber.

5.5 Optical diagnostics

Further, in our studies, to analyze the experimental results, we have also used optical diagnostics viz., emission spectra, absorption spectra and ICCD camera.

5.5.1 Emission spectra

In physics, it is the continuous spectrum or pattern of bright lines or bands seen when the electromagnetic radiation emitted by a substance is passed into a spectrometer. The spectrum is characteristic of the emitting substance and the type of excitation to which it is subjected[98].

In other source, it is defined as the pattern of dark lines and colors made when electromagnetic energy, such as light, passes through a substanc and excites its atoms. The excited atoms give off energy in the form of light. Because each type of atoms gives off light having a unique range of colors, the emission spectrum can be used to determine the substance's chamical composition.

Therefore, the emission spectra is the result of the electron dropping from an excited state to the lower state. And the energy of emission is as discrete amount of energy corresponding to the difference between two electronic level. Also, since there are usually a number of electronic levels to which an electron in an atom can be promoted, there are a number of

possible discrete energy jumps back to the lower energy states. These represent a number of distinct wavelengths of light to be emitted. Each kind of atom is different in terms of the separation between energy levels and the line emission spectra are therefore different.

The primary goal is to investigate the early development of the plasma channel to detect any mechanism that contributes in the development by given knowledge of well-defined emission lines and transitions. In this work the role of electrode material during the discharge process in the liquid dielectric medium (ex: water) explored. The details of spectra will be discussed in chapter 5 and 6. For this purpose, 0.5 m visible spectrometer (Princeton Instruments, model no. SP 2500i) operated with 600 grooves/mm grating is used. The spectrometer is having reciprocal linear dispersion of 3.2 nm/mm and gives a wavelength coverage of 85 nm when coupled to a CCD (Andor Technology, model no. DU440BU) having 2048 x 512 no. of pixel. Light was collected though a chord viewing both the electrodes and water in between them.

5.5.2 Absorption spectra

In physics, the absorption spectra is the characteristic pattern of dark lines or bands that occurs when electromagnetic radiation is passed through an absorbing medium into a spectroscope. An equivalent pattern occurs as colored lines or bands in the emission spectrum of that medium.

The pattern of dark lines and colors made when the light passes through an absorbing medium, such as a gas or liquid. The dark lines represent the colors that are absorbed. Because each type of atom absorbs a unique range of colors, the absorption spectrum can be used to identify the composition of distant substances, such as the gaseous outer layers of stars.

In our work, Fourier transform infrared spectroscopy (FTIR) [99]is used to identify the signatures of chemical compounds and substantial groups in the pre and post breakdown

samples of liquid dielectric medium. Thermo scientific, Nicolet-6700 model FTIR spectrometer is used for this purpose. FTIR is a technique, which is used to identify the signatures of chemical compounds and substantial groups in the sample. Spectra have been performed with resolution 4 cm^{-1} and wave number range from 650-4000 cm^{-1} on the original as well as post treated liquids.

5.5.3 Intensified CCD (ICCD)Camera

Intensified CCD's are also cameras, which can exploit gain to overcome the read noise limit but also have the added feature of being able to achieve very fast gate times. The gating and amplification occurs in the image intensifier tube[100].

The Image intensifier tube is an evacuated tube which comprises the Photocathode, Micro channel plate (MCP) and a Phosphor screen, and the properties of these determine the performance of the device.

The output of the image intensifier is coupled to the CCD typically by a fiber optic coupler. Fiber coupled systems are physically compact with low optical distortion levels. The high efficiency fiber optic coupling means that the image intensifier can be operated at lower gains, and this in turn results in better dynamic range performance from the image intensifier (better than 15 bit).

ICCD cameras are used in spectroscopy and imaging applications involving transient phenomena at ultralow-light levels. Detection and time resolution of low light are two unique strengths of ICCDs. Low-light detection is achieved by high amplification of incoming photons by the intensifier, whereas time resolution is possible due to the fact that the intensifier can be switched on and off (gated) in very short intervals.

Further to understand the process of discharge initiation and propagation in liquid dielectric medium in between the electrodes of the test chamber single shot fast camera (Stanford

computer optics, 4Picos model) is used. The obtained images will be of help in understanding the inherent breakdown mechanism in the water as discussed in the chapter 8.

5.6 Other diagnostics

5.6.1 Conductivity meter

In order to understand the discharge breakdown characteristics, conductivity measurements were carried out on the original and post treated liquid samples. Eutech Cyber scan PC 300 model conductivity meter was used for this purpose. The conductivity meter had accuracy (±1 % Full Scale + 1 digit)[101], which gives measurement error ± 0.21 μS/cm Prior to the measurement on each sample, the meter was calibrated using standard calibrating liquids

5.7 Summary

In this chapter, designed self-integrating Rogowski coil is discussed, its working principle, designing and calibration for nanosecond and micro second pulse details are demonstrated. The capacitive voltage sensor for measurement of nanosecond high voltage pulse is presented. In this work, two sensors are used. The working principle, mode of operation, designing and calibration are discussed. Further, the optical diagnostics such as emission, absorption spectra and ICCD camera are introduced which are used for analyzing the experimental data. The details of conductivity meter for measurement of pre and post breakdown conductivity are given.

Chapter 6
Water breakdown properties

6 Introduction

As discussed in the chapter 2, considering the advantages of liquid dielectrics for development of high voltage compact pulsed power applications, in this work an attempt has been made to experimentally study the breakdown behavior of liquids especially deionized water.

The advantage of deionized water dielectric properties such as high dielectric constant (ε_r =78) and moderate dielectric strength (in comparison to transformer oil) makes the most suitable for developing the compact pulsed power systems.

6.1 Water properties

The higher relative permittivity (ε_r) of water is due to the consequence of correlations between the permanent dipoles in the closely related hydrogen-bonded network [102][103]. An additional factor contributing to the high value of ε_r is the collective polarization. A water molecule has an appreciable polarizability and the short-range anti ferroelectric order arising from the hydrogen bonding induces a finite average electronic moment pointing along the direction of the permanent dipole. Experimental estimates indicate that the average total dipole moment is increased from 1.85 D in the gas phase to 2.6 D in ice[102]. The value in the bulk liquid is most likely not much lower than this. The structure of water and the hydrogen bonds are shown in Figure 6.1 (a) and (b).

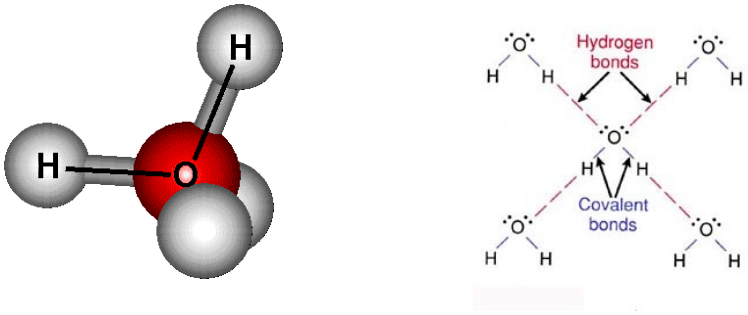

(a) (b)

Figure 6.1 (a) The structure of water, (b) shows the hydrogen bonds

The key feature of liquid water is the hydrogen bonding of a molecule and its four nearest neighbors[104]. There is ample evidence from experiment for this local tetrahedral structure in the liquid. Closely related to the hydrogen bonding is another important property, the dielectric constant (ε_r) which is considerably higher for water than for non-associative liquids with comparable (gas phase) dipole moments.

De-ionized (DI) water is mechanically filtered or ionic mineral salts removed (in various fashions) such as cations like sodium, calcium, iron and copper, and anions such as chloride and sulfate[105]. De ionization is a chemical process that uses specifically manufactured ion-exchange resin, which exchange hydrogen and hydroxide ions for dissolved minerals, and then recombine to form water.

Dielectric breakdown properties of water depend on many other parameters like electrode material, temperature, applied pulse duration and polarity[38][31], etc. Various studies have been made considering these parameters but the findings and conclusions are not very clear.

Further understanding the breakdown properties of deionized water (ε_r = ~ 78), experiments are performed in nanosecond regime. The analysis of breakdown in nanosecond regime may be of significance as it may aid in understanding the inherent close packed features of water dielectrics. Understanding the breakdown process in deionized water may lead to further improvement in its dielectric properties.

In this work the effect of electrode material, and distance between the electrodes are analyzed. Further, the effect of electrode material on deionized water breakdown properties is attempted to analyze via emission spectra during discharge.

6.2 Experimental procedure

Experiments are performed[90] with deionized water ($\varepsilon_r \sim 78$ at room temperature ~ 26^{o}C) as a dielectric medium in the test chamber using Tesla based pulse generator. The experimental conditions are uniform electric field and pulse duration of tens of nanosecond. In this, hemisphere electrodes of diameter 44, 42 millimeter, are used which makes the inter electrode gap as 6 mm, 8 mm respectively. The conductivity of water is maintained at 0.45 µS/cm with continuous circulation of water through deionizer plant.

Voltage is applied in incremental steps in steps of tens of kilo volts until the breakdown occur in the water. Then the breakdown strength (E_B) is defined as the maximum stress experienced without breakdown for a series of tests (for the present case 10). Initially the experiments are performed with pair of stainless steel (SS 304) electrodes, with 6, 8 mm gap between the electrodes. The same sets of experiments are repeated with pair of brass electrodes for same experimental conditions.

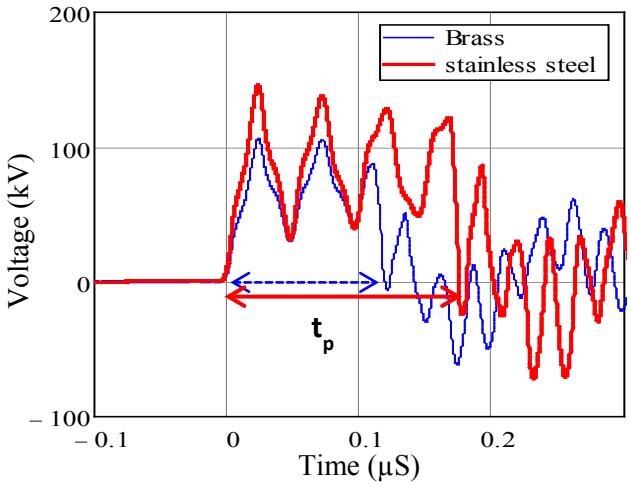

Figure 6.2 Voltage waveform vs time for 6 mm inter electrode gap

6.3 Observations

The experimental observations are shown in Figure 6.2 and Figure 6.3 obtained from both the cases suggest that the stainless steel electrodes hold more charge and for long duration compared to brass electrodes. Figure 6.4 shows the variation of breakdown voltage for number of shots for all the experimental parameters.

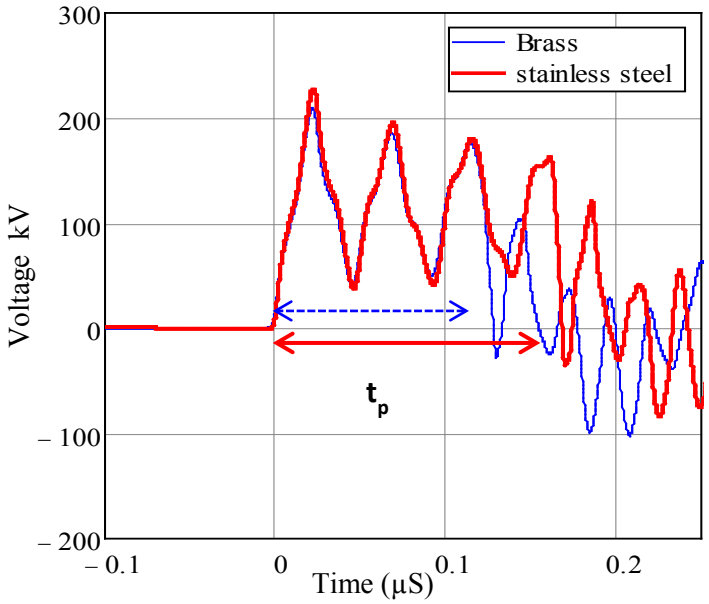

Figure 6.3 Voltage Vs. time plot for 8 mm inter electrode gap

Based on the experimental results, it is observed that water show satisfactory with the stainless steel (SS) as electrode material compared to the brass material. It is also observed that, in case of SS electrode material charge hold for long duration compared to brass electrode material.

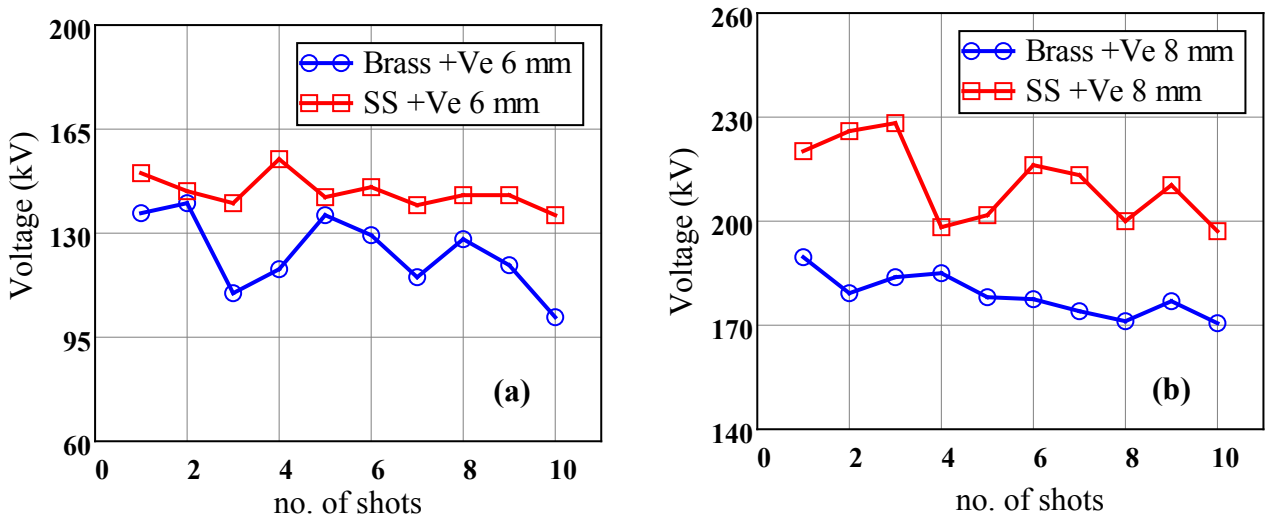

Figure 6.4 Voltage vs no. of shots. Brass and SS (a) for 6 mm (b) for 8 mm inter electrode gap

The voltage vs no of successive breakdown shots data for all the experiments are presented in the Figure 6.4.

Further understanding of effect of electrode material on breakdown properties, emission spectra is used. In this, 0.5 m visible spectrometer (Princeton Instruments, model no. SP 2500i) operated with 600 grooves/mm grating is used. The spectrometer is having reciprocal linear dispersion of 3.2 nm/mm and gives a wavelength coverage of 85 nm when coupled to a CCD (Andor Technology, model no. DU440BU) having 2048 x 512 no. of pixel. Light was collected though a chord viewing both the electrodes and water in between them. The spectra obtained for 400-700 nm range collected from four similar discharges.

In case of brass, the spectra as shown in Figure 6.5 the presence of copper (Cu) and Zinc (Zn) ions in the test sample whereas Iron (Fe) ions Figure 6.6 with SS electrodes during discharge. In this the prominent visible lines are identified with help of NIST [106] database. Zahn et al.[107][108][109][110] have observed that, Cu is the probable injector of positive ions and Zn injects negative charges in to the test sample under micro second discharges and the same also observed in our very small applied pulse durations (i.e. nanosecond scales). In case of stainless steel, the positive charge due to the Fe ions may result in a shielding effect at

electrode (anode) surface, which aids in the reduction of the field [111]. Hence, the discharges with SS electrodes withstand high voltage. It is not clear in case of discharges with brass electrodes, whether the presence of Cu ions is at the anode or at the cathode. However, we speculate that, the presence of Zinc i.e. negative ions at anode might have resulted in a field enhancement at anode, leading to a lower voltage breakdown. Based on the results obtained with optical and electrical diagnostics, it is understood that discharges with SS electrodes show enhanced voltage withstand capacity for the nanosecond pulsed conditions in comparison to discharges with Brass electrodes.

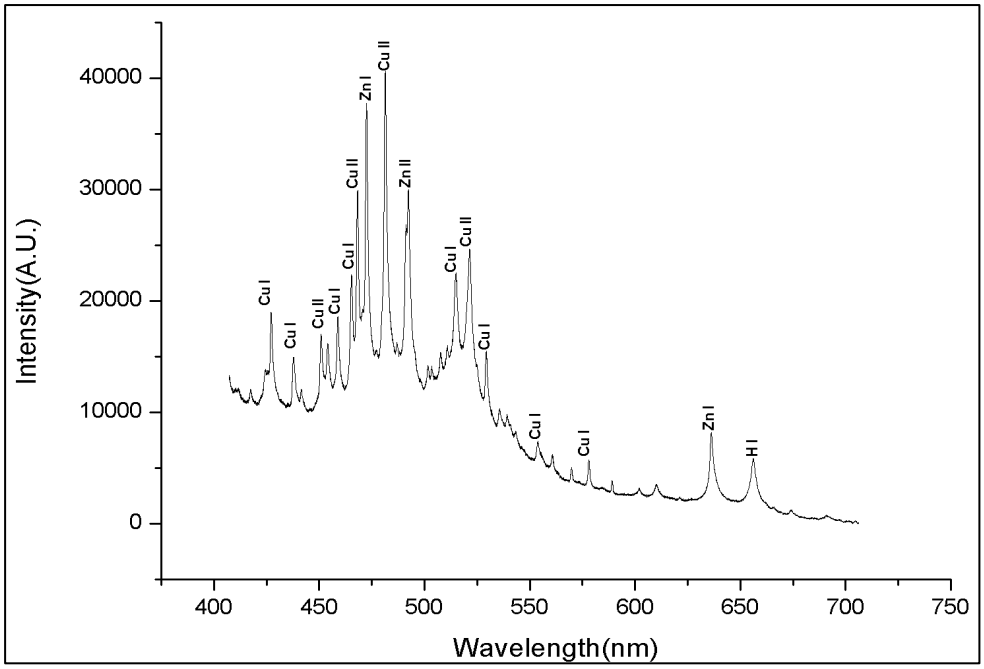

Figure 6.5 Emission spectra for discharge in water with brass as electrode material

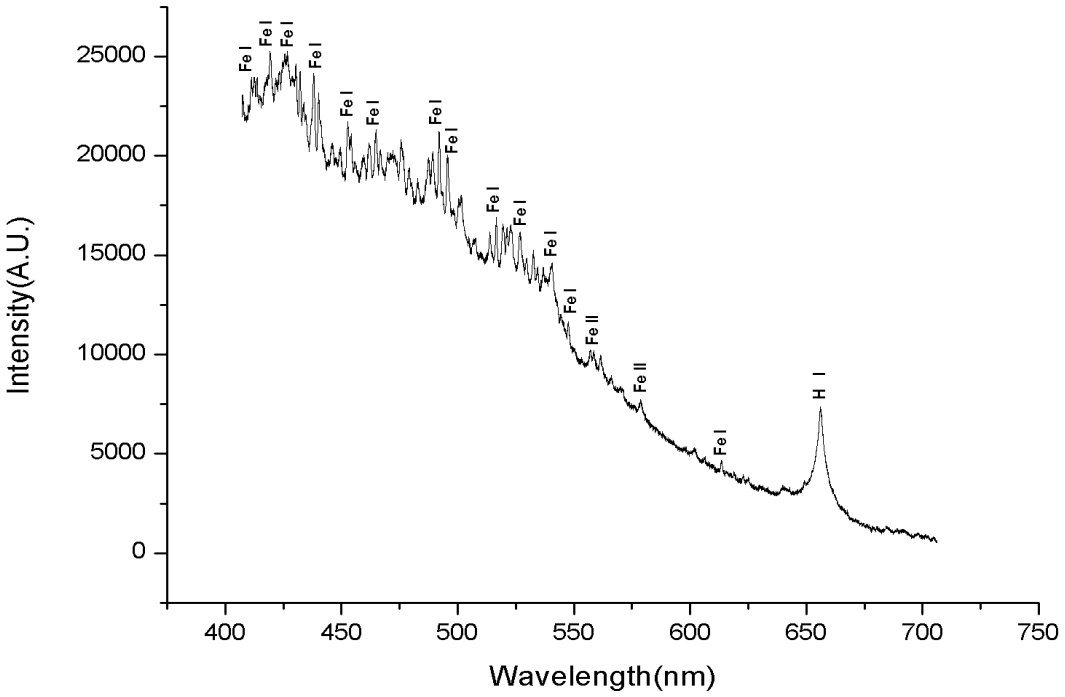

Figure 6.6 Emission spectra for discharge in water with stainless steel as electrode material

Further, the effect of inter electrode gap is studied. In this work, 6 mm, 8 mm inter electrode gap are made using the 46, 44 mm diameter electrodes. The 3 mm breakdown voltage point is taken from the work carried in chapter 7 for plotting the breakdown voltage vs inter electrode distance graph as shown in Figure 6.7. From the figure, the breakdown behavior for deionized water does not follows linearity.

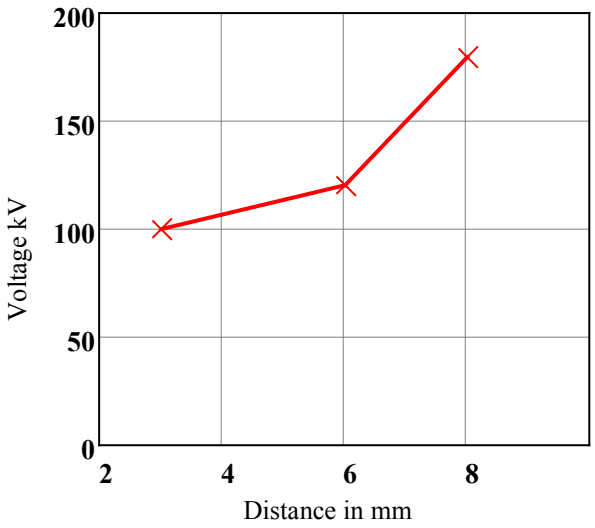

Figure 6.7 Voltage Vs. distance between the electrodes

6.4 Summary

In the present chapter, electrical breakdown properties of water in nanosecond time scales and uniform filed conditions are studied. In this, the effect of electrode material and inter electrode gap are studied. It is observed that with stainless steel electrodes the water can hold comparatively higher voltages even for long durations as compared to the brass as electrode material. The reason is tried to analyzed using emission spectra, which reveals the information of presence of bipolar charge (Cu and Zn) in case of brass electrodes in comparison to stainless steel electrodes (where only unipolar charge) are observed. Further the effect of inter electrode gap is examined which shows the nonlinear behavior of water breakdown voltage. Hence, the suitability of stainless steel as electrode material for nanosecond pulsed power makes the system efficient and compact than the brass.

Chapter 7
Comparative study of Electrical Breakdown properties of Water and Heavy water

7 Introduction

As discussed in the chapter 2, the compact pulsed power can be achieved by two ways. One is to find the medium having good dielectric properties and use it to develop a compact system. Other is to understand the breakdown properties of available dielectric materials and use the knowledge to avoid the breakdown for large extent. These techniques may be of help in achieving compact systems.

In the process of finding the alternate dielectric medium for developing the compact pulsed power systems, in this chapter, the study is focused to understand the suitability of heavy water (D_2O) for pulsed power applications.

For this work, the intuition is taken from the fact that, considering the advantages of Deuterium (D_2), it is preferred in high voltage switching applications [74][75] than that of hydrogen (H_2). This leads us to think whether similar effects can be generated by using D_2O in place of H_2O to enhance the efficacy of pulsed power systems. To examine this aspect, the breakdown study has been extended to D_2O, analyzed and compared with H_2O results. Another aspect considered is the exploration of the breakdown behavior of heavy water in nano-second time scales, due to the interest of inherent breakdown properties for several nanosecond pulsed power applications. To the best of our knowledge, none of the literature is found reporting the breakdown behavior in heavy water (D_2O) for pulsed power applications.

The study is performed using various electrical and optical diagnostics with different operating parameters to find the suitability of heavy water for developing compact pulsed power systems.

7.1 Heavy water properties

Hydrogen is the most abundant element in the universe. It is composed of one proton and one electron with an atomic mass of unity. Deuterium is an isotope of hydrogen, with one proton, one neutron, and one electron and an atomic mass of two, i.e., twice the mass of the common hydrogen atom. It is so unique it has its own element symbol "D." Deuterium Oxide, or heavy water (D_2O), is composed of two deuterium atoms and one oxygen atom, with the chemical symbol D_2O. Because D2O contains two more neutrons than water made with normal hydrogen, it is about 11% more dense. Since deuterium has twice the mass of normal hydrogen, this difference in mass means there may significant [112][113][114] differences between the properties of hydrogen and deuterium. This may cause noticeable differences in bonding energies. In natural water there is about a 17 mM (mill molar) concentration of deuterium is present.

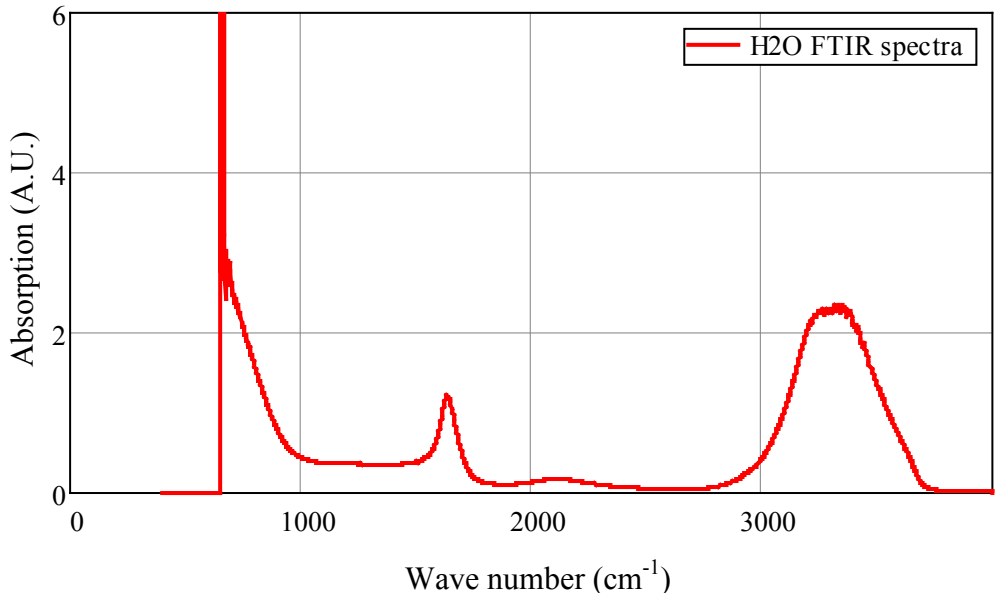

Figure 7.1 FTIR spectra for pure water (H2O)

However, water is one of the most abundant resources on our planet, and D_2O occurs naturally, visually (to the naked human eye), all water looks the same. There is no way for the human eye to tell the difference between H_2O and D_2O. However, spectroscopically, these two waters are very different. The FTIR spectra for pure water (H_2O) and heavy water (D_2O) used in our experiments are shown in Figure 7.1 and Figure 7.2 respectively.

Heavy water (D_2O), though chemically similar to normal water (H_2O), is not exactly identical with the later due to the presence of an additional neutron in the nucleus of Deuterium. Deuterium is unique among heavy stable isotopes in being twice as heavy as the lightest isotope this difference increases the strength of water's hydrogen-oxygen bonds" [3]-[5]. This doubled mass increases the strength of hydrogen-oxygen bonds in heavy water, as a result of which D_2O less self-ionizes compared to H_2O.

The number of hydrogen bonds per molecule of water is higher in heavy water (D_2O), giving its molecule a definite tetrahedral shape[12] as compared to the broader structure of normal water molecule. D_2O has higher density (~11%), dynamic viscosity, heat of fusion and heat of vaporization in comparison to normal water, whereas H_2O has higher surface tension and refractive index compared to D_2O. The low self-ionization, higher density and the structural rigidity of D_2O, in comparison with H_2O, point to a different, possibly better, breakdown and dielectric property of D_2O. However, an experimental study in this area is highly incomplete.

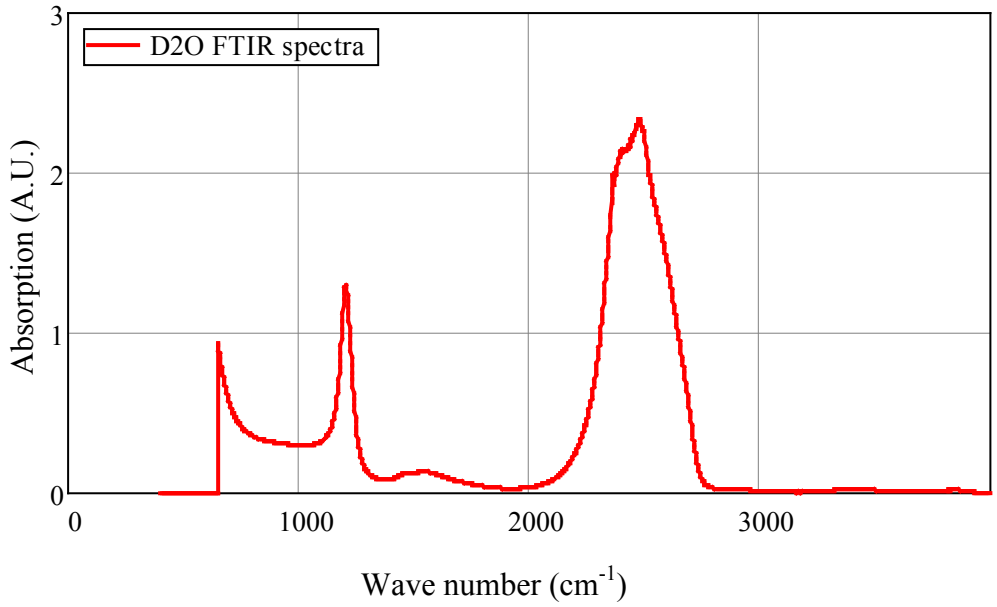

Figure 7.2 FTIR spectra for pure Heavy water (D2O)

There are few literatures discussed the structures of heavy and light water at ambient conditions with the combined techniques of x-ray diffraction, neutron diffraction, and computer simulation[114]. They concluded that heavy water is a more structured liquid than light water. Further, OH bond length in H_2O is 3% longer than the OD bond length in D_2O. This is a much larger change than current predictions. Corresponding to this, the hydrogen bond in light water is 4% shorter than in heavy water, while the intermolecular H-H distance is 2% longer.

Under standard conditions, heavy water less dissociates than ordinary water as it is a weaker acid than ordinary water[115]. The smaller dissociation constant and thus pH (7.435)_for heavy water is a reflection of the somewhat stronger bond between D and O. The physical properties of Heavy water (D_2O) and water (H_2O) are given in Table 7.1[116]

Table 7.1 Physical properties of heavy water and water

Properties	**D_2O (Heavy water)**	**H_2O (Light water)**
Freezing point	3.82 °C (38.9 °F)	0.0 °C (32 °F)
Boiling point	101.4 °C (214.5 °F)	100.0 °C (212 °F)
Density at STP (g/mL)	1.1056	0.9982
Temp. of maximum density	11.6 °C	3.98 °C[8]
Dynamic viscosity (at 20 °C, mPa·s)	1.2467	1.0016
Surface tension (at 25 °C, N/m)	0.07187	0.07198
Heat of fusion (kJ/mol)	6.132	6.00678
Heat of vaporization (kJ/mol)	41.521	40.657
pH (at 25 °C)	7.43 (sometimes "pD")	6.9996
Refractive index (at 20 °C, 0.5893 μm)	1.32844	1.33335

It may not be immediately obvious why simply increasing the mass of what would otherwise be just another H atom should make this bond a bit stronger. Since it is determined by the electric charges, the shape of the potential energy well is not all that different for HO or DO but the reduced mass of the oscillator they form determines how deep in the well the zero

point energy of the oscillator is located. The greater reduced mass of the DO puts it deeper. This makes the DO bond length shorter as the well narrows toward the bottom, all of which means it will take a greater amount of energy to separate D from O[115].

The reason for overall hydrogen bond energy in heavy water D_2O is given by reference[114]. In that it is given as nuclear quantum effects are particularly important in the different properties of light (H_2O) and heavy water (D_2O), where the more restricted atomic vibrations in D_2O reduce the negative effect of its van der Waals repulsive core so increasing its overall hydrogen bond energy.[117]

Many of the properties of heavy water differ from those of ordinary water. A fairly well referenced comparative list of these properties can be found at [116]

In the present work, an effort has been made to study the electrical breakdown properties of heavy water and compare the results with those of deionized water. Dependence of the breakdown properties on the electrode material has been studied, using SS and Brass as the electrodes in different experiments. Further, experiments are also performed to understand the role of polarity of the electrodes on the discharge characteristics. Attempts are also made to correlate the observations on breakdown properties with conductivity measurements of the original and post treated liquids. In order to understand the observed dependence of electrical characteristics on the type of liquid, electrode material and the polarity chosen, optical studies i.e. Fourier Transform Infrared (FTIR) and emission spectroscopy also have been carried out on the samples.

7.2 Experimental procedure:

Experiments have been conducted with laboratory developed Tesla based pulse generator [90] as shown in Figure 7.3. In this work water (H_2O) of conductivity ~ 0.65 μS/cm, dielectric constant ε_r~ 78, pH 6.99 and density 0.999 g/ml and heavy water (Nuclear grade) of

conductivity 0.9 μS/cm , dielectric constant (ε_r) ~78[114], pH 7.6, density 1.10199 g/ml and Isotopic purity % D_2O 99.96 (obtained from Heavy water plant, Vadodara, Government of India) has been used. Hemispherical electrodes of diameter 50 mm are used for the experiment and gap between the electrodes is ~ 3 mm. All the tests are performed at room temperature (~ 28^o C). In all the experiments, the test chamber is filled with pure samples, and is not circulated through purifier. Utmost care is taken when deionized water is replaced by heavy water by cleaning the entire chamber to ensure that no trace of deionized water or any other debris are present in the chamber. For all the experimental campaigns, discharges were initially started at low voltages (~70 kV) and the voltage is increased in steps until breakdown occurred in the liquid. For a given dielectric liquid (deionized water or heavy water), experiments were conducted by using both Stainless Steel and Brass electrodes, keeping positive as well as negative polarities in each case. For any dielectric-material-polarity combination, an average of results from fifteen shots is considered as the breakdown voltage. In order to understand the discharge breakdown characteristics, conductivity measurements were carried out on the original and post treated liquid samples. Eutech Cyber scan PC 300 model conductivity meter(had accuracy (±1 % Full Scale + 1 digit)[101])was used for this purpose. Prior to the measurement on each sample, the meter was calibrated using standard calibrating liquids. Fourier Transform Infrared (FTIR) spectroscopy performed on the original as well as post treated liquids further supplement the electrical measurements mentioned above. Thermo scientific made Nicolet-6700 model FTIR spectrometer has been used for this purpose. In addition, the emission spectroscopy has been performed using 0.5 m visible spectrometer (Princeton Instruments, model no. SP 2500 i) to analyze the effect of electrodes on liquid breakdown characteristics.

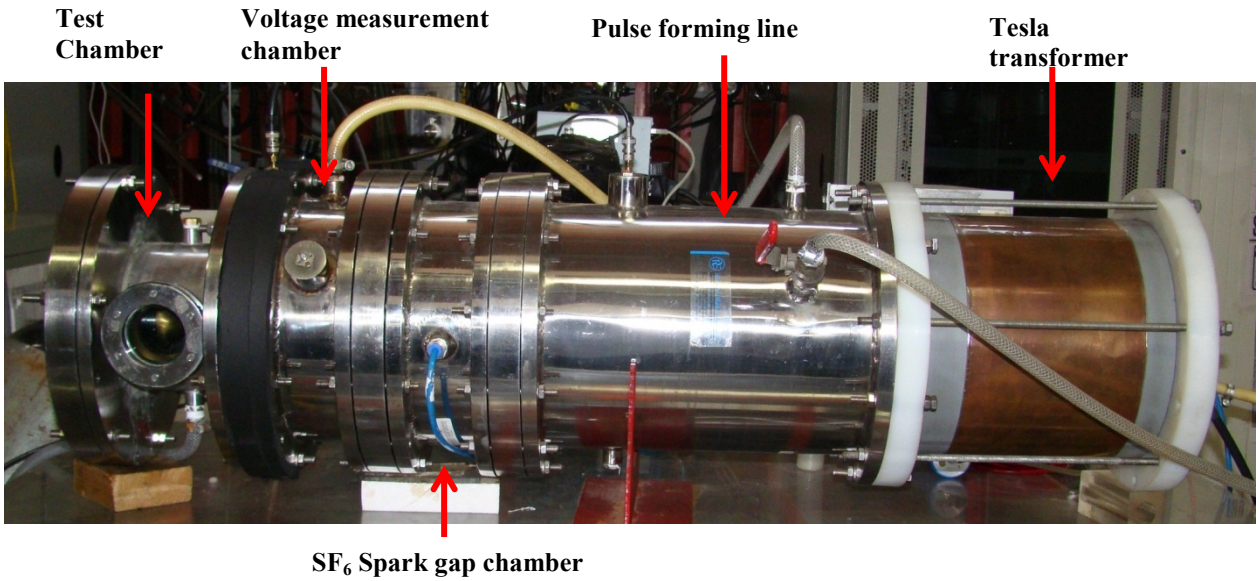

Figure 7.3 Overall view of Tesla based pulse generator

7.3 Results and discussion

Figure 7.4 shows the electrical breakdown voltage, averaged over 15 shots, obtained in case of deionized water (thick curves)) and D_2O (Thin curves). The plots in Figure 7.4 (a) and (b) the breakdown behavior using Brass electrodes, similarly, the plots in Figure 7.4(c) and (d) correspond to experiments with SS electrodes for positive and negative applied voltage respectively. For a typical choice of parameters, the repeatability of the shots is shown by the statistical representation in Figure 7.5, where the breakdown voltage and pulse duration with respect to shot number are shown.

It is observed consistently that irrespective of the combination of electrodes or polarity, discharges with D_2O exhibit less breakdown voltage and sustenance in comparison to the discharges with deionized water. The deviation in voltage holding time is more pronounced when SS electrode is used, as compared to the discharge with Brass electrode, for any given polarity. It is further observed that for both the liquids chosen as the dielectric medium, discharges with SS electrodes are sustained for larger durations compared to those with Brass electrodes. A yet another observation is the enhanced holding time obtained when the

electrodes (SS or Brass) are maintained at negative polarity for either deionized water or D_2O used as the dielectric. The charge holding capability of the dielectrics is further tested by observation of the discharge current behavior and comparing the time integration for various shots. A typical current waveform is shown in Figure 7.6.

As discussed in section 7.1, the chemical properties of heavy water makes it slightly denser compared to H_2O and have higher bond strength [113][114][118][119]. Therefore, it is anticipated that heavy water hold higher voltages compared to Deionized water (H_2O). The experimental results, however, show a conflicting behavior. In order to understand the results further, the conductivity measurements are carried out on all the original and post treated samples.

The measurements on conductivity, tabulated in Table 7.2 give observations supporting our observations on the breakdown behavior. It is observed that, for all the parametric combinations, the conductivity of the post-treated liquid is higher as compared to the original sample. However, the relative enhancement in conductivity is considerably higher in case of heavy water as compared to deionized water. Further, liquids treated with brass electrodes show higher relative increase in conductivity compared to those treated with SS electrodes. It is also observed that maintaining +ve polarity results in the post treated liquids having higher conductivity as compared to the discharges with –ve polarity.

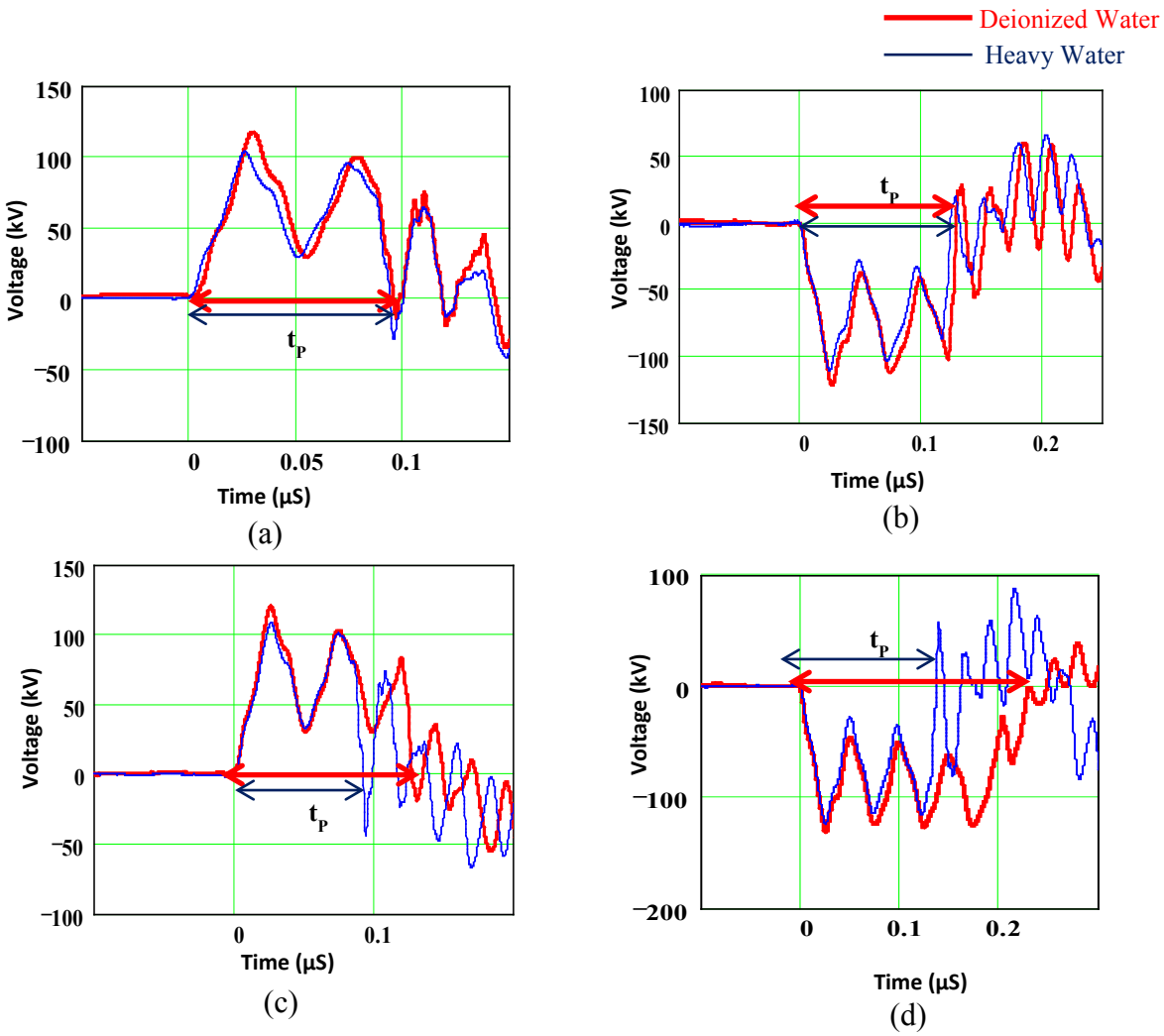

Figure 7.4 Experimental voltage waveforms of Deionized water (H_2O) and Heavy water (D_2O). (a) Pair of Brass electrodes with positive applied voltage, (b) Pair of Brass electrodes with negative applied voltage, (c) Pair of stainless steel electrodes positive applied voltage, (d) Pair of stainless steel electrodes with negative applied voltage. Oscillations in the voltage waveforms are due to stray capacitances formed at the electrodes of SF_6 spark gap switch and test chamber electrodes as explained in reference [90] Pulse duration (t_p) considered as the voltage falls to zero at the time of breakdown.

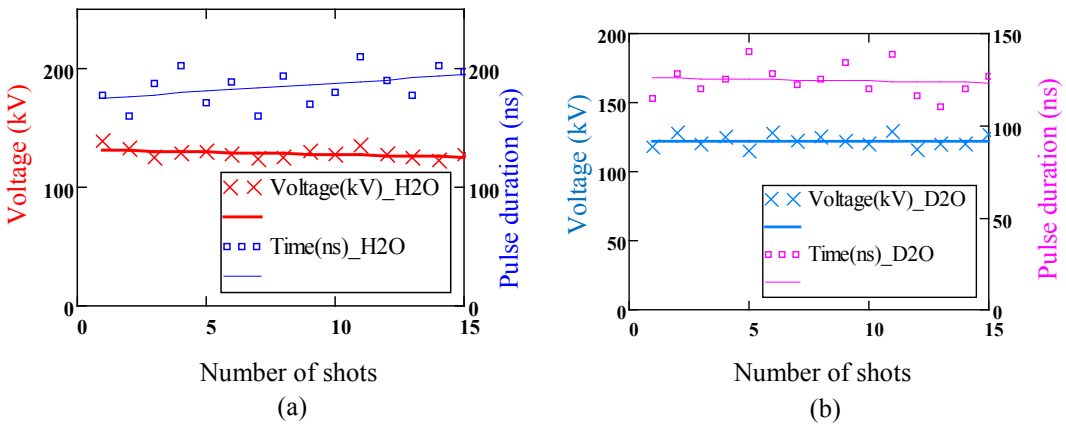

Figure 7.5 Statistic chart of Voltage, pulse duration with respect to number of shots. (a) Pair of SS electrodes with negative applied voltage for water, (b) Pair of SS electrodes with negative applied voltage for heavy water

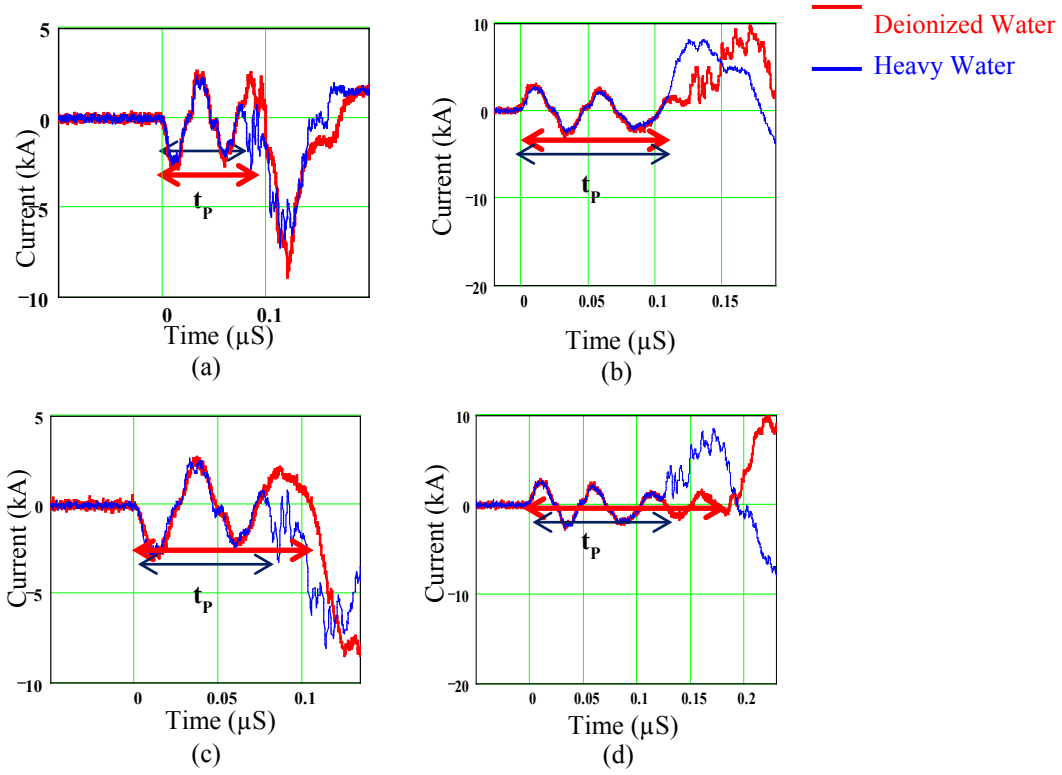

Figure 7.6 Experimental current waveforms of Deionized water (H_2O) and Heavy water (D_2O). (a) Pair of Brass electrodes with positive applied voltage, (b) Pair of Brass electrodes with negative applied voltage, (c) Pair of stainless steel electrodes positive applied voltage, (d) Pair of stainless steel electrodes with negative applied voltage.

Table 7.2 Approximate measured conductivity values of H_2O and D_2O for pre and post experiments.

Polarity	Material	H_2O (Original liquid is ~0.65 µS/cm)	D_2O (Original liquid is ~0.9 µS/cm)
Positive	Brass	1.27	3.2
	Stainless steel	1.11	2.8
Negative	Brass	1.20	2.1
	Stainless steel	1.11	1.7

FTIR is a technique, which is used to identify the signatures of chemical compounds and substantial groups in the sample. Spectra are performed with resolution 4 cm^{-1} and wave number range from 650-4000 cm^{-1}. After completion of each set of experiment, liquid samples are collected from the test chamber through an outlet of the test chamber and a spectrum has been taken within few minutes. The FTIR spectroscopy was carried out on both original as well as post treated samples of H_2O and D_2O for all the experiments.

In the case of heavy water (D_2O), the peaks obtained correspond to wave numbers 1205, 1467, 2480, 3405 and 3850 cm^{-1} as shown in Figure 7.7. The wave number 1205 cm^{-1} represents bending vibrations, 1467 cm-1 bending plus broadband librations, and 2480 cm^{-1} complex band with double the bending vibrations, and symmetrical and asymmetrical vibrations [120]. A week band at 3404 cm^{-1} is due to O-H stretching vibrations of HOD (Hydrogen deuterium oxide) from traces of H_2O in D_2O. In case of deionized water, spectra show three peaks at 1635, 2120 and 3317 cm^{-1} wave numbers as shown in Figure 7.8. The wave number 1635 cm^{-1} represents bending vibration, 2120 cm^{-1} combination of bending plus libration and 3317 cm^{-1} symmetric, asymmetric and overtone of bending vibrations [121][122] . When it is compared with respective original samples, H_2O exhibits only

marginal increase in intensity of spectral lines corresponding to different wavelengths, whereas D_2O exhibits significant increase in intensity for all wavelengths. In case of Heavy water the significant change in intensity is observed at 1465 and 3405 cm^{-1}. The intensity enhancement is stronger in case of positive polarity for both stainless steel and brass electrode. Further, it is also seen that for brass electrode, the intensity change is higher as compared to the case with SS. To enable better clarity regarding relative intensity enhancement in case of both the liquids the plot of intensity against wavenumber is shown in Figure 7.9 and Figure 7.10. It may be observed that, in case of Heavy water ~ 3%, 14%, increment in intensity in case of brass and stainless steel electrode material with positive polarity with reference to the original liquid at the 1465, 3405 cm^{-1} wave numbers. In case of water, the intensity enhancement is marginal. The relative enhancement in intensity observed in case of D_2O and H_2O indicates possibility of chemical reactions during the process of electrical breakdown. In the case of water breakdown or discharge, the molecules dissociate into H and OH radicals whereas in case of D_2O the corresponding radicals are D and OD [123][124][4]. These radicals combine into other combinations and the concentration of compounds depends on formation of number of H, OH in case of H_2O and D, OD in case of D_2O.

During electric discharge, electric current from a high voltage pulse in water forms highly conductive channels called streamers between the anode and cathode. In the streamer or discharge channel, the water molecules are dissociated into H and OH radicals, which react to form molecular hydrogen, oxygen. A mathematical model that describes the primary reactions in the plasma channel includes the following reaction steps:

$$H_2O \longrightarrow H + OH$$

$$H + H \longrightarrow H_2$$

$OH+OH \longrightarrow H_2O + O$

$O+ OH \longrightarrow O_2 + H$

$D_2O \longrightarrow D+ OD$

$OD + OD \longrightarrow D_2O + O$

In our case, the considerably high intensity enhancement at wave number 3405 cm^{-1} in case of D_2O suggests that there is a higher concentration of HOD molecules compared to the original sample, pointing to the formation of D^+ and OD^- ions in D_2O due to the breakdown. Deuterium is known to react more slowly in comparison to ordinary hydrogen [124][125], and hence the D^+ and OD^- ions in D_2O would have remained for longer durations compared to the corresponding ions in H_2O. This could be the possible reason for increase in conductivity and reduced charge holding capability of D_2O.

The use of Brass electrodes is known [126][108][109] to cause injection of positive charges due to Cu and negative charges due to Zn in to the test liquids and thus to result in weak charge holding capability of discharge, as compared to many other electrodes. However, these studies were carried out in discharges those are much longer (a few microseconds) compared to the discharges of the present work. It is not clear whether such ion injections can be effective in nanosecond duration discharges. In order to understand the week charge holding capability of discharges with Brass electrodes as compared to the case with SS electrodes in the present case, in situ, emission spectroscopy has been carried out on deionized water using an 0.5 m visible spectrometer (Princeton Instruments, model no. SP 2500i) operated with 600 grooves/mm grating. The spectrometer is having reciprocal linear dispersion of 3.2 nm/mm and gives a wavelength coverage of 85 nm when coupled to a CCD (Andor Technology, model no. DU440BU) having 2048 x 512 no. of pixel. Light was collected though a chord viewing both the electrodes and water in between them. The spectra

obtained for deionized water (H_2O) with brass and SS as electrode materials, which are shown in Figure 7.11 and Figure 7.12, respectively. The entire spectra obtained for 400-700 nm wavelength range collected from four similar discharges. The spectra clearly reveal presence of Cu and Zn ions in the test liquids in case of discharges with Brass electrodes, whereas with the use of SS electrodes, the spectra show presence of Fe ions. These results clearly indicate that even short (nanoseconds) discharges have ions introduced into the test liquids from the electrodes used, although the exact mechanism of ion generation is presently not yet clear, however, it is assumed that, this could be due to the high temperature plasma causing electrode melting, vaporization and ionization. The results further indicate additional amount of ions in case of discharges with Brass electrodes as compared to the ones with SS electrodes, leading to the weak charge holding capacity of the former. In both the spectra, only prominent visible lines are identified with help of NIST [127] database.

The experimental observations also reveal that keeping negative polarity results in the liquids having better (~5% enhanced) charge holding capacity. In case of electrode configurations, such as point – plane, having non-uniform field distribution, it is established[128] theoretically and experimentally that keeping the pointed electrode at negative polarity results in approximately doubling of the breakdown voltage. Although the field distribution is uniform in the present case, how the electrode surface irregularities in the realistic experimental situation contributes to the breakdown is not clearly understood. However, there has been a report [38] discussing about 5 % enhancement in breakdown voltage observed adopting negative polarity configuration, with hemispherical electrodes, which support our observations.

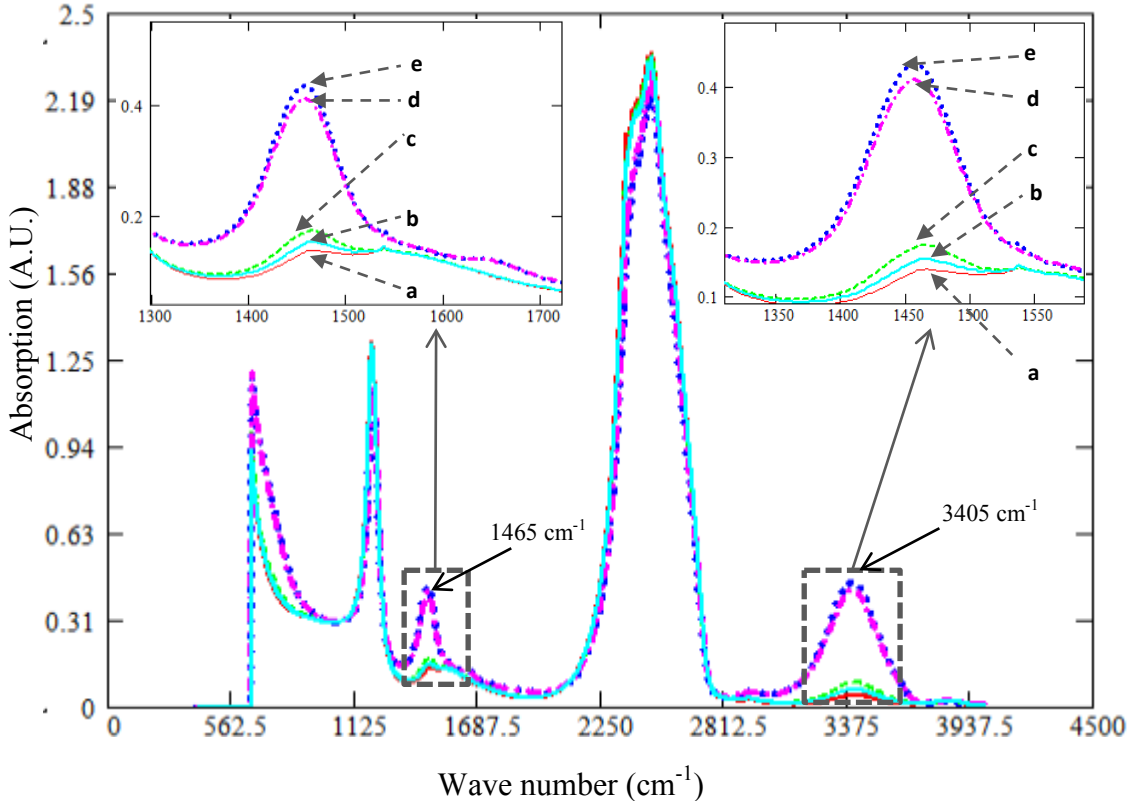

Figure 7.7 : FTIR spectra of D_2O for all the four cases, which are, a =original D_2O for reference spectra, b = stainless steel electrodes with negative polarity, c = brass electrodes with negative polarity, d = stainless steel electrodes with positive polarity, e = Brass electrodes with positive polarity. The spectra evidence change in intensity levels at wave number 3405, 1465 cm^{-1} majorly for positive applied voltage polarity.

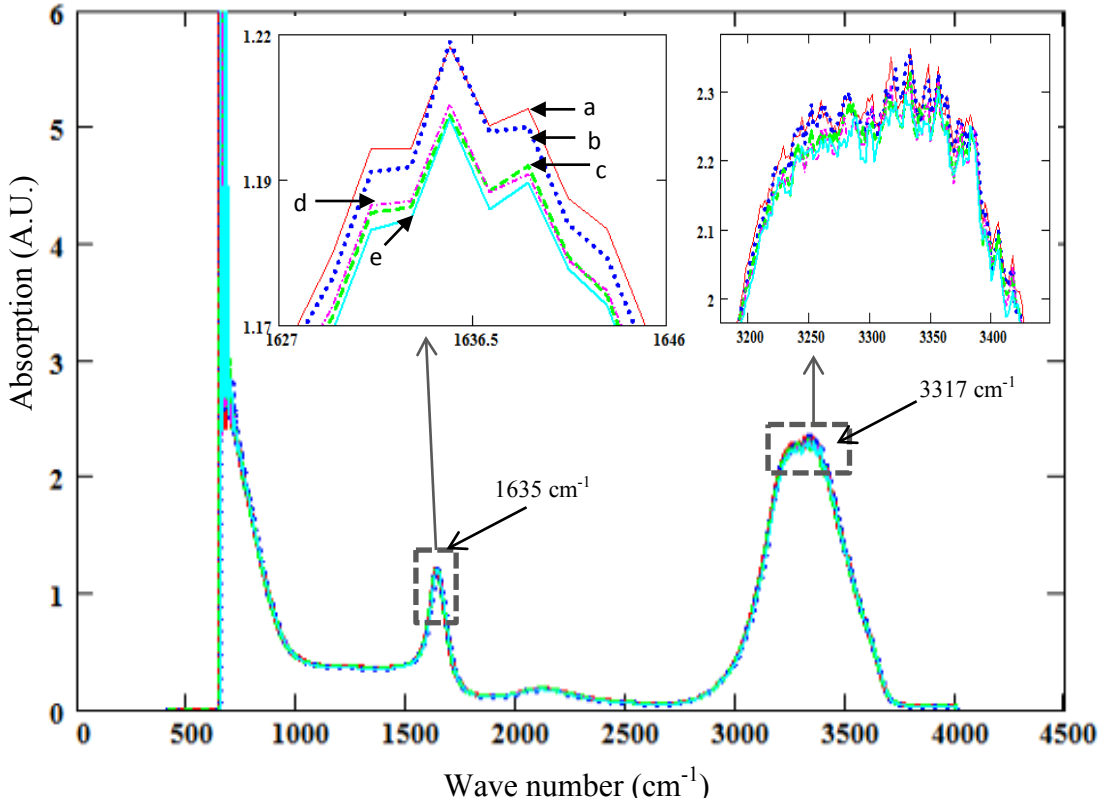

Figure 7.8 FTIR spectra of H_2O for all the four cases, which are, a = Original H_2O reference spectra, spectra, b = Brass electrodes with positive polarity, c = Brass electrodes with negative polarity, d = stainless steel electrodes with positive polarity, e = stainless steel electrodes with negative polarity. The spectra evidence for change in intensity at 3317, 1635 cm^{-1}.

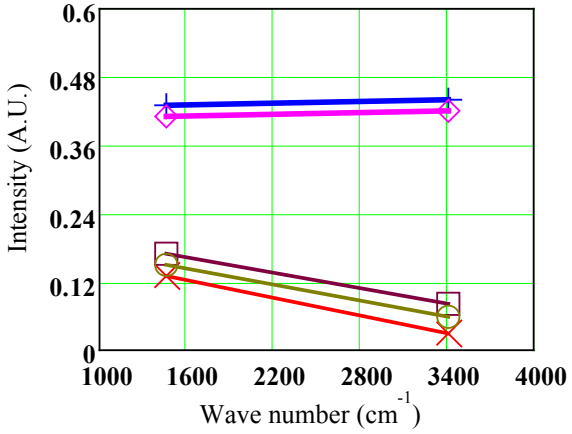

Figure 7.9 Observed Intensity values of D_2O spectra. Reference sample for 3405 cm^{-1}, 1465 cm^{-1} are 0.03 and 0.13 respectively.

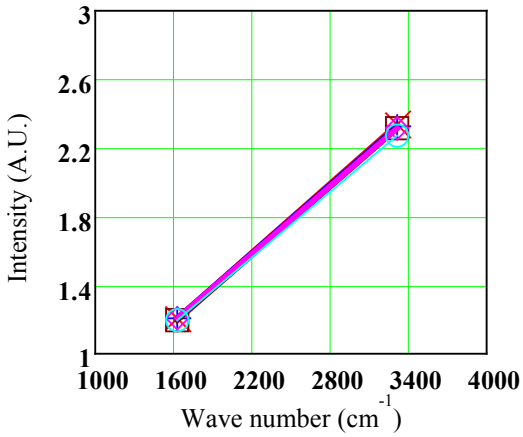

Figure 7.10 Observed intensity values from H_2O spectra.

Reference sample 3317 cm-1 and 1635 cm-1 are 2.34 and 1.21 respectively

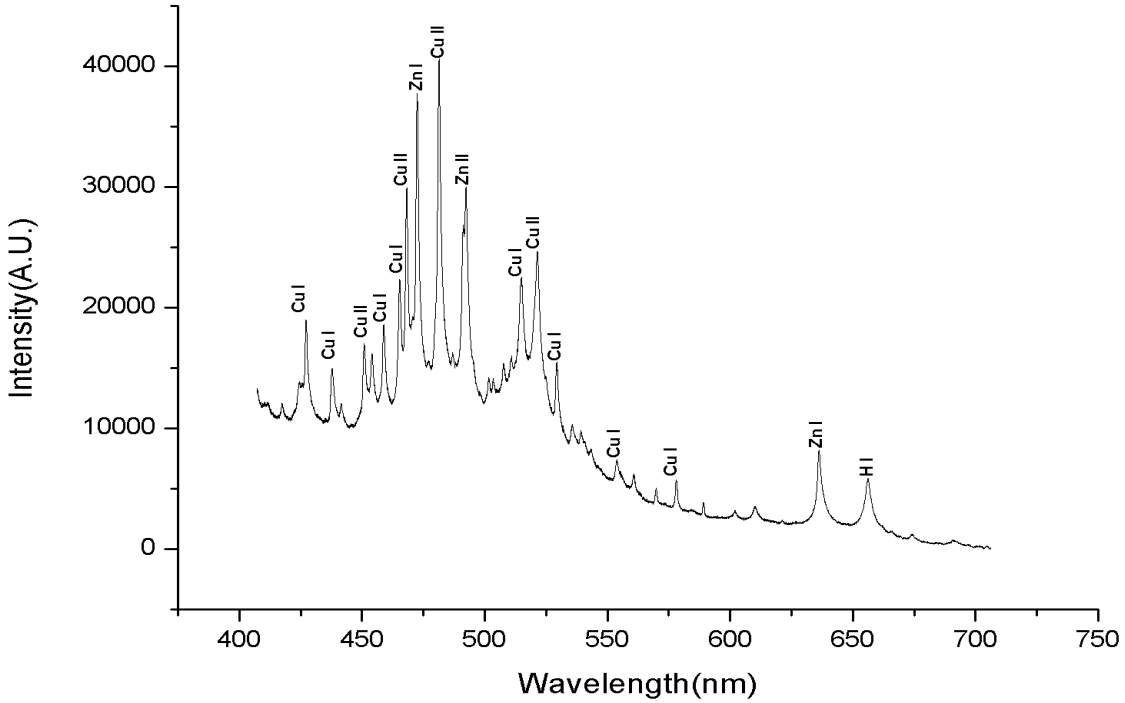

Figure 7.11 Emission spectra plot for deionized water (H_2O) with Brass as electrode material. It indicates the emission of copper and zinc ions from electrode material.

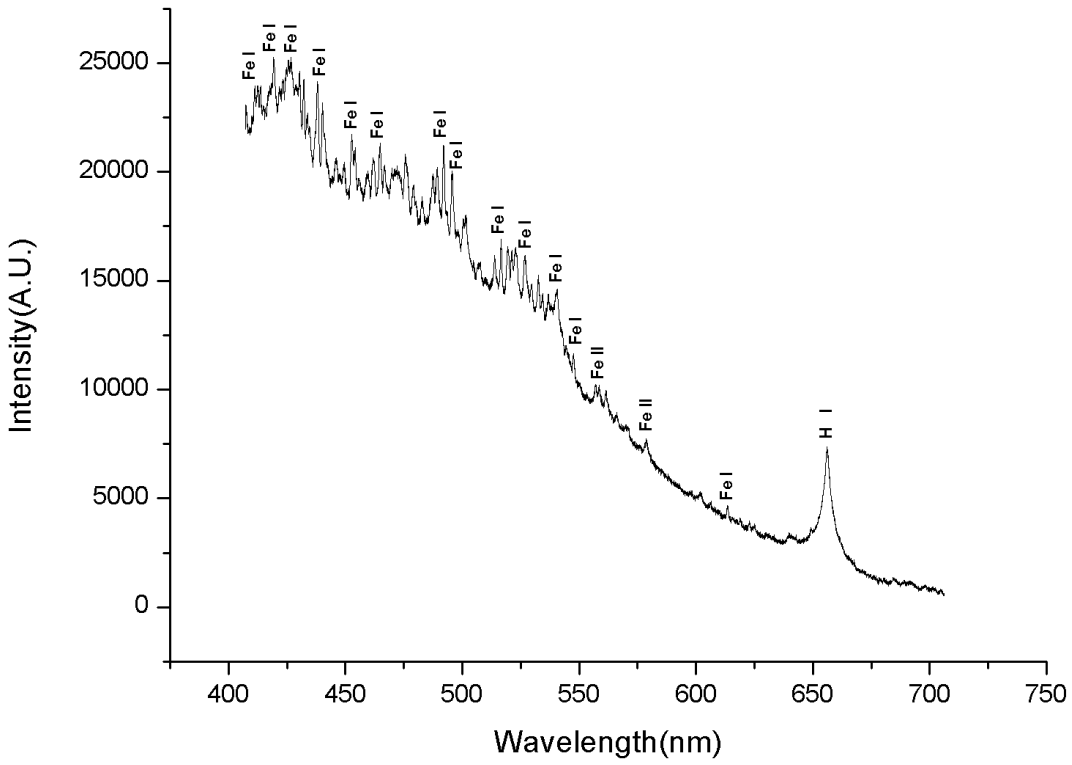

Figure 7.12 Emission spectra plot for deionized water (H2O) with SS as electrode material. The spectrum indicates the injection of iron ions from electrode in to the water.

7.4 Summary

Experiment has been conducted on Deionized water and Heavy water under unifrom electrical field conditions to understand electrical breakdown properties. Discharges were carried out with positve and negative polarities with Brass and Stainless steel as electrode materials, in different experiments. In all cases it is observed that heavy water holds less charge and for less durations compared to deionized water, irrespective of the electrode material and applied voltage polarity chosen. SS electrodes are seen to perform better in terms of the voltage withstand capacity of the liquid dielectric as compared Brass electrodes. It is further observed that keeping negative polarity of the electrode gives enhanced discharge breakdown voltage when compared with discharges with positive polarity. The observations corroborate well with conductivity measurements carried out on original and post treated liquid samples. An interpretation of the observations is attempted using FTIR measurements on original and post treated liquids as well as in situ emission spectra studies. Adding to the existing literature on emission spectra of long (microsecond) discharges, observations in the present study reveal that even short (nansecond) duration discharges result in formation of considerable amount of ions introduced into the liquid from the electrodes. The experimental results reported thus show that deionised water is better suited for high voltage applications and also offer a comparison of the discharge behaviour with different electrodes and polarities.

Chapter 8
Anode breakdown initiation in water

8 Introduction

Understanding the physical processes of discharge initiation in the pulsed breakdown of liquids and the basic laws of formation and propagation of discharges in nanosecond regime may further help in improving the system geometry. One of the ways this can be realized by using fast optical camera.

Present work discusses the investigation of experimental results of discharge development from anode, in water under uniform electric field conditions with nanosecond high voltage pulses. Details of a high-speed photo recording, triggering mechanism and observations are discussed

8.1 Experimental details and results

Experiments are performed using Tesla based pulse generator [136]. The impulse voltage had amplitude ~100-150 kV and rise time of 20 ns and pulse duration of ~100-140 ns. Hemisphere electrodes made of stainless steel (#304), each of diameter 44 mm and the distance between the electrodes is 6 mm. The test chamber is filled with deionized water of conductivity 0.65 μS/cm. Experiments conducted at room temperature (~26^{o}C). Figure 8.1 shows the schematic diagram of the experimental setup, which includes the pulse generator, electrical diagnostics, and arrangement of the ICCD camera and its synchronization method used in this work. Tesla based pulse generator [13] is used as a voltage source to get the required voltage and pulse duration, which is fed to the anode.

The high-speed camera (Stanford computer optics, 4 Picos, ICCD) [137] having minimum exposure time of 1 ns is used to observe the temporal development of streamer discharges. The trigger for ICCD camera is provided by digital oscilloscope (Agilent Technologies, DSO-X 2024 A digital oscilloscope)[138] . The oscilloscope has the provision to deliver TTL trigger out (i.e., every time the oscilloscope captures the waveform on its screen; there is a TTL compatible output pulse on the trigger out provision).

The voltage across the pulse forming line [136] is measured with this oscilloscope, which triggers the oscilloscope 500 ns before the beginning of the discharge event in the test chamber.

The internal delays of camera (40 ns)[137] and oscilloscope (25 ns) [138] are very less than this 500 ns time; hence, the temporal development of the streamer discharge at particular time of breakdown can be covered with the ICCD camera. The images of streamer development are captured in single frame regime with exposure time of ~3 ns.

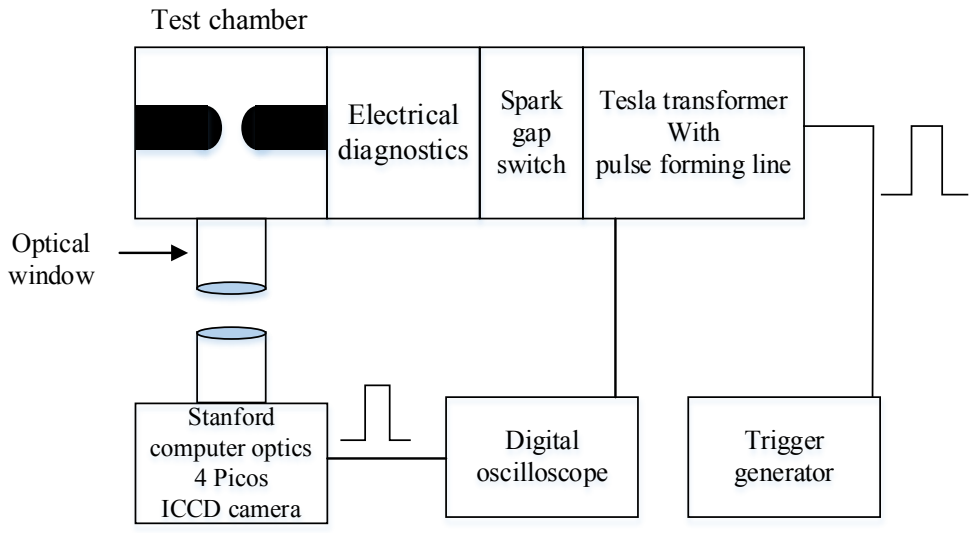

Figure 8.1 Schematic of experimental setup with camera synchronization

Figure 8.2 show the single frame images of streamer development in deionized water from anode to opposite ground electrode taken form ICCD camera with exposure time of 3 ns. The optical settings for each case kept same for each image, they correspond to 130 kV at anode

and the inter electrode gap is 6 mm. In this, each photograph taken at different shot for adjusted delay from the onset of voltage application. However, the general features of the streamer discharges are similar from shot to shot. The origin point of discharge is observed on anode surface. The localized plasma recorded after 20 ns. The emission until ~60 ns is preceded as a single stem or thick channel after that it split into branches of two and further it split in to sub branches. Formation of sub branches observed near to the ground electrode. The gap breakdown occurred after the streamers completely reach the opposite electrode.

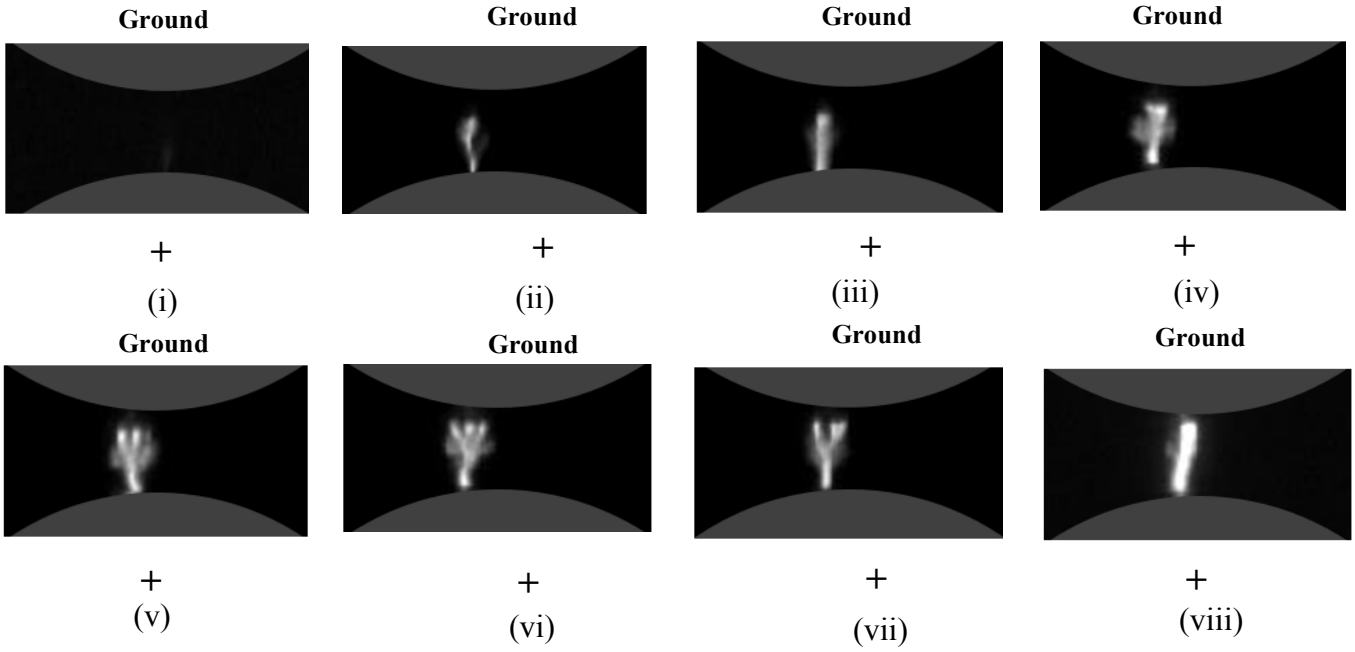

Figure 8.2 Temporal evolution of electric discharge in distilled water, for 3 ns exposure duration of camera, inter electrode distance between electrodes, 6 mm

It is observed from the Figure 8.2, image number (i), (ii) and (iii), the discharge is started as a single stem (root) from the anode and develops and extends to reach the opposite ground electrode. In these three images, it is observed that, there are no branches formed. The stem reaches some extent in the gap; the formation of two branches had started and after that, it is further increased in the path of sub branches in the one of the branch as shown in Figure 8.2 images iv, v, vi and vii. All the branch channels emerge from a central channel called stem, which is connected to the anode electrode surface.

The streamer increases in diameter and intensity with decrease in distance to the opposite electrode. The first stage is due to the local release of energy near the electrode surface. As the field strength increased with respect to time, the growth of the streamers increased and at particular, the streamer split into branches and propagates to opposite electrode as shown in Figure 8.2. This may be due to variation in field due to space charge in the liquid. The image-to-image evolution of streamer is presented as intensity plot with reference to pixel position in Figure 8.3. The rate of intensity of the discharge is increased up to 80 ns duration, after that the intensity fall in consequence propagation. The streamer velocity in the initial stage until the branches formed was high. Once the initiation of the branches started, the velocity of streamer propagation comes down. This reduction of velocity may be due to the ion current density distributed in to the branches.

8.2 Streamer initiation

V.F.Klimkin [139] has considered the breakdown mechanism at anode under uniform field as bubble and ionization mechanism of breakdown. In general, shadow graphic technique is well known for information on phase changes in the liquid which includes discharge channels, gas-vapor bubbles, cavitation voids etc.,. Similar experiments were reported[12], that the breakdown initiation in their case has started due to bubble formation under the application of high voltages at the anode, there the ionization process starts, and are confirmed using laser schlieren photograph techniques. However, in these experiments this techniques is not used but the experimental results are compared with earlier reports, with that it is assumed that the breakdown in process in the present case is due to ionization process at the anode electrode.

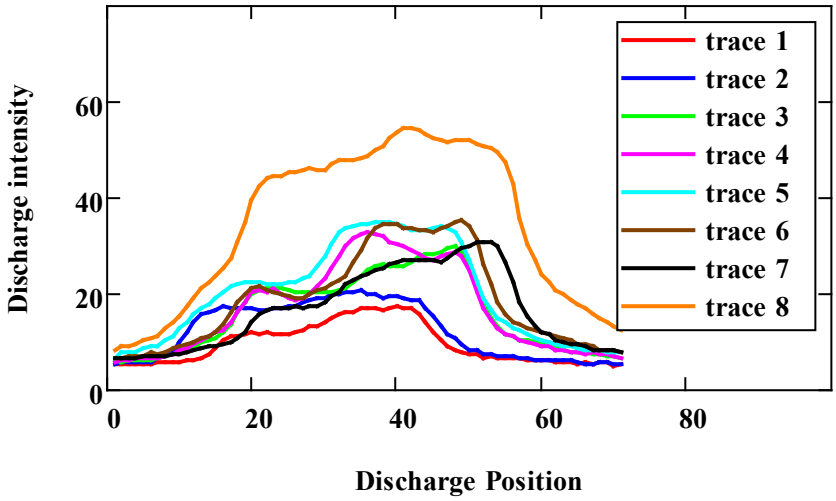

Figure 8.3 Streamer evolution in the inter electrode gap

8.2.1 Streamer propagation:

The general mechanism for streamer propagation is due to thermal process at the streamer head and other is a field driven propagation. Positive ions near the plasma-water boundary layer are accelerated by the enhanced electric field due to the space charge in the streamer. Streamer initiation and propagation mechanism for several liquid dielectrics are discussed reported in the reference [140][141]. If the electrode is positively charged, the electrons quickly neutralized on the electrode, and the remaining positive charge becomes a non-uniform electric field source, which leads to the creation of inhomogeneity at the electrode surface. As shown in Figure 8.4 the discharge initially started as a single stem in all cases for some duration (approximately less than half of the distance between the electrodes), there after the formation of branches started, which further split in to sub branches. In the case of highly stressed anode, highest ionization activity occurs at the anode.

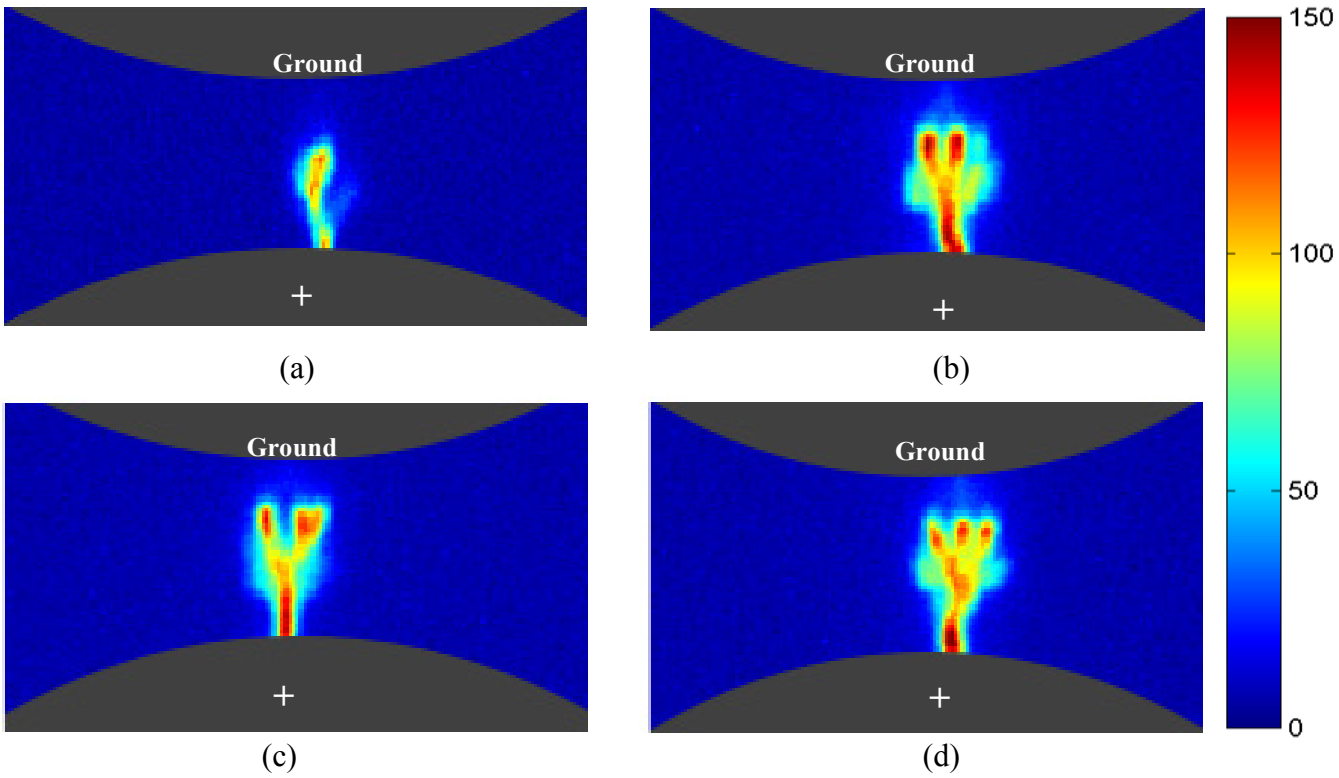

Figure 8.4 Temporal development of discharge in deionized water. (a) Represents the initiation of discharge (b) Discharge stem split into two-streamer branches (c) branch further split into two branches in one of the branch (d) evolution of split streamer branches

The amount of charge in the streamer head is mainly determined [142]by conductivity of the streamer column and ionic current. If a large amount of charge is delivered to the streamer, the streamer head will increase temporally, resulting in increase in the electric field at the boundary. This increased electric field is quickly suppressed by the expansion of the streamer head, due to splitting the streamer channel. The evolution of discharge is shown in Figure 8.5

In the case of applied voltage is increased to more than the breakdown threshold voltage (150 kV) [143][4], it is observed that, the multiple channels initiated from the surface of electrode itself as shown in Figure 8.6. The discharge in present experiments does not emerge from the same site as the preceding discharge channels.

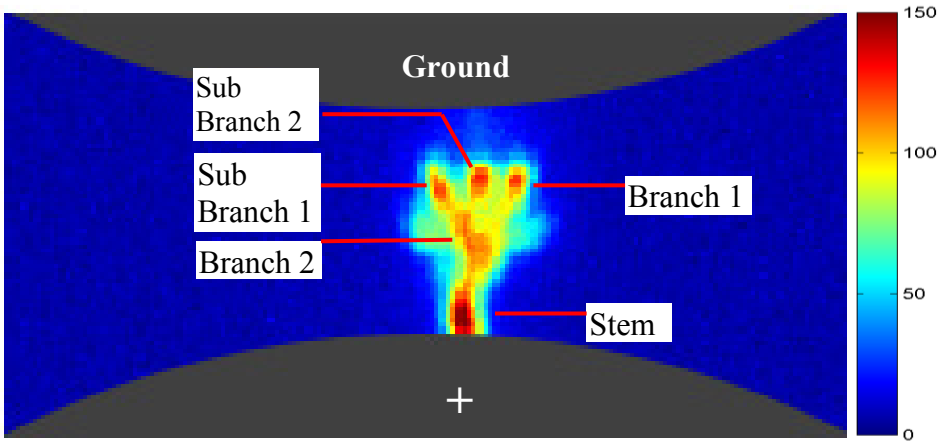

Figure 8.5 Evolution of discharge as stem, branches and sub branches

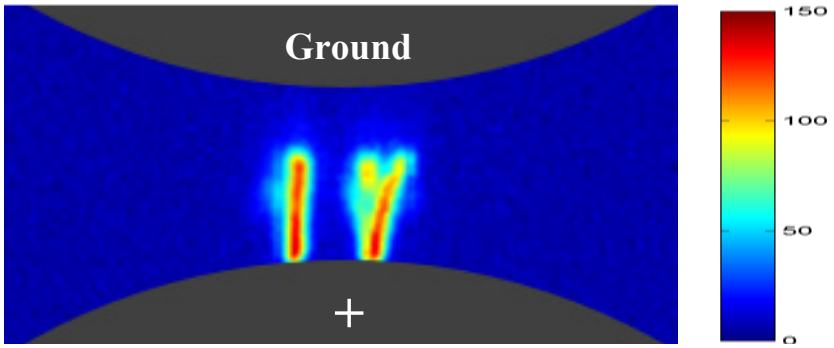

Figure 8.6 Evolution of multiple discharges on the application of more than the breakdown voltage for deionized water.

8.3 Summary

The anode discharges in deionized water (ε_r) under uniform electric field conditions, using Tesla based pulse generator are investigated by means of optical fast camera diagnostics. These discharges were studied by applying positive high voltage to one of the electrode and keeping other at ground potential. The temporal development of streamers is recorded using high-speed camera with 3 ns shutter time in single frame regime. The branches were observed from the main stem after 80 ns duration of the applied voltage pulse. The discharge velocities are found high (~3 x 10^6 cm/s) at initial stages but after few nanoseconds the velocities were found reduced. In the case of increased applied voltage, i.e. more than the

breakdown voltage, it is observed that multiple discharge channels started from initiated from the surface of the electrodes.

Chapter 9
Conclusion and future scope

In this thesis, we have studied liquid dielectric breakdown properties for developing compact and efficient intermediate storage devices towards the development of compact pulsed power systems. For this, we have developed a suitable pulse generator and voltage and current sensors. The experiments are performed in nanosecond time scales under uniform electric field conditions. We have also tried to explore the suitability of alternate dielectric medium for developing the compact pulsed power system. The chemical changes due to breakdown in the dielectric medium and presence of charge in the dielectric medium due to discharge are tried to understand using optical diagnostics viz. absorption spectroscopy and emission spectroscopy respectively. Further, the discharge characteristics i.e. discharge initiation and propagation in the water is studied with fast camera.

The experiments to fulfill the motivation have been performed and the important outcomes of the studies are as follows:

1. In the process of developing the compact and efficient energy storage devices towards the development of compact pulsed power applications, liquid dielectric breakdown properties are tried to study. For this, a suitable Tesla based pulse generator is designed and developed. The pulse generator can deliver maximum voltage up to 300 kV and pulse duration of several tens of nanosecond. The system is very compact and required low maintenance compared to the other conventional systems. Calculated system parameters are experimentally verified. Overall, the experimental setup is characterized by using PSPICE (student version 9.1) simulation software and the

simulation results are in good agreement with experimental results as discussed in the chapter 3.

2. Further, in order to understand to estimate the electrical breakdown properties of liquids, fast response electrical diagnostics *viz.*, capacitive voltage sensor and self-integrating Rogowski coil are indigenously developed and calibrated using standard commercial probes.

3. Considering the advantages of dielectric properties of deionized water and to overcome the limitations of it for developing the compact pulsed power systems, we have attempted to study the electrical breakdown properties of deionized water in nanosecond time scale with uniform electric field conditions. Experiments are performed with deionized water (ε_r=80) and conductivity of 0.45 μS/cm is used. In this work the effect of electrode material viz. stainless steel and, Brass with variation in inter electrode gap (6, 8 mm) are studied. All the experiments are performed at room temperature (~26^o C).Considering the average of number of experimental data it is observed that the discharge with SS electrodes occur at higher voltage and sustain for longer duration in comparison to those with Brass electrodes, which are discussed in the chapter 5. The variation in inter electrode gap shows the nonlinear behavior of breakdown characteristics in case of water as discussed in chapter 5.

4. In addition, to understand the observed effect of electrode material (i.e. stainless steel and brass) is analyzed by using the optical emission spectra during the discharge. The details of the spectrometer are discussed in the chapter 4. The spectra showed the presence of copper (Cu) and Zinc (Zn) ions in case of brass whereas iron ions (Fe) in case of stainless steel electrode. It is assumed that the presence of bipolar ions in case of brass as electrode material may be the cause for early breakdown in comparison to

unipolar ions case of stainless steel. Based on this, the SS material is shown to be advantageous for the nanosecond compact pulsed power applications than that in case of Brass.

5. In the process of searching an alternate dielectric for developing the compact pulsed power systems, further in this work, the suitability of Heavy water (D_2O) is examined. The experiments are performed using developed Tesla based pulse generator under nanosecond time scales. The experimental results are compared with results of H_2O at same experimental conditions. For this experiments, the heavy water (D_2O) and pure water (H_2O) of conductivity <1 μS/cm (ASTM type II water) are used. The effect of electrode material viz. stainless steel and brass, voltage polarity i.e. positive and negative are examined with ~3 mm inter electrode gap. The obtained experimental results are compared with the results of pure water (H_2O). It is observed that irrespective of the combination of electrodes or polarity, discharges with D_2O exhibit less breakdown voltage and less sustenance time as compared to the discharges with deionized water. Further, in order to validate the above experimental observations, the conductivity measurements (Eutech Cyber scan PC 300 model conductivity meter was used for this purpose.)are carried out on pre and post breakdown test samples, for all the combinations of parameters (i.e. dielectric liquid, polarity and electrode material). The conductivity measurements are consistent with the observed breakdown behavior.
6. Further, to understand the above observation it is attempted to know the change in chemical behavior in both liquids due to discharge by using optical Fourier transform infrared (FTIR) absorption spectroscopy. The details of FTIR are discussed in the diagnostics chapter in this thesis. The FTIR spectra are performed on pre and post breakdown discharge samples covering all the typical parametric combination. The observations clearly reveal evidence of chemical reactions during breakdown and

found more prominent in case of D_2O in comparison to H_2O samples as discussed in chapter 6. This enables a qualitative interpretation of the superior performance exhibited by H_2O as a dielectric for compact pulsed power applications.

7. In order to understand the physical processes of discharge initiation in the pulsed breakdown of liquids and the basic laws of formation and propagation of discharges in liquid a high speed fast optical photo recording(Stanford computer optics, 4 Picos, ICCD) camera has been used. The trigger for camera with low jitter (~4-6 ns) is provided by oscilloscope as discussed in the chapter 7. The optical images are taken in frame regime with exposure time of 3 ns and inter frame delay of 20 ns. It is observed that, in nanosecond time scales and uniform electric field conditions for positive applied voltage, the breakdown is initiated at single point on the electrode surface and the discharge propagate as a single stem for a finite duration (~80 ns) and after that, the discharge split into branches. This may be due to the difference in the field generation by space charge in the dielectric medium. It is assumed the discharge initiation is due to hole tunneling process in the medium itself as discussed in the chapter 7.

Future scope:

Future research issues are open to study the dielectrics and understanding its properties in designing the efficient components of pulsed power system viz. in switch medium in spark gaps, energy storage devices that may lead to develop compact pulsed power system. The understanding of breakdown properties can be carried out by theoretical modeling or using available computational software.

The search for utilizing new dielectric materials, metals, and interface in the design of compact pulsed power systems is never ending requirement. The breakdown characteristics

may be well understood visually by using optical diagnostics *viz.,* fast ICCD camera, spectroscopy, etc., which gives in deep knowledge of breakdown mechanism at atomic levels.

Understanding the mechanism of discharge initiation at nanosecond or less may assist to develop the techniques, which may extend or avoid the breakdown of dielectric medium.

The studies may be extended to quantify the charge injection due to the discharge in the dielectric medium; this may assist to control the breakdown initiation and propagation.

Alternative topologies and novel engineering techniques must be required to investigate for developing the compact pulsed power systems.

References

[1] P.W.Smith, “pulsed power for particle accelerators,” in *May 8-12th*, 2004.

[2] H. Bluhm and P. P. Systems, *Pulsed power systems, principles and applications*. .

[3] M. Kristiansen, “Pulsed Power Applications,” *Ninth IEEE Int. Pulsed Power Conf.*, vol. 1, 1993.

[4] P. Šunka, “Pulse electrical discharges in water and their applications,” *Phys. Plasmas*, vol. 8, no. 5 II, pp. 2587–2594, 2001.

[5] W. Jiang and K. Yatsui, “Pulsed wire discharge for nanosize powder synthesis,” *Plasma Sci. IEEE Trans.*, vol. 26, no. 5, pp. 1498–1501, 1998.

[6] F. DeVito, “Application of Pulsed Electric Field (PEF) Techniques in Food Processing,” *Chem. Eng.*, p. 116, 2006.

[7] A. Mizuno and Y. Hori, “Destruction of living cells by pulsed high-voltage application,” *Ind. Appl. IEEE Trans.*, vol. 24, no. 3, pp. 387–394, 1988.

[8] M. J. Löffler, R. Hensel, B. Siegert, F. Schnell, D. Spitzer, G. Cassagnou, and A. Voronov, “Al-wire Explosions in Glass Tubes : Experimental Results.”

[9] G. W. Carter and A. V Tsangaris, “Plasma gasification of biomedical waste,” Georgia Institute of Technology, Atlanta, GA (United States), 1995.

[10] S. H. R. Hosseini and H. Akiyama, “High repetitive pulsed streamer discharges in water , their induced shock waves and medical applications,” *28th Int. Symp. Shock Waves*, pp. 2–3, 2011.

[11] C. Eing, M. Goettel, R. Straessner, C. Gusbeth, and W. Frey, “Pulsed Electric Field Treatment of Microalgae—Benefits for Microalgae Biomass Processing,” *IEEE Trans. Plasma Sci.*, vol. 41, no. 10, pp. 2901–2907, 2013.

[12] Y. Yang, Y. I. Cho, and A. Fridman, *Plasma Discharge in Liquid: Water Treatment and Applications*. CRC Press, 2012.

[13] C. Gordon, “~TAL FOILS FOR USE IN PULSED LASER APPLICATIONS by.”

[14] M. G. Haines, T. W. L. Sanford, and V. P. Smirnov, “Wire-array z-pinch: a powerful x-ray source for ICF,” *Plasma Phys. Control. fusion*, vol. 47, no. 12B, p. B1, 2005.

[15] P. J. Turchi, C. Chairman, P. S. Society, D. Advanced, D. N. Agency, D. Command, N. Surface, A. Force, A. F. Aero-, I. Fusion, P. Services, and E. Engineers, “5th IEEE Pulsed Power Conference,” no. 84, 1985.

[16] H. C. Claiborne, “NEUTRON-INDUCED TRANSMUTATION OF HIGH-LEVEL RADIOACTIVE WASTE.,” Oak Ridge National Lab., Tenn., 1972.

[17] M. Pulsed and P. Systems, “J R Starkey DRA Military Systems RARDE Chobham Lane, Chertsey, Surrey, KTI6 0EE, U.K.,” pp. 834–837.

[18] “Pulsed_Power,” 2012.

[19] R. Kumar, “A miniaturized plasma-opening switch based axial,” pp. 1–4.

[20] W. Jiang, X. Wang, J. Yuan, K. Liu, J. Qiu, T. Yokoo, K. Takayama, M. Wake, N.

Shimizu, and a. Tokuchi, “Compact pulsed power and its industrial applications,” *PPC2009 - 17th IEEE Int. Pulsed Power Conf.*, no. 10675049, pp. 1–10, 2009.

[21] F. Report and C. Mansson, “Pulsed Power Technology and Applications – Scandinavia,” *Power*, no. April, 1999.

[22] S. J Beebe, “Applications for Pulse Power using Nanosecond Pulsed Electric Fields (nsPEFs) in Cell Biology and Cancer Treatment,” *J. Nanomedine. Biotherapeutic Discov.*, vol. 03, no. 01, pp. 1–2, 2013.

[23] Https://en.wikipedia.org/wiki/Pulsed_power, “Pulsed power.” .

[24] S. T. Pai and Q. Zhang, *Introduction to High Power Pulse Technology*. World Scientific, 1995.

[25] J. a Gaudet, R. J. Barker, C. J. Buchenauer, C. Christodoulou, J. Dickens, M. a Gundersen, R. P. Joshi, H. G. Krompholz, J. F. Kolb, a Kuthi, M. Laroussi, a Neuber, W. Nunnally, E. Schamiloglu, K. H. Schoenbach, J. S. Tyo, and R. J. Vidmar, “Research issues in developing compact pulsed power for high peak power applications on mobile platforms,” *Proc. IEEE*, vol. 92, no. 7, pp. 1144–1165, 2004.

[26] E. Schamiloglu, K. Schoenbach, and R. Vidmari, “Basic research leading to compact, portable pulsed power,” DTIC Document, 2007.

[27] M. Joler, C. G. Christodoulou, S. Bakim, and E. Schamiloglu, “Study of high energy storage Blumlein transmission lines as high power microwave drivers,” *IEEE Conf. Rec. - Abstr. 2002 IEEE Int. Conf. Plasma Sci. (Cat. No.02CH37340)*, 2002.

[28] R. Bartnikas, *Engineering Dielectrics: Volume III Electrical Insulating Liquids*. 1994.

[29] G. A. Mesyats, *Pulsed power*. Springer Science & Business Media, 2007.

[30] C. L. Wadhwa, *High Voltage Engineering*. New Age International (P) Limited, 2007.

[31] E. Kuffel, W. Zaengl, and J. Kuffel, “High voltage engineering fundamentals,” p. 556, 2000.

[32] J. R. Lucas, “Breakdown of Gaseous Insulation,” *High Volt. Eng.*, pp. 1–21, 2001.

[33] C. L. Wadhwa, “Breakdown Mechanism of Gaseous, Liquid and Solid Materials,” *High Volt. Eng.*, pp. 1–55, 271AD.

[34] Spellman High Voltage Electronics Corporation, *High Voltage Reference Manual*, vol. 104, no. 3. 2014.

[35] W. J. Wijker, “The electrical breakdown in vacuum,” *Appl. Sci. Res. Sect. B*, vol. 9, no. 1, pp. 1–20, 1961.

[36] A. S. Denholm, “The electrical breakdown of small gaps in vacuum,” *Can. J. Phys.*, vol. 36, no. 4, pp. 476–493, 1958.

[37] Z. Krasucki, “Breakdown of Liquid Dielectrics,” *Proc. R. Soc. A Math. Phys. Eng. Sci.*, vol. 294, no. 1438, pp. 393–404, 1966.

[38] A. I. Gerasimov, “Water as an insulator in pulsed facilities (Review),” *Instruments Exp. Tech.*, vol. 48, no. 2, pp. 141–167, 2005.

[39] J. Kolb, S. Kono, S. Xiao, B. Goan, X. Lu, C. Bickes, M. Laroussi, R. P. Joshi, K. H. Schoenbach, and E. Schamiloglu, “Water and propylene carbonate as storage and switching media in pulsed power systems,” in *Pulsed Power Conference, 2003. Digest of Technical Papers. PPC-2003. 14th IEEE International*, 2003, vol. 1, pp. 715–718.

[40] W. Jue, Y. Ping, Z. Shichang, and S. Yaohong, “Transformer oil breakdown under

nanosecond pulse," *Conf. Rec. Int. Power Modul. Symp. High Volt. Work.*, no. 50437020, pp. 100–103, 2006.

[41] V. Ushakov and I. Breakdown, *Impulse Breakdown of Liquids*. 2007.

[42] V. Y. Ushakov and V. I. A. Ushakov, *Insulation of High-Voltage Equipment*. Springer, 2004.

[43] S. Naidu and V. Kamaraju, *High Voltage Engineering*. McGraw-Hill Education (India) Pte Limited, 2013.

[44] T. J. Lewis, "A new model for the primary process of electrical breakdown in liquids," *Dielectr. Electr. Insul. IEEE Trans.*, vol. 5, no. 3, pp. 306–315, 1998.

[45] R. P. Joshi and S. M. Thagard, "Streamer-like electrical discharges in water: Part I. fundamental mechanisms," *Plasma Chem. Plasma Process.*, vol. 33, no. 1, pp. 1–15, 2013.

[46] J. F. Kolb, R. P. Joshi, S. Xiao, and K. H. Schoenbach, "Streamers in water and other dielectric liquids," *J. Phys. D. Appl. Phys.*, vol. 41, no. 23, p. 234007, 2008.

[47] M. Kim and R. E. Hebner, "Initiation from a point anode in a dielectric liquid," *IEEE Trans. Dielectr. Electr. Insul.*, vol. 13, no. 6, pp. 1254–1260, 2006.

[48] Y. Seepersad, A. Fridman, and D. Dobrynin, "Anode initiated impulse breakdown in water: the dependence on pulse rise time for nanosecond and sub-nanosecond pulses and initiation mechanism based on electrostriction," pp. 11–17.

[49] T. J. Lewis, *The Liquid State and Its Electrical Properties*, vol. 193. 1989.

[50] M. Szklarczyk, "On the Dielectric Breakdown of Water: An Electrochemical Approach," *J. Electrochem. Soc.*, vol. 136, no. 9, p. 2512, 1989.

[51] F. Macdougall, J. Ennis, X. Hui, C. Yang, R. a Cooper, J. E. Gilbert, J. F. Bates, C. Naruo, M. Schneider, N. Keller, S. Joshi, G. Lane, S. Diego, T. R. Jow, J. Ho, C. J. S. Scozzie, P. M. Road, and W. Dc, "High Energy Density Capacitors for Pulsed Power Applications," 2009.

[52] J. P. Vandevender and T. H. Martin, "Scieice, Vot.NS-22," vol. 5, no. 3, pp. 979–982, 1975.

[53] R. P. Joshi, J. Qian, J. Kolb, and K. H. Schoenbach, "Model analysis of breakdown in high-voltage, water-based switches," *Dig. Tech. Pap. PPC-2003. 14th IEEE Int. Pulsed Power Conf. (IEEE Cat. No.03CH37472)*, vol. 1, pp. 293–296, 2003.

[54] Dingjiu Li and Shoushen Chen, "The breakdown Voltage of deionized water and transformer oil in the microsecond and nanosecond regions," *Proceedings., Second Int. Conf. Prop. Appl. of, Beijing*, vol. vol.1, pp. 63–66, 1988.

[55] K. K. and T. S. H. Yamada, T. Murakami, "Positive streamer propagation and breakdown time lag in cyclohexane under micro-second rectangular pulse voltage," *Conf. Rec. 10th Int. Conf. on, Grenoble*, pp. pp. 410–414, 1990.

[56] " L. G. Christophorou and H. Faidas, "Dielectric-liquid pulsed power switch," *Conduct. Break. Dielectr. Liq. 1990. ICDL 1990. Conf. Rec. 10th Int. Conf. on, Grenoble*, pp. 454–458, 1990.

[57] M. A. G. and B. R. V. D. W. Auckland, K. Chandraker, "Water treeing in insulating liquids," *IEE Proc. - Sci. Meas. Technol.*, vol. vol. 142, no. no.2, pp. pp. 157–161.

[58] B. T. J. Lewis, B. S. Eng, M. Sc, D. Ph, and A. Member, "ELECTRICAL

BREAKDOWN IN ORGANIC LIQUIDS," vol. 100, no. 1488, 1953.

[59] S. N. Komin and E. A. Morozov, "Investigation of prebreakdown processes in deionized water by Mach-Zehnder interferometer," *Conduction and Breakdown in Dielectric Liquids, 1990. ICDL 1990. Conference Record., 10th International Conference on*. pp. 459–463, 1990.

[60] E. Husain and S. M. Islam, "Effect of electrode shape, material and chemical structure on electric strength of some liquid hydrocarbons," *Conduction and Breakdown in Dielectric Liquids, 1990. ICDL 1990. Conference Record., 10th International Conference on*. pp. 552–556, 1990.

[61] I. M. Gavrilov, V. R. Kukhta, and V. V Lopatin, "The effect of heating and EHD events on breakdown in water," *Conduction and Breakdown in Dielectric Liquids, 1990. ICDL 1990. Conference Record., 10th International Conference on*. pp. 593–597, 1990.

[62] E. Forster and S. Patrissi, "The Effect of the Electrode Gap on Breakdown in Liquid Dielectrics," vol. 1, no. 3, pp. 440–446, 1994.

[63] H. M. Jones, "The Influence of Pressure and Conductivity on the Pulsed Breakdown of Water," vol. 1, no. 6, pp. 1016–1025, 1994.

[64] T. J. Lewis, "The basic processes of conduction in dielectric liquids," *Conduction and Breakdown in Dielectric Liquids,1993., ICDL '93., IEEE 11th International Conference on*. pp. 32–41, 1993.

[65] T. J. Lewis, J. P. Llewellyn, M. J. Van Der Sluijs, J. Freestone, and R. N. Hampton, "A NEW MODEL FOR ELECTRICAL AGEING AND BREAKDOWN IN DIELECTRICS," no. 4, pp. 23–26, 1996.

[66] M. Marci, "Electric breakdown strength measurement in liquid dielectrics," no. 1, pp. 1–4.

[67] J. F. Kolb, S. Xiao, B. Goan, X. P. Lu, K. H. Schoenbach, M. Laroussi, J. P. Joshi, J. Dickens, A. Neuber, H. Krompholz, M. Cevallos, and M. Butcher, "Nanosecond, optical diagnostics for liquid dielectric switches," *Plasma Science, 2004. ICOPS 2004. IEEE Conference Record - Abstracts. The 31st IEEE International Conference on*. p. 402, 2004.

[68] K. C. Kao, "Theory of High-Field Electric Conduction and Breakdown in Dielectric Liquids," no. 4, 1976.

[69] B. A. M. Sletten, T. J. Lewis, M. Sc, D. Ph, and A. Member, "CHARACTERISTICS OF THE TRIGATRON SPARK-GAP," no. 193, pp. 54–61, 1956.

[70] "Introduction to High Power Pulse Technology S. T.Pai Q.Zhang World 1995 WW.pdf." .

[71] R. Bischoff, S. Pinguet, and J. Duperoux, "THE APPLICATION OF LIQUID DIELECTRICS IN MARX GENERATORS," pp. 6–9.

[72] S. Naidu and V. Kamaraju, *High Voltage Engineering*. Tata McGraw Hill Education Private Limited, 2009.

[73] A. I. Gerasimov, "Water as an insulator in pulsed facilities (Review)," *Instruments Exp. Tech.*, vol. 48, no. 2, pp. 141–167, 2005.

[74] C. A. Pirrie and H. Menown, "The evolution of the hydrogen thyratron," *Power Modulator Symposium, 2000. Conference Record of the 2000 Twenty-Fourth*

International. pp. 9–16, 2000.

[75] K. G. Cook and G. G. Isaacs, “Deuterium-filled thyratrons,” *Br. J. Appl. Phys.*, vol. 9, no. 12, p. 497, 1958.

[76] P. . Ottinger, R. J. Commisso, W. H. Lupton, and J. J.D. Shipman, “System Study for an Inductive Generator,” pp. 12–15.

[77] W. Heise and F. T. D. I. V. W.-P. A. F. B. OHIO., *Tesla Transformers*. Defense Technical Information Center, 1971.

[78] J. C. Martin, P. D. Champney, D. A. Hammer, and C. U. S. of Electrical Engineering, *Notes on the construction methods of a Martin high-voltage pulse transformer*. School of Electrical Engineering, 1967.

[79] M. Denicolai, “Optimal performance for Tesla transformers,” *Rev. Sci. Instrum.*, vol. 73, no. 9, p. 3332, 2002.

[80] K. K. Jain, D. Chennareddy, P. I. John, and Y. C. Saxena, “Design and performance of a Tesla transformer type relativistic electron beam generator,” *Sadhana*, vol. 9, no. 1, pp. 19–29, 1986.

[81] D. Finkelstein, “High Voltage Impulse System,” *Rev. Sci. Instrum.*, vol. 37, no. 2, p. 159, Dec. 1966.

[82] C. R. J. Hoffmann, “A Tesla transformer high−voltage generator,” *Rev. Sci. Instrum.*, vol. 46, no. 1, p. 1, Sep. 1975.

[83] H. Matsuzawa and S. Suganomata, “Design charts for Tesla-transformer-type relativistic electron beam generators,” *Rev. Sci. Instrum.*, 1982.

[84] J. L. Reed, “Greater voltage gain for Tesla-transformer accelerators,” *Rev. Sci. Instrum.*, vol. 59, no. 10, p. 2300, 1988.

[85] T. Korkeakoulu, “Tesla Transformer for Experimentation and Research,” no. May, 2001.

[86] A. Upadhyay, S. Pirmohammad, H. Ganeshkumar, and G. Vasimmahamad, “Working model of tesla coil,” no. May, 2011.

[87] “High power Tesla driven miniature plasma opening switch.”

[88] N. Miura and K. Nakao, “Computer Analysis of Megagauss Field Generation by Condenser Bank Discharge,” *Jpn. J. Appl. Phys.*, vol. 29, no. Part 1, No. 8, pp. 1580–1599, 1990.

[89] F. W. Grover, “Inductance Calculations: Working Formulas and Tables,” *Instrum. Soc. Am.*, 1946.

[90] G. Veda Prakash, R. Kumar, J. Patel, K. Saurabh, and a. Shyam, “Note: Tesla based pulse generator for electrical breakdown study of liquid dielectrics,” *Rev. Sci. Instrum.*, vol. 84, no. 12, 2013.

[91] D. G. Pellinen, M. S. Di Capua, S. E. Sampayan, H. Gerbracht, and M. Wang, “Rogowski coil for measuring fast, high-level pulsed currents,” *Rev. Sci. Instrum.*, vol. 51, no. 11, pp. 1535–1540, 1980.

[92] D. E. Shepard and D. W. Yauch, “an Overview of Rogowski Coil Current Sensing Technology,” 2010.

[93] D. a. Ward and J. L. T. Exon, “Using Rogowski coils for transient current measurements,” *Eng. Sci. Educ. J.*, vol. 2, no. 3, p. 105, 1993.

[94] M. Argüeso, G. Robles, and J. Sanz, “Measurement of high frequency currents with a Rogowski coil,” *IX Spanish-Portuguese Conf. Electr. Eng.*, 2005.

[95] F. Hegeler, G. Masten, and H. Krompholz, “Fast Electrical and Optical Diagnostics of the Early Phase of Current Luminosity,” pp. 0–3, 1894.

[96] C. a. Ekdahl, “Voltage and current sensors for a high-density z-pinch experiment,” *Rev. Sci. Instrum.*, vol. 51, no. 12, p. 1645, 1980.

[97] C. a. Ekdahl, “Capacitively-coupled inductive sensors for measurements of pulsed currents and pulsed magnetic fields,” *Rev. Sci. Instrum.*, vol. 51, no. 12, pp. 1649–1651, 1980.

[98] “Emission spectra.” .

[99] “Fourier Transform Infrared spectroscopy,” *http://www.thermoscientific.com/content/tfs/en/products/fourier-transform-infrared-spectroscopy-ftir.html*. .

[100] “4 Picos ICCD camera,” *http://www.stanfordcomputeroptics.com/products/pic*. .

[101] “No Title.” [Online]. Available: http://www.4oakton.com/Assets/Manual_pdfs/EOK_PC300_Oct02.pdf.

[102] M. Sprik and M. Sprik, “Hydrogen bonding and the static dielectric constant in liquid water,” *J. Chem. Phys.*, vol. 95, no. 9, p. 6762, 1991.

[103] C. G. Malmberg, “Dielectric constant of deuterium oxide,” *...of Res. Natl. Bur. Stand.*, 1958.

[104] M. Chaplin, “hydrogen bonding in water,” *http://www1.lsbu.ac.uk/water/water_hydrogen_bonding.html*. .

[105] “Deionized water,” *https://en.wikipedia.org/wiki/Purified_water*. .

[106] “NIST: Atomic Spectra Database Lines Form.” .

[107] M. Zahn, T. Takada, Y. Ohki, and J. Gottwald, “Charge Injection and Transport Analysis and Measurements in Highly Purified Water,” pp. 312–315.

[108] M. Zahn, Y. Ohki, K. Rhoads, M. LaGasse, and H. Matsuzawa, “Electro-Optic Charge Injection and Tramsport Measurements in Highly Purified Water and Water/Ethylene Glycol Mixtures,” *IEEE Trans. Electr. Insul.*, vol. EI-20, no. 2, pp. 199–211, 1985.

[109] M. Zahn, “Electro-optic field and space-charge mapping measurements in high-voltage stressed dielectrics,” *Phys. Technol.*, vol. 16, no. 6, pp. 288–295, 1985.

[110] M. Zahn, S. Voldman, T. Takada, and D. B. Fenneman, “Charge injection and transport in high voltage water/glycol capacitors,” *J. Appl. Phys.*, vol. 54, no. 1, p. 315, 1983.

[111] R. Arora and W. Mosch, *High Voltage and Electrical Insulation Engineering*. Wiley, 2011.

[112] G. A. Vidulich, D. F. Evans, and R. L. Kay, “The dielectric constant of water and heavy water between 0 and 40.degree.,” *J. Phys. Chem.*, vol. 71, no. 3, pp. 656–662, Feb. 1967.

[113] Boundless, “Isotopes of Hydrogen,” Jul. 2015.

[114] A. K. Soper and C. J. Benmore, “Quantum Differences between Heavy and Light Water,” *Phys. Rev. Lett.*, vol. 101, no. 6, p. 65502, Aug. 2008.

[115] T. Aug, P. By, C. Cole, and E. Physics, “MadSci Network : Chemistry Query : Re : what is the pH of heavy water (D2O),” pp. 2–3, 2015.

[116] “Water properties,” *http://www.lsbu.ac.uk/water/data.html*. .

[117] M. Chaplin, “Water’s Hydrogen Bond Strength,” *arXiv*, vol. cond-mat.s, pp. 1–20, 2007.

[118] “Heavy water,” *https://en.wikipedia.org/wiki/Heavy_water*. .

[119] “deuterium | chemical isotope | Britannica.com.” .

[120] “Water absorption spectrum.” .

[121] J. G. Bayly, V. B. Kartha, and W. H. Stevens, “The absorption spectra of liquid phase H2O, HDO and D2O from 0·7 μm to 10 μm,” *Infrared Phys.*, vol. 3, no. 4, pp. 211–222, 1963.

[122] M. Chaplin, “Water absorption spectrum,” vol. 7, pp. 1–7, 2014.

[123] S. M. Thagard, K. Takashima, and A. Mizuno, “Electrical discharges in polar organic liquids,” *Plasma Process. Polym.*, vol. 6, no. 11, pp. 741–750, 2009.

[124] S. Mededovic, “Chemical Processes In Aqueous Phase Pulsed Electrical Discharges : Fundamental Mechanisms And Applications To Organic Compound Degradation,” 2007.

[125] S. Mededovic, W. C. Finney, and B. R. Locke, “Electrical Discharges in Mixtures of Light and Heavy Water,” *Plasma Process. Polym.*, vol. 5, no. 1, pp. 76–83, Jan. 2008.

[126] M. Zahn, “Charge Injection and Transport in a Lossy Capacitor Stressed by a Marx Generator,” *IEEE Trans. Electr. Insul.*, vol. EI-19, no. 3, pp. 179–182, 1984.

[127] N. US Department of Commerce, “NIST Atomic Spectra Database.”

[128] X. Lu, J. F. Kolb, S. Xiao, M. Laroussi, K. H. Schoenbach, and E. Schamiloglu, “Dielectric strength of sub-millimeter water gaps subjected to microsecond and sub-microsecond voltage pulses,” *Dig. Tech. Pap. Int. Pulsed Power Conf.*, pp. 600–603, 2007.

[129] *Impulse Breakdown of Liquids*. Berlin, Heidelberg: Springer Berlin Heidelberg, 2007.

[130] D. B. Fenneman and R. J. Gripshover, “Experiments on electrical breakdown in water in the microsecond regime,” *...Science, IEEE Trans.*, 1980.

[131] K. Schoenbach, J. Kolb, S. Xiao, S. Katsuki, Y. Minamitani, and R. Joshi, “Electrical breakdown of water in microgaps,” *Plasma Sources Sci. Technol.*, vol. 17, no. 2, p. 024010, 2008.

[132] G. R. Jones, *Electrical Engineer’s Reference Book*. Elsevier Science, 2013.

[133] M. Szklarczyk, “Electrical breakdown of liquids,” in *Modern Aspects of Electrochemistry*, Springer, 1993, pp. 253–296.

[134] V. ya. ushakov V. Lopatin, “Initiation and development of nano secodn discharge in liquids,” no. 3, pp. 376–381, 1975.

[135] F. W. (Frank W. Peek, *Dielectric phenomena in high-voltage engineering*, 3rd ed. New York [etc.] : McGraw-Hill Book Company, inc, 1929.

[136] G. Veda Prakash, R. Kumar, J. Patel, K. Saurabh, and A. Shyam, “Note: Tesla based pulse generator for electrical breakdown study of liquid dielectrics.,” *Rev. Sci. Instrum.*, vol. 84, no. 12, p. 126108, Dec. 2013.

[137] “4 picos ICCD,” *http://www.stanfordcomputeroptics.com/products/picosecond-iccd.html*. .

[138] “Agilent Technologies, DSO-X 2024 A,” *http://www.keysight.com/en/pd-1945124-pn-DSOX2024A/oscilloscope-200-mhz-4-channels?cc=IN&lc=eng*. .

[139] V. F. Klimkin, “Super high-speed anode pre-breakdown phenomena in liquiddielectrics under uniform fields,” *Proc. 1993 IEEE 11th Int. Conf. Conduct. Break. Dielectr. Liq. (ICDL ’93)*, pp. 299–303, 1993.

[140] J. Jadidian, M. Zahn, N. Lavesson, O. Widlund, and K. Borg, “Stochastic and deterministic causes of streamer branching in liquid dielectrics,” *J. Appl. Phys.*, vol. 114, no. 6, 2013.

[141] Y. Seepersad, M. Pekker, M. N. Shneider, A. Fridman, and D. Dobrynin, “Investigation of positive and negative modes of nanosecond pulsed discharge in water and electrostriction model of initiation,” *J. Phys. D. Appl. Phys.*, vol. 46, no. 35, p. 355201, 2013.

[142] P. H. Ceccato, O. Guaitella, M. R. Le Gloahec, and a Rousseau, “Time-resolved nanosecond imaging of the propagation of a corona-like plasma discharge in water at positive applied voltage polarity,” *J. Phys. D. Appl. Phys.*, vol. 43, no. 17, p. 175202, 2010.

[143] S. Katsuki, H. Akiyama, A. Abou-Ghazala, and K. H. Schoenbach, “Parallel streamer discharges between wire and plane electrodes in water,” *IEEE Trans. Dielectr. Electr. Insul.*, vol. 9, no. 4, pp. 498–506, 2002.

Appendix-I

Stainless steel (SS 304) material details:

Test sample : 45 mm SS Hemisphere

Method of analysis: Spectroscopy

Elements	Content (in %)	Standard value (in %)
Carbon	0.065	0.08 Max
Silicon	0.395	2.00 Max
Manganese	1.190	1.50 Max
Phosphorus	0.024	0.040 Max
Sulphur	0.020	0.040 Max
Chromium	18.600	18.0-21.0
Nickel	8.300	8.0-11.0
Molybdenum	0.165	0.50 Max

Remarks: The above elements conform to ASTM A351, Gr-CF8 [S.S. 304].

Brass material details:

Elements	Percentage (%)
Zinc	40.220
Tin	0.450
Lead	2.970
Iron	0.360
Nickel	0.280

Phosphorous	0.005
Silicon	0.008
Manganese	0.023
Antimony	0.014
Arsenic	0.010
Copper	55.640